ABSTRACT

Title of Document: ORBITAL FLOOR REGENERATION USING CYCLIC ACETAL HYDROGELS THROUGH ENHANCED OSTEOGENIC CELL SIGNALING OF MESENCHYMAL STEM CELLS

Martha Wheaton Betz, Doctor of Philosophy, 2009

Directed By: Associate Professor John P. Fisher, Fischell Department of Bioengineering

Orbital floor fractures are a serious consequence of craniofacial trauma and account for approximately 60-70% of all orbital fractures. Unfortunately, the body's natural response to orbital floor defects generally does not restore proper function and facial aesthetics which is complicated by the thin bone and adjacent sinuses. We propose using a tissue engineering strategy to regenerate orbital floor bone. To this end, a functional biomaterial was investigated to enhance orbital floor regeneration.

First, a bone marrow stromal cell population was isolated and differentiation assessed via coculture with chondrocytes and osteogenic media supplements. A cyclic acetal biomaterial composed of the cyclic acetal monomer 5-ethyl-5-(hydroxymethyl)-β,β-dimethyl-1,3-dioxane-2-ethanol diacrylate (EHD) and poly(ethylene glycol) diacrylate (PEGDA) was then developed for cell encapsulation. The previously investigated bone marrow stromal cells were then used to determine

the effects of the ammonium persulfate/N,N,N',N'-tetramethylethylenediamine initiator system used to crosslink the EH-PEG hydrogels on cell viability, metabolic activity, and osteogenic differentiation. Next, EH-PEG hydrogels were implanted into orbital floor defects with bone morphogenetic protein-2, where tissue response and surrounding bone growth was analyzed. To improve surrounding tissue interaction and cell infiltration, macroporous EH-PEG hydrogels were created using porogen-leaching. These hydrogels were characterized using optical coherence tomography for pore size, porosity, and cell viability. In addition, these macroporous hydrogels were created with varying architecture to analyze the effects on osteogenic signaling and differentiation. This work outlines the potential application of EH-PEG hydrogels for use in orbital floor repair.

ORBITAL FLOOR REGENERATION USING CYCLIC ACETAL HYDROGELS THROUGH ENHANCED OSTEOGENIC CELL SIGNALING OF MESENCHYMAL STEM CELLS

By

Martha Wheaton Betz

Dissertation submitted to the Faculty of the Graduate School of the
University of Maryland, College Park, in partial fulfillment
of the requirements for the degree of
Doctor of Philosophy
2009

Advisory Committee:
Associate Professor John P. Fisher, Chair
Assistant Professor John F. Caccamese
Assistant Professor Domenick P. Coletti
Professor David M. Mosser
Assistant Professor Sameer B. Shah

Dedication

This work is dedicated to my grandfather, Victor Betz, who has always let me know how proud he is of me.

Acknowledgements

I would like to thank my advisor, Dr. John Fisher, for his guidance throughout this project, for without him it would not have been possible. I would also like to thank Dr. John Caccamese and Dr. Domenick Coletti for their invaluable input into my project and assistance with the *in vivo* studies. I would like to thank Dr. John Sauk for his direction with my histology samples. I would like to thank Dr. Yu Chen for introducing me to optical coherence tomography and all of his help with my project; in addition to the members of his lab including Chao-Wei Chen and Andrew Paek. I want to thank the undergraduates I worked with throughout my career at Maryland who significantly contributed to my work, Andrew Thompson, Parth Modi, and William Richbourg. I would also like to thank the other members of my dissertation committee, Dr. David Mosser and Dr. Sameer Shah for their guidance and support. A huge thanks to the other members, past and present, of the tissue engineering and biomaterials laboratory for assistance in lab, encouragement along the way, and of course friendship. Also, thanks to my family and friends for their support!

Table of Contents

List of Tables

List of Figures

Chapter 1: Introduction

Orbital floor fractures are a severe form of craniofacial trauma. In addition, the orbital floor is the wall most likely involved in orbital injuries. Unfortunately, the body's natural healing response to orbital floor fractures does not restore proper function and aesthetics; therefore, clinical intervention is necessary. Current common clinical treatments include alloplastic implants and autologous grafts; however, each has associated disadvantages.

This project investigates the use of a tissue engineering approach to orbital floor repair. An optimized orbital floor implant should regenerate orbital bone while supporting the orbital contents and eliciting minimal inflammatory response from the surrounding tissues. As scaffold properties are very important to the success and function of the implant a number of polymers are currently under investigation; however, an ideal biomaterial has yet to be developed. Our laboratory has developed a novel class of biomaterials based upon a cyclic acetal unit. These materials may be advantageous as they degrade by hydrolysis into neutral primary degradation products of diols and carbonyls, and thus many not experience a change in local acidity associated with many synthetic biomaterials. The acidity of hydrogel degradation products may be a concern to the stable phenotypic function of encapsulated cell populations. Furthermore, acidic byproducts are thought to increase the inflammatory response and slow wound healing. In addition, an increase in acidity is associated with an increase in the degradation rate which may affect the mechanical support the construct is providing.

In order to create a cyclic acetal based hydrogel for cell delivery, we followed the well described route of incorporating the hydrophilic polymer poly(ethylene glycol) (PEG). Specifically, by including poly(ethylene glycol) diacrylate (PEGDA) within the radical polymerization of the cyclic acetal monomer 5-ethyl-5-(hydroxymethyl)-β,β-dimethyl-1,3-dioxane-2-ethanol diacrylate (EHD). This hydrogel can act as a platform for orbital floor repair by incorporation of mesenchymal stem cells and osteoinductive signals such as bone morphogenetic proteins.

Chapter 2: Polymeric Scaffolds for Bone Tissue Engineering[1]

Orthopaedic injuries resulting from trauma or improper development often require surgical intervention to restore natural tissue function. Currently, over one million operations are completed annually for bone surgical reconstruction[1]. The well known limitations associated with autografts, allografts, and bone cements have led to the investigation of synthetic polymers as support matrices for bone tissue engineering. Polymers are long chain molecules that are formed by linking repetitive monomer units and have been extensively studied for tissue engineering applications. Constructs designed from these polymers can act as a support matrix to deliver cell populations or induce surrounding tissue ingrowth. Scaffold properties directly determine their success in tissue engineering and must be designed specifically for each application. A successful scaffold provides initial support, growth factors, and transitions through degradation to allow tissue regeneration and returned function. This chapter will discuss the fabrication and properties of polymeric tissue engineering scaffolds including curing methods, polymer assembly, scaffold fabrication, surface properties, macrostructure, mechanical properties, biodegradation and biocompatibility, in addition to current synthetic polymers being investigated.

[1] As published in MW Betz, DM Yoon, and JP Fisher. Engineering Polymeric Scaffolds for Bone Grafts. In: Engineering of Functional Skeletal Tissues. Topics in Bone Biology (Bronner, Farach-Carson, Mikos eds.) Springer, New York, NY. 3: 81-94. (2006).

2.1 Scaffold Formation

2.1.1 Curing Methods

Scaffold curing method describes how polymer chains are formed into a bulk material and is dependant on the chemical nature of the polymer, specifically polymer length and functionality[2]. Two major curing methods often used are polymer entanglement and crosslinking.

Polymer entanglement is based on the principle that many polymers associate with one another in solution. This is common with long, linear, as well as branched polymers. The polymer is dissolved in an appropriate solvent and placed in a mold. The solvent is removed by evaporation, leaving the polymer in the shape of the mold using pressure, temperature, or both[3]. The process is advantageous because it is relatively simple, however there can be a lack of mechanical stability in the constructs formed exclusively by polymer entanglement.

Crosslinking of individual polymers through chemical bonds to form a bulk material is another curing method. Individual polymer chains can form hydrogen or ionic bonds with one another through non-covalent interactions[2]. For the formation of covalent bonds, the polymer must contain a reactive site for crosslinking, such as a carbon-carbon double bond. Covalent crosslinking is generally induced by a free radical that is initiated by heat, light, chemical accelerant, or time[4]. For example, photopolymerization is a commonly used technique based on photopolymer polymerization initiated by electromagnetic radiation[5]. The photopolymers used are typically low molecular weight monomers that react to form long-chain polymers when activated by a specific wavelength. In addition, since scaffold formation is in

response to a signal, the polymer may be used as an injectable material, and when exposed to the signal can form *in situ*. However, the chemical reactions that are necessary for crosslinking are often associated with unreacted components as well as reaction byproducts that may be harmful to the surrounding tissue.

2.1.2 Polymer Assembly

Polymer assembly may occur before implantation into the body, known as prefabrication, or during implantation *in situ*[6]. Prefabrication is common because the scaffold is formed outside of the body and any cytotoxic or non-biocompatible byproducts may be removed prior to transplantation. In addition, this method allows for cell encapsulation and *in vitro* preculture before implantation. However, the geometry of the construct generally will not precisely fit the host site. This imperfect match may lead to host immune reactions such as fibrosis and therefore construct failure. *In situ* fabrication techniques have been developed to address this concern. This technique involves curing the construct at the tissue defect site[4]. Liquid components are injected into the desired site and their deformability allows for improved integration into the host tissue. Furthermore, as this method uses liquid components, it is less invasive than the surgical procedures sometimes necessary for prefabricated constructs. However, *in situ* fabrication does not allow for the removal of harmful byproducts, and therefore the surrounding tissue can be exposed to toxic components. This concern effectively reduces the possible chemical components that can be used to form the construct *in situ*.

2.1.3 Conventional Scaffold Fabrication Methods

Fabrication is the process of forming a cured or curing polymer into a scaffold. Scaffold fabrication can occur using conventional or rapid prototyping / solid freeform practices (See Table 1). There are a number of conventional techniques that are used to create porous scaffolds including fiber bonding, solvent-casting particulate leaching, phase separation, melt molding, freeze drying, and gas foaming.

Fabrication Method	Scaffold Characteristics	Materials	References
Fiber Bonding	High porosity Low mechanical strength	PGA, PCL	[7-9]
Solvent-Casting Particulate-Leaching	Controlled porosity Lack of mechanical strength	PLA, PLGA, PPF	[10-14]
Phase Separation	Porous Biomolecule incorporation	PLLA, PLGA, PLA	[15-18]
Melt Molding	Controlled porosity & pore size Biomolecule incorporation	PLGA	[6,19]
Freeze Drying	Controlled pore size	PLGA	[20-22]
Gas Foaming	Controlled porosity Controlled pore structure	PLLA, PLGA, PLA	[23-25]
Three-dimensional Printing	Controlled mechanical strength	PCL, PEO, PLGA, PLA	[26-28]

Sheet Lamination	Porous	PLA, PLGA	[29]
Laser Stereolithography	Biomolecule incorporation	PPF, PEGDA	[30-32]
Fused Deposition	Controlled pore size	PCL	[33-36]

Table 1: Fabrication methods and associated characteristics of synthetic polymers used in bone tissue engineering scaffolds.

2.1.3.1 Fiber Bonding

Fibers are commonly processed from semicrystalline polymers, including poly(glycolic acid) (PGA). These fibers can be used to create a fiber mesh, or a three-dimensional patterned structure with variable pore size through weaving or knitting. These mesh constructs allow a large surface area and high porosity corresponding with greater cell attachment, nutrient diffusion, and waste removal[6]. However, due to the increased porosity these scaffolds tend to be mechanically unstable. This led to the formation of a fiber bonding technique to alleviate this issue[6,7]. Fiber bonding method has been used to dissolve poly(lactic acid) (PLA) in a solvent and cast it over a PGA mesh that is aligned in the desired shape[6]. Heating the construct above the melting temperature of PGA evaporates the solvent. The PGA mesh becomes connected at fiber cross points when the construct is cooled and PLA is re-dissolved. Fiber bonding has also been used to fabricate scaffolds from poly(ε-caprolactone) (PCL)[9]. While this technique allows for greater structural stability, there are a few disadvantages. The porosity varies and cannot be finely

controlled. In addition, the solvent used to dissolve the polymer can be harmful to an incorporated cell population and the surrounding tissue.

2.1.3.2 Solvent-Casting Particulate Leaching

Solvent-casting particulate leaching is a technique where dispersed particles such as sodium chloride, tartrate, citrate, or saccharose, are mixed in solution with a polymer and mold casted[6,10]. Casting or freeze-drying is performed to evaporate the solvent. The dispersed particles are leached out of the scaffold, leaving void spaces that form a porous and highly interconnected structure. This process allows the independent control of porosity and pore size[6]. This technique has been used to form constructs with PLA, poly (D,L-lactic acid-co-glycolic acid) (PLGA) and poly(propylene fumarate) (PPF)[10-14].

2.1.3.3 Phase Separation

Phase separation is used to isolate components of a heterogeneous mixture. In this process the polymer is first dissolved in a solvent such as molten phenol, naphthalene, or dioxane[6,15]. The polymer solvent solution is cooled, causing liquid-liquid or solid-liquid phase separation with the polymer in a separate phase than the solvent. The solvent is then evaporated forming a porous polymer membrane[6,16,37]. One considerable advantage of this technique is the ability to incorporate biomolecules into the scaffold without exposing it to harsh chemical or thermal conditions. In addition, changes to the polymer composition, polymer concentration, and solvent to nonsolvent ratio can be utilized to augment the scaffold structure.

However, the effect of these modifications may be difficult to predict. Phase separation has been used to create scaffolds of poly(L)lactic acid (PLLA), PLGA, and PLA[15-18].

2.1.3.4 Melt Molding

Melt molding combines a polymer powder and microspheres to form a scaffold[6]. This technique has been used with a fine PLGA powder and gelatin microspheres heated in a Teflon mold[6,19]. Heating the polymer above the glass transition temperature allows the polymer powder to melt. The molded polymer is then removed and placed in water where the entrapped microspheres are removed, resulting in a three-dimensional porous structure. There are a number of advantages to using this technique. Pore size is directly related to the microsphere diameter, and changing the polymer to gelatin ratio modifies the porosity. Furthermore, biomolecules can be incorporated into the scaffold, since this process is completed in a moderate environment without organic solvents. Also, a defined construct shape can be chosen and created by changing the shape of the mold. However, a disadvantage is that this technique may often require very high temperatures to heat semicrystalline polymers above their glass transition temperature[6].

2.1.3.5 Freeze Drying

Freeze drying is another method that uses temperature change to create a porous structure[20]. In this technique synthetic polymers such as PLGA are dissolved in extremely cold solvents, for example glacial acetic acid or benzene[20-22]. This

solution is combined with water creating an emulsion[22]. Next, the emulsion is quickly frozen, creating ice crystals of solvent and water. These crystals are removed through a freeze-drying technique, leaving a highly connected porous matrix. An advantage to this technique is that the pore size can be controlled by altering the freezing rate; in general, a faster rate creates smaller pores[21]. Pore structure is difficult to control with freeze drying alone; however, it may be controlled by combining freeze drying with other techniques such as the above-described particulate-leaching method[38].

2.1.3.6 Gas Foaming

In gas foaming, pores are created within a scaffold from pressurized gases or gases created from a chemical reaction[24]. The presence of bubbles within the polymer leads to the formation of pores in the construct. Variations in gas volume, rate of gas nucleation and diffusion modify the porosity and pore structure of the scaffold. This method is advantageous because the scaffold is formed in a moderate environment without the use of organic solvents. Similar to freeze-drying, this method can also be improved through combination with particulate leaching[25]. Gas foaming has been used with PLLA, PLGA and PLA to create scaffolds for bone tissue engineering applications[23-25].

2.1.4 Rapid Prototyping / Solid Free Form Fabrication

The conventional techniques described above are all generally limited in their control of scaffold parameters such as pore size, pore shape, pore interconnectivity,

and pore wall thickness. This lack of fine control has led to the development of new techniques to produce scaffolds often directly from a computer-aided design model. Rapid prototyping, also known as solid freeform fabrication, has been used to guide surgical procedures based on patient computerized topography[5]. These techniques generally form reproducible three-dimensional scaffolds in a layer-by-layer fashion. The computer model used for scaffold formation can be precisely designed to form specific architecture. In addition to the fine control of scaffold formation, this technique typically also has the advantage of being performed at room temperature. This moderate environment can allow for cell encapsulation and biomolecule incorporation without significantly affecting their viability. However, this technique is not applicable to all polymers and therefore fabrication in this method is limited. Rapid prototyping techniques include sheet lamination, three-dimensional printing, laser stereolithography, and fused deposition modeling[5,32,39,40].

2.1.4.1 Sheet Lamination

Sheet lamination is a technique that creates scaffolds using a layer-by-layer approach. A three-dimensional cross-section of the scaffold is built out of a roll of sheets that have been lined with an adhesive[5]. The layers are cut by a carbon dioxide laser and bonded by heat and or pressure. One disadvantage to this method is that this technique does not allow for formation of small inner holes within the scaffold[5]. This can affect transport of nutrients and waste within the construct.

2.1.4.2 Three-dimensional Printing

Three-dimensional printing forms sequential powder layers of the scaffold by ink-jet printing a binder[39,40]. In this technique a computer model is used to create a slicing algorithm defining the morphology of each layer of the scaffold. A thin layer of powder is distributed over a powder bed, and then a binder material is printed on top where the scaffold is to be formed. A piston is lowered to allow the next layer of powder to be spread and bonded. An advantage of this technique is that the packing density of the powder particles can be used to control the adhesive bonding of the material and therefore mechanical strength[40]. This technique has been used to create scaffolds from polyethylene oxides (PEOs), PLA, PCL and PLGA[26-28,39,40].

2.1.4.3 Laser Stereolithography

Laser stereolithography is another computer aided design method that allows for three-dimensional scaffold formation. This method is similar to three-dimensional printing described above but utilizes a liquid polymer to fabricate a scaffold[39]. The computer model creates two-dimensional slices of the scaffold model and uses this to control a platform submerged in liquid photopolymer. This liquid is then exposed to a focused laser light, which cures the polymer forming a solid at specific points. A significant advantage of this technique is the ability to produce complex internal architecture. Furthermore, different liquid solutions containing biomolecules can be used while forming each layer for incorporation into the scaffold[39]. This technique was used with crosslinking of diethyl fumarate (DEF) and PPF demonstrating a range

of pore sizes from 150-800 μm and porosity up to 90 percent[32]. Laser stereolithography has also been used to create scaffolds with PEG diacrylate[31].

2.1.4.4 Fused Deposition Modeling

Fused deposition modeling is a technique where the polymer is deposited in thin layers on a base which solidifies attaching to the previous layer[40]. Initially this technique was only used with non-resorbable materials but has recently be expanded to PCL and PCL/Hyaluronic acid scaffolds[33-35,40]. As with the other computer techniques, this process is highly reproducible. Fused deposition modeling also supports incorporation of pores into the scaffold affecting mechanical strength and molecule diffusion.

2.2 Synthetic Polymers for Scaffolds

The molecular structure and properties of synthetic polymers can be designed for specific applications, such as to support cell and tissue processes for engineered bone. This is perhaps an advantage over natural polymers whose modification is often less precise due to their variable molecular structure. Synthetic polymers are most often present in a semicrystalline or an amorphous state. A semicrystalline polymer contains dense chain regions randomly distributed throughout the material. These regions act as physical crosslinks and contribute to the mechanical strength of the polymer network. Amorphous polymers act similar to rubber above their glass transition temperature and analogous to glass below. The structure of amorphous polymers can be altered by chemical bonding, copolymerization, physical mixing, or

blending[41]. In their unmodified form, synthetic polymers lack biomolecules that are present in some natural polymers that can aid in cell attachment. Advances have been made to modify synthetic polymer surfaces with biomolecules and therefore stimulate cell attachment and proliferation[42]. Common synthetic polymers include polyesters, polyanhydrides, polyphosphazenes, polycarbonates and poly(ethylene glycol).

2.2.1 Polyesters

2.2.1.1 Poly(D,L-lactic acid-co-glycolic acid)

Poly (D,L-lactic acid-co-glycolic acid) (PLGA), is a copolymer of poly(lactic acid) (PLA) and poly(glycolic acid) (PGA), and has distinct properties from the two homopolymers[22]. For example, PGA and PLA are semicrystalline polymers while PLGA is amorphous, and therefore a solid, non-crystalline structure. Furthermore, PGA degrades slowly while PLGA can degrade rapidly[6,19,43,44]. When using comonomers, their ratio can be varied to achieve different mechanical, physical and degradation properties[25]. Degradation times have been shown to vary from six to twelve months with a monomer ratio of 85/15 to one to two months with a 50/50 ratio, demonstrating the ability of this polymer to be engineered for an appropriate degradation rate[41]. PLGA is also known to degrade via bulk degradation (see Biodegradation Section below) due to its ester linkages, affecting its mechanical properties as it degrades[41]. The degradation products include glycolic acid and lactic acid, both which are present in the body and can be removed naturally through metabolic pathways[21,22,25].

The ability to engineer PLGA properties has caused it to be of great interest for tissue engineering applications and has been found to support a variety of cell types. Osteoblasts have been shown to attach to PLGA[45,46]. Furthermore, extracellular matrix components such as osteopontin and osteonectin, known markers for osteogenic differentiation, were produced and present in abundant concentrations in addition to collagen, fibronectin, vitronectin and laminin[46]. The presence of these components is important to simulate the mature extracellular environment that osteoblasts require.

2.2.1.2 Poly(ε-caprolactone)

Poly(ε-caprolactone) (PCL) is an aliphatic polyester with a repeating molecular structure of five nonpolar methylene groups and a single polar ester group[6]. A semicrystalline polymer, PCL has a melting point of approximately 60°C and is formed by the ring-opening polymerization of ε-capolactone [6]. PCL is known to be highly water soluble and degrades by hydrolytic mechanism at physiologic conditions[47]. Degradation occurs by bulk or surface mechanism into the byproduct caproic acid. This acidic byproduct can affect the local environment of the scaffold and therefore degradation rate and byproduct concentration should be kept to a low level[6]. PCL is known to degrade very slowly and has a degradation time of approximately two years[6]. To modify the degradation rate and make it more appropriate for certain tissue engineering applications, PCL has been copolymerized with collagen, PGA, PLA and PEG[48-50]. In addition, PCL may have the ability to

support load-bearing applications and can maintain mechanical strength for an extended period of time[44].

PCL has been used as a scaffold to support osteoblast growth. A porous PCL scaffold facilitated osteoblast production of alkaline phosphatase, a known marker of bone mineralization, and attachment and proliferation of osteoblasts[51]. It has also been combined with hyaluronic acid to improve the compressive strength associated with the polymer and thus enhance its application in bone tissue engineering[51].

2.2.1.3 Poly(propylene fumarate)

Poly(propylene fumarate) (PPF) is an aliphatic linear polyester composed of repeating units of two ester groups and one central unsaturated carbon-carbon double bond[52]. The polymer degrades by hydrolysis of an ester bond into degradation products of fumaric acid and propylene glycol[52]. These byproducts have been shown to cause mild and short inflammation suggesting that it is a biocompatible polymer[52]. PPF's double bonds allow it to be covalently crosslinked. This ability of crosslinking in response to a trigger allows scaffold fabrication *in situ*, therefore acting as an injectable biomaterial[53]. In addition, the cured form of PPF has demonstrated significant compressive and tensile strength and is a possible scaffold material for bone tissue engineering[53].

PPF has been investigated for a number of different applications in bone tissue engineering. PPF scaffolds with varying porosities and pore sizes were investigated to analyze tissue response in cranial defects. In all cases the scaffolds only induced a mild tissue response and allowed for vascularization of the area[54]. In addition, PPF

scaffolds coated with transforming growth factor-β1 induced significant bone formation in cranial defects[42].

2.2.1.4 Polyorthoester

Polyorthoesters (POEs) are a family of bioerodible polymers[55]. They are formed through a reaction of ketene acetals with hydroxy-containing molecules, such as diols[56]. POEs are hydrophobic substances and undergo surface degradation[56,57]. However, properties of POEs can be modified through copolymerization. For example, degradation of the polymer can be adjusted to an appropriate rate by incorporating short acid groups such as glycolic or lactic acid[57,58]. In addition, the orthoester linkages present within POEs have been found to be more susceptible to hydrolytic cleavage in acids than bases demonstrating another method of degradation control[41,47].

POE polymers are desirable for bone tissue engineering because they degrade by surface degradation and maintain mechanical stability. Therefore, they can be used in load bearing applications while the host tissue is reforming. Scaffolds constructed of POEs were implanted into calvarial defects and analyzed for bone regrowth and demonstrated promotion of new bone formation[58].

2.2.2 Other Synthetic Polymers

2.2.2.1 Polyanhydrides

Polyanhydrides have a polymer backbone containing an anhydride bond[59]. They contain bonds which easily react with water causing degradation via surface

erosion[60]. Polyanhydrides are synthesized by a dehydration reaction of diacids, and degrade into these non-toxic diacid monomers which are removed from the body within weeks to months[59]. Polyanhydride degradation rate can be modified by changing the monomer concentrations: increasing hydrophobicity decreases degradation rate. For example, polyanhydrides synthesized with carboxyphenoxypropane degrade over a period of 3-4 years. However, when synthesized with 79% sebacic acid the construct degrades over two weeks[60]. Furthermore, polyanhydride synthesis can be activated by a trigger such as photocrosslinking and therefore can be cured *in situ* [61,62].

Polyanhydrides have initially been studied as a method for controlled release of bioactive molecules[59,63]. They tend to have limited mechanical stability and therefore may not be appropriate for load bearing applications involved in most bone tissue engineering. However, research on polyanhydrides led to incorporation of imides into crosslinkable networks[44,64]. This increases the mechanical stability of the construct and it is thought that the strength is related to the rigidity of the aromatic imide group[64]. Specifically, scaffolds containing succinic acid have shown compressive strengths of 50-60 MPa and were degraded by hydrolysis of the anhydride bonds then imide bonds[63,64]. In addition, photocrosslinking has been used to increase mechanical properties of the polymer[61,65,66].

2.2.2.2 Polyphosphazene

Polyphosphazene contains a backbone composed of alternating nitrogen and phosphorous atoms with two side groups attached to each atom[67]. Polyphosphazene

is hydrophobic and degrades by surface degradation into phosphate and ammonium salt byproducts. Variation in polyphosphazene constructs can be achieved by adding different hydrolytically labile substituents to the phosphorous atoms[68]. The degradation rate of phosphazenes are unable to be altered significantly and generally degrade slowly *in vivo*[68].

Polyphosphazenes have been investigated for a number of different tissue engineering applications because of their ability to be highly modified. Their slow degradation rate makes them of interest for long term controlled release devices[68]. It has also been applied as a material for orthopaedic uses due to its high strength and surface degradation properties[69]. Osteoblast cells have been seeded on three-dimensional polyphosphazene scaffolds and shown to support proliferation and skeletal tissue formation[70].

2.2.2.3 Polycarbonate

Tyrosine-derived polycarbonate (P(DTR carbonate)) is an amorphous polycarbonate, and is modifiable due to the presence of alkyl ester pendant groups located within its linear chain[71]. P(DTR carbonate) structure contains three bonds that can be hydrolytically degraded: amide, carbonate, and ester[71]. Carbonate bonds have been found to degrade faster than the ester bonds, and the amide bond is stable to hydrolysis at physiological temperature[71,72]. The ester bond is known to degrade into carboxylic acid and alcohol while the carbonate bond byproducts include two alcohols and carbon dioxide[71]. P(DTR carbonate) is suggested to be a biocompatible

material because it is based on the natural amino acid tyrosine and degrades mostly into non-acidic byproducts[73].

P(DTR carbonate) can be modified to degrade over months or years[73]. It has been investigated as a bone scaffold and shown to elicit a response of bone ingrowth at the bone-polymer interface[73]. In addition, research has demonstrated the ability of osteoblast cells to attach onto the surface of P(DTR carbonate) and maintain their phenotype[74]. Other investigations with poly(deasminotyrosyl-tyrosine ethyl ester carbonate) (poly(DTE carbonate)) have demonstrated that bone ingrowth occurs in cranial defects and that the patterns of bone formation mimicked the morphology of the scaffold[75]. This suggests that polycarbonate scaffolds can be designed to reflect the morphology of different bone tissue and therefore induce growth appropriate to the location. Further studies with poly(DTE carbonate) show that it elicits more direct bone apposition when compared with other polycarbonates, and it is thought to occur due to the ethyl ester pendant group in the polymer[76]. The hydrolysis of these groups produces calcium chelation sites on the polymer surface which appear to be related to polymer-bone bonding[76].

2.2.2.4 Poly(ethylene glycol)

Poly(ethylene glycol) (PEG) is a linear-chained polymer with an oxygen-carbon-carbon repeating unit. The number of units can be varied, which changes the length and molecular weight of the polymer[4,77]. PEG homopolymer is non-degradable, however it can be copolymerized with degradable polymers to allow degradation[78]. PEG is highly water soluble due to the oxygen molecule present in the polymer

backbone. Copolymerization of PEG with other materials causes an increase in hydrophilicity of the subsequent material. This property has led to investigation of its ability to function as a hydrogel. However, linear PEG chains are susceptible to rapid diffusion and also low mechanical stability[79]. Networks of PEG can be formed by attaching functional groups to the ends of PEG chains and initiating their crosslinking[80-82].

PEG has low mechanical stability and is therefore not often used in bone tissue engineering for load bearing applications. However, its ability to be crosslinked into a network with other synthetic materials and affect degradation of those materials makes it attractive as a copolymer. It can be copolymerized with various polymers to engineer a construct with controlled erosion methods and degradation rates. PEG was copolymerized with poly(lactic acid), combined with a hydroxyapatite ceramic, and used to deliver bone morphogenetic protein and demonstrated complete repair of bone defects[83]. Similarly, PEG was combined with PLA and p-dioxanone and used to deliver bone morphogenetic protein where it exhibited osteoconductive capacity[84]. PEG hydrogels have also been modified with cell adhesion peptides and used in tissue engineering. These gels delivered growth factors, resulting in efficient and highly localized bone regeneration[85]. In addition, PEG has been copolymerized with PLGA to form a foam to deliver periosteal cells *in vivo* supporting osteochondral repair[86].

2.3 Scaffold Design Properties

Scaffold properties can be modified to mimic the mature tissue that is being regenerated, or engineered to induce ingrowth and proliferation of cells. Properties that can be altered are discussed below and include: surface properties, macrostructure, mechanical properties, biodegradation, and biocompatibility.

2.3.1 Surface Properties

The majority of cell types used in bone tissue engineering are anchorage dependant and thus the engineered scaffold should facilitate cell attachment. The surface of the scaffold is the initial and primary interaction site to the surrounding tissue. Therefore, tissue engineering strategies favor scaffolds that cells attach to abundantly and easily, making scaffolds with large accessible surface areas more favorable. In addition, the surface of the scaffold should support cell proliferation. It has been shown that strong cell adhesion promotes cell proliferation while a rounded morphology demonstrates their differentiation[43]. A highly wettable surface is present on hydrophilic polymers and this allows cells to be encapsulated through capillary action[87]. However, the most significant surface property of polymers is the ability to provide an environment for scaffold-host interaction. Many natural polymers have the innate ability to facilitate attachment because they can contain a number of functional groups that vary in polarity, electrostatic charge, hydrophobicity, and the ability to interact via van der Waal's forces. In addition, natural polymer chemistry uses covalent and non-covalent assembly which can be varied and precisely controlled with association constants[88]. A strategy for synthetic

polymers in tissue engineering is to mimic these natural polymer characteristics. Advances in polymer synthesis now allow for control of the polymer and side-chain architecture. This enables inclusion of functional groups at the surface in addition to within the material. The surface of the polymer can therefore be modified with short peptide sequences or long protein chains to promote interaction with the surrounding tissue[89]. Specifically, ligands that are common in the extracellular matrix such as, fibronectin, vitronectin, and laminin have been used as surface molecules[89]. This surface modification technique is being widely investigated for tissue engineering applications[88-90].

2.3.2 Macrostructure

A highly porous scaffold allows cells to integrate into the porous void space. In addition, the porous nature of the scaffold is important for diffusion of nutrients and waste removal. In general, it is advantageous for the scaffold to have a high surface area to volume ratio, which promotes small diameter pores that are larger than the diameter of the cell. However, high porosity scaffolds are associated with poor mechanical integrity. Engineering these properties to allow for appropriate diffusion and mechanical strength are important challenges in the construction of bone tissue engineering scaffolds. Fiber meshes, foam scaffolds, and hydrogels demonstrate the varying polymer macrostructure of foams possible for bone tissue engineering applications.

Fiber meshes are formed into three-dimensional structures by knitting or weaving individual polymer fibers. They are advantageous for tissue engineering because they

provide a large surface area to promote cell attachment[6]. In addition fiber mesh scaffolds are similar to the structure of the extracellular matrix allowing for nutrient diffusion and waste removal. These scaffolds tend to have low mechanical integrity, however fiber bonding has been used to create a more stable structure[7].

Foam scaffolds act as a three-dimensional structure for cell integration. These scaffolds are generally prefabricated before implantation. Similar to fiber meshes, the structure of foam scaffolds allow for sufficient nutrient diffusion and waste removal. However, foams tend to be more mechanically stable than fiber meshes, but still lack strong mechanical integrity. Porosity and pore structure can be modified by using different processing techniques such as, solvent-casting particulate leaching, melt molding, freeze drying and gas foaming.

Hydrogels are formed from hydrophilic polymers by physical polymer entanglements or crosslinking[4,91]. The hydrophilic polymers are able to absorb large quantities of water, up to a thousand times their own dry weight[91]. The aqueous environment created in hydrogels simulates *in vivo* environments and therefore are an ideal setting for cell encapsulation. In addition, the aqueous environment supports quick diffusion of nutrients, proteins, and waste, thus promoting cell growth and proliferation. Some hydrogels, including PEG based hydrogels, are easily injectable and capable of being molded, allowing minimally invasive implantation[92]. Disadvantages of hydrogels include lack of strong mechanical stability and sterilization difficulty[91,92].

2.3.3 Mechanical Properties

The ability of a scaffold to provide the necessary mechanical support is a critical component of the construct. However, the relatively strong mechanical strength of bone, compared to other tissues, presents challenges to tissue engineers. Mechanically, compact bone acts as a semibrittle, viscoelastic and orientation dependant material[93]. In the longitudinal orientation, a range of strengths has been reported for compact bone reported of 78.8 to 151 MPa and 131 to 224 MPa for tension and compression, respectively[94]. The elastic moduli for compact bone has been demonstrated to be 17.0 to 20.0 GPa in the longitudinal direction with a shear modulus of 3.30 GPa and a structural density of 1.80 g/cm^3[94]. In contrast to compact bone, cancellous bone is spongy and highly porous with a structural density of 0.20 g/cm^3. In general, cancellous bone is oriented along the principal stress directions due to the external loading environment[93]. The strength of cancellous bone is based upon its apparent density and has values of 2.00 to 5.00 MPa and 90.0 to 400 MPa for strength and modulus, respectively[95].

For proper tissue regeneration without significant deformation, it has been suggested a scaffold should provide a mechanical modulus of 10-1,500 MPa for hard tissues and 0.4 to 350 MPa for soft tissues[96]. Mechanical requirements are therefore very important for orthopaedic hard tissues and dictate the fabrication method of the polymer. For example, it is suggested that fabrication with particulate leaching and gas foaming have a maximum compressive moduli of 0.4 MPa and therefore are not appropriate for scaffolds to be implanted for hard tissue regeneration[96]. The lack of mechanical stability associated with many of the conventional fabrication techniques

emphasizes the utility of rapid prototyping techniques for bone tissue engineered scaffolds. These precise methods of fabrication have the capability of creating scaffolds with significant mechanical stability.

Finally, scaffolds should provide interim support while the tissue regenerates. It is important that the material does not degrade before the tissue can provide sufficient load-bearing support for the area and stress dissipation. There are two common scaffold design properties to support bone ingrowth with proper mechanical support. One strategy is for the physical scaffold to provide mechanical support for the polymer/cell/tissue construct from initial seeding to remodeling by the host[97]. Therefore, the scaffold matrix must provide sufficient mechanical support to withstand *in vivo* stresses and loading. The other strategy imposes transitional support. Here the scaffold provides mechanical support while cells proliferate and differentiate *in vitro*[97]. Once implanted, the scaffold is designed to degrade at the same rate as the cells produce the extracellular matrix for support.

2.3.4 Biodegradation

The majority of tissue engineering scaffolds are designed to degrade so that when the tissue is completely formed, the scaffold should be wholly degraded. For synthetic polymers, degradation occurs primarily by chemical hydrolysis of hydrolytically unstable polymer backbones[41]. The polymer can also be designed to degrade enzymatically relying on catalysts present in the surrounding environment or embedded within the scaffold. Degradation can alter the mechanical properties of the construct, which subsequently can affect the effectiveness of the implant. In addition,

the degradation products can modify the local environment of the implant. This is dependant on the biocompatibility of the degradation products and whether they are harmful to the surrounding tissue. Both of these properties are dependant on the structure, components, and fabrication techniques of the material and how it degrades over time. In addition, degradation is dependant on the location and geometry of the implant as well as the presence of catalysts, impurities and other additives[41].

Hydrolysis of the polymer backbone occurs in two phases[41]. First, water penetrates in the bulk of the polymer converting the long chains into shorter water-soluble degradation products by attacking the chemical bonds in the amorphous phase. Next, the fragments are enzymatically degraded causing a rapid decrease in polymer mass. These two phases are part of two overall mechanisms of degradation.

In addition to the characteristics of polymer degradation, overall scaffold degradation has been well described in literature. Polymeric scaffolds undergo bulk, or surface degradation, or a combination of both. In bulk degradation, the erosion at the surface is slower than in the interior[41]. Initially the surface begins to degrade when the construct is in contact with water, then as water penetrates to the inside of the material, the bulk of the scaffold begins to degrade. Bulk degradation is associated with a decrease in mass while the volume of the construct stays the same, which causes a decrease in density and as a result, mechanical strength.

One concern with bulk degradation is a phenomena known as the autocatalytic effect[98]. This often occurs with synthetic polymers whose degradation products are acidic. When degradation occurs the interior degradation products are unable to diffuse through the polymer network and cause a local increase in acidity. This

elevated acidic environment causes a rapid increase in degradation by catalyzing hydrolysis of labile linkages.

Surface degradation of a scaffold is similar to the dissolution of soap. In this mechanism, the rate at which the material degrades at the surface is constant. As the size of the construct decreases or thins over time, the bulk integrity and structure is maintained. This mechanism is common with polyanhydrides and polyorthoesters. These materials are hydrophobic, but highly susceptible to hydrolysis and degrade at the surface. As the material degrades the size of the construct decreases as mass is loss allowing for constant density. This property allows the polymer to maintain mechanical integrity, which can be critical for bone tissue engineering applications.

The preferable method of degradation varies between tissue engineering uses, the host tissue, and mechanical integrity requirements. The speed at which a scaffold degrades can be engineered by varying the polymer properties. For example, more hydrophilic monomers and acidic end groups, more hydrolytically reactive backbone, less crystallinity, and smaller device size all tend to increase the degradation rate of the material[41]. The location of the implant can also affect the speed of degradation. A poorly vascularized area with low diffusion will not be able to remove degradation products as quickly causing an increase in acidity, similar to the interior of the scaffold during bulk degradation, and an overall increase in degradation rate. All of these factors are important in engineering an appropriate rate and method for degradation specific to the tissue of interest.

2.3.5 Biocompatibility

All implanted materials elicit a reaction from the host, but materials vary in the degree of response produced. Reactions to injury include inflammation, wound healing, and foreign body responses[99]. A material may be considered to be biocompatible if it produces minimal inflammatory and immune response, and is able to function properly without significant harm to the host. The goal of designing a material for implantation is to minimize the magnitude of the response and its duration.

The response to an implanted scaffold can be divided into three phases[99]. Phase one occurs during the first one to two weeks after implantation and includes acute and chronic inflammatory responses. Acute inflammation is short and generally lasts minutes to days and is dependant on the extent of the injury[100]. Chronic inflammation is due to long-term presence of inflammatory stimuli and is confined to the implant site. In general, the phase one response is independent of the degradation rate of the polymer[99]. Initiation of phase two response occurs with an increase in monocytes and macrophages. In addition, phase two includes the initiation of fibrous encapsulation of the foreign material. In contrast to phase one, the length of phase two is a function of the rate of biodegradation of the scaffold[99]. Fibrous encapsulation continues in phase three. The length of the phase is dependant on the degradation rate of the polymer. Slowly degrading polymers have been shown to have a phase three response lasting several weeks to months and the phase three response of rapidly degrading polymers can be as short as one to two weeks[99].

The immune response has a direct effect on bone tissue engineering. Specifically, degradation products are thought to be the cause of failure in many orthopaedic implants[101]. These degradation particles can be phagocytosed by macrophages when less than 20 μm in diameter[101]. It is thought that these particles indirectly affect bone cells through the secretory products of macrophages drawn to the area from the immune response[101]. Studies have shown that microparticles of PLLA and PLGA suppress osteoblast differentiation early in culture[101]. Others suggest that degradation particles directly interact with osteoblasts and affect their proliferation[102]. In addition, dense fibrous capsule formation composed of macrophages and foreign body giant cells have formed in response to PLLA bone plates and screws[103]. Clearly biomaterial properties significantly affect the magnitude and duration of the host response. Characteristics of the material that can alter the immune response include the size, shape, and chemical and physical properties[99]. Finally, when designing a biomaterial one must consider not only consider the initial properties of the scaffold but also the degradation products and their effect on the host.

2.4 Summary

Scaffold design is an intricate process and must be tailored for different bone tissue engineering applications. Scaffolds must be able to induce growth, support cell adhesion and proliferation, and provide mechanical stability as necessary for different locations. Synthetic polymers can be easily modified to provide appropriate properties for bone tissue engineering. The properties are affected by the fabrication

method: both conventional and rapid-prototyping techniques have successfully produced viable bone tissue engineering scaffolds. Fundamental design parameters are dependant of the needs of the regenerated tissue and include polymer assembly, curing methods, surface properties, macrostructure, mechanical properties, biodegradation and biocompatibility.

Chapter 3: Regeneration of Orbital Floor Bone

Orbital floor fractures are a common form of craniofacial trauma and can result in significant functional limitation. In addition, the floor is the orbital wall most likely involved in orbital trauma. The thin bone of the orbital floor and the adjacent dead space of the maxillary sinus are not conducive to proper healing sometimes resulting in poor function and facial aesthetics; therefore a clinical intervention is often necessary. Current clinical treatments have associated disadvantages, increasing the need for the development of an ideal implant.

3.1 Orbital Bone Development and Anatomy

The orbital region is central to the functional success and aesthetic features of the facial skeleton.[104] Initially the ocular globes, as the growth center, grow rapidly causing an increase in the orbits. The growth of this bony structure is 85% complete by 5 years and is finalized between seven years of age and puberty.[105,106]

The main purpose of the floor is to support the globe and separate the orbital contents from the maxillary sinus; it is therefore very thin, approximately 0.5 mm.[105,107] It is composed of portions of three bones, the maxilla, zygomatic, and palantine.[107,108] The floor is not completely horizontal, but has a slight convex curve where the posteromedial section is higher than the flatter anterolateral area.[108] The orbital floor is also lined on the ocular side by periosteum.[105,109] In addition, when compared to the other orbital walls, the orbital floor demonstrates the highest degree

of deformation with static loading, possibly explaining the high number of orbital fractures associated with blunt trauma.[107]

3.2 Orbital Floor Injuries and Mechanisms

Orbital floor injuries, most commonly caused by assault and traffic accidents, can be a devastating form of craniofacial trauma.[110,111] Studies have shown that the floor is the wall most frequently involved in orbital trauma accounting for approximately 60-70% of all orbital fractures.[112,113](See Figure 1) As the floor is continuous with the thin medial wall, it may also act as a natural crumple zone and be involved in significant orbital traumas.

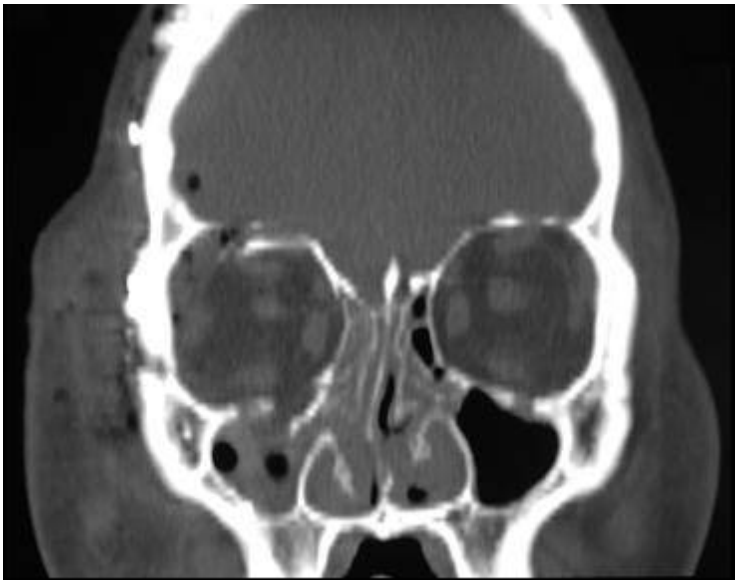

Figure 1: CT Scan of an orbital floor fracture. (An orbital roof fracture is also present)
Image courtesy of Dr. Domenick Coletti

If left untreated, orbital floor fractures might not provide adequate support to the globe through standard primary and secondary bone healing mechanisms. The

thin bone fragments often paired with injured periosteum and disrupted blood supply provides a poor conduit for bone healing. Furthermore there is generally insufficient contact with surrounding bony edges to conduct bone formation which leads to fibrous scar formation. This change in orbital architecture provides inadequate globe support and increased orbital volume, and as a result, altered globe function. Therefore, the endogenous response to orbital fractures, in contrast to many other bone fractures, is not sufficient for proper healing.

The majority of orbital floor injuries occur from trauma, and there are two main biomechanical mechanisms proposed to explain how orbital floor defects occur. The hydraulic theory suggests that force applied to the globe results in increased intraorbital hydraulic pressure and transmission of this pressure to the walls of the orbit results in the fracture at the weakest point, which is generally the thin orbital floor.[107,114,115] The buckling theory offers that trauma to the infraorbital rim transmits force directly to the orbital floor, causing disruption of the bone without fracture of the rim and displacement of orbital contents.[107,114,115]

3.3 Current Clinical Solutions

To treat a clinically significant orbital floor fracture, it is critical to restore the orbit to its original volume in order to ensure proper globe function.[107] During surgery the herniated orbital tissues are repositioned into the orbit and an implant is used to span the defect in the floor to prevent reherniation.[116] There are a wide variety of implants available, each associated with very specific advantages and disadvantages; however, literature suggests that ophthalmologists tend towards using

alloplastic implants while plastic and craniofacial surgeons tend towards using autologous materials.[111,116] The decision for which type of implant should take into consideration the size and shape of the defect, the presence or absence of peripheral bony ledges, the age of the patient, donor site issues, and to a degree, patient preferences.

There are a number of alloplastic implants that are currently in clinical use. Frequently used materials include Medpor (high-density polypropylene), poly(L-lactic acid) or poly(glycolic acid), and titanium (See Figure 2).[107,111,117] The benefits of using alloplastic implants include their ease of availability, they can be adapted to fractures of any defect shape before use, and they are reasonably priced.[111,116] However, these implants are foreign bodies and following implantation, these relatively inert alloplastic materials develop a fibrous capsule.[116] Other complications have been described with these implants including infection, implant migration or extrusion, extraocular muscle entrapment, cyst formation, residual diploplia, globe elevation, and visual loss.[111,116,118] Treatment then involves additional surgery including removing or re-exploring and repositioning the implant.[111,116]

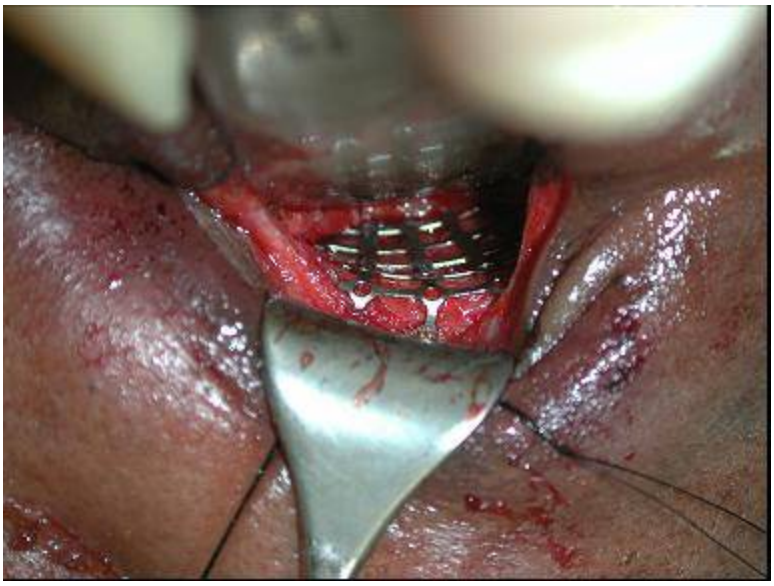

Figure 2: Orbital repair with titanium mesh. *Image Courtesy of Dr. Domenick Coletti.*

Autologous grafts are frequently used for the repair of orbital floor defects, and a number of donor sites have been employed such as iliac crest, ribs, calvaria, maxillary bone, the outer cortex of the mandible, and also cartilage donor sites have been described.[111,119-122] The advantages to using autologous grafts include good graft stability, reduced implant associated costs, and limited adverse reactions.[111] However, there are a number of associated disadvantages such as, morbidity of the donor site, increase in surgical time, limited availability, unpredictable resorption, adaptability, and the modeling properties of the graft.[111,118] In addition, there may be significant risk to the donor site. Furthermore, it is vital that the orbit is restored to its original volume to promote proper function and aesthetics. There are a number of variables that account for volume maintenance including position (inlay versus onlay), membranous or endochondral, cancellous or cortical, mechanical stress, recipient site, method of fixation, graft orientation, presence or absence of the

periosteum, and rate of vascularization.[123] However, grafts harvested from calvarial and facial sites tend to resorb less than those from rib, tibia, or iliac crest which is important to consider when choosing a donor site.[123]

Other grafts that have been used in the past, or are currently in use, however they are less common. Allogenic implants, such as lyophilized dura mater was successfully used until cases involving disease transmission were reported.[111] New sterilization techniques have shown promise with dura mater implants, however it is only appropriate for use with small to moderate-sized defects, and long-term outcome studies have not yet been completed.[118] In addition, solvent preserved cadaveric calvarial bone grafts have been used with some success.[104] These grafts showed implant vascularization and tissue ingrowth, however studies showing the effects of solvent treatment on graft survival are limited and long term effects of these implants still need to be studied.[104] Other graft types including xenografts, specifically swine bone cortex, show good integration into the surrounding tissue, however they do not have good modeling properties.[111]

3.4 Sequelae

The endogenous response to bone healing is not adequate for proper regrowth of the orbital floor causing a number of associated problems. In addition, the current clinical solutions are not without their share of disadvantages. Therefore there are a number of general sequelae that are associated with orbital floor injuries, with the two most frequent complications being enophthalmos and diploplia.[108,124] Enophthalmos is defined as recession of the globe into the orbit when compared to the contralateral

globe, and this is readily visible at greater than 3 mm.[111] Enophthalmos is thought to be caused by changes in orbital volume, destruction of restraining ligaments, fat atrophy, and remodeling of the soft tissues into a more round shape.[104,108,111,124] Diplopia (double vision) is thought to be caused from extraocular muscle dysfunction; specifically, entrapment, ischemia, hemorrhage, or nerve injury.[125] Other common sequelae include decreased sensation on the injured side of the face (in the distribution area of the infraorbital nerve) and this is shown to be present in more than half of cases in recovery studies.[112,124,125] In addition, unsatisfactory facial aesthetics have been associated with orbital floor fractures.[112] Proper treatment alleviates sequelae by supporting the orbital contents, preventing soft tissue fibrosis, and restoring continuity of the orbital floor.[111]

3.5 Tissue Engineering Approach

In order to create an improved orbital floor implant tissue engineering has been explored. In bone tissue engineering, cells act as the osteogenic stimulation to form new bone.[123] In contrast, specific growth factors and cytokines can act as the osteoinductive stimulation, which recruit and induce osteoprogenitor cells to grow into mature bone tissue through chemotaxis, mitosis, and differentiation.[123] Finally, a scaffold acts as an osteoconductive medium where the scaffold serves as a surface on which the cells can attach, migrate, grow, divide, and new blood vessels can invade.[123]

The scaffold should provide enough structural support for the globe and associated tissues for orbital floor repair. In addition, it should return the orbit to the

original orbital volume to decrease the likelihood of enophthalmos.[107] Also, the implant should degrade as the tissue grows. Furthermore, it should only elicit a moderate immune response and not induce fibrous encapsulation. Lastly, it should be easy to work with, easily molded and shaped to the floor defect, and easily placeable. A scaffold that has all of these properties would be the optimal device for orbital floor repair.

3.5.1 Cell Source

In order to regenerate bone tissue an appropriate cell population needs to be delivered or recruited to the injured area. A number of cell types have been used in craniofacial tissue engineering with success; however, the most widely investigated are mesenchymal stem cells (MSCs).

During natural injuries such as bone fractures, MSCs are recruited to the area and differentiate into osteoblasts through a number of environmental cues.[126] MSCs have the ability to replicate as undifferentiated cells and also the potential to differentiate into a number of lineages such as bone, cartilage, adipose, tendon, ligament, and marrow stroma.[127,128] However, in order to be induced down the osteogenic differentiation pathway, a sufficient and appropriate amount of extracellular signals must be available.[126]

MSCs are capable of proliferating *in vitro* allowing large numbers of cells to be cultured from a small harvest amounts.[129] Furthermore, studies have demonstrated that transplanted allogenic MSCs did not elicit a significant immune

response.[129] Lastly, stem cells have been shown to withstand low-oxygen conditions, which may be present following transplantation.[129] The ease of isolation and capacity to be induced down the osteogenic differentiation pathway make MSCs an ideal cell type for bone tissue engineering.[130-132]

3.5.2 Signals

Bone morphogenetic proteins (BMPs) are members of the TGF-β superfamily and are known to be secreted signaling molecules.[133,134] BMPs are present at different periods of growth: the early stages of embryogenesis, during the organogenesis phase and growth period, and in adults during fracture repair.[133,135] Currently, 16 BMPs have been identified, and the most widely investigated for bone tissue engineering are BMP-2, 4, and 7 (also known as osteogenic protein-1).[136-141] BMP-2 and BMP-7 are currently the only BMPs with recombinant human products developed for clinical applications[129,138,142].

The family of BMPs is known to induce formation of cartilage, bone, and other like tissues of the skeleton through recruitment, commitment, and differentiation of osteoprogenitor cells.[133,141] Specifically, BMP-2 through 7 and BMP-9 have demonstrated the ability to induce the differentiation of mesenchymal stem cells into osteoblasts.[138] Furthermore, BMP-2 and 7 have both shown to have chemotactic effects on osteoblasts and osteoprogenitor cells.[143] In addition, BMP-2 is known to induce mesenchymal stem cell chemotaxis, proliferation, and differentiation.[144]

As related to orbital defects, many studies have demonstrated the use of BMPs in increasing bone formation in maxillofacial defects.[136] In addition, when implanted in a defect, BMP-2 has demonstrated induction throughout the defects and bony healing.[133] It has been shown that the amount of BMP required is small relative to the volume of bone it is capable of producing.[133] However, a kilogram of bone contains only a few micrograms of BMPs, but milligram doses have been shown to be required for efficacy in human models.[145]

Other growth factors are being investigated for use in bone tissue engineering including: transforming growth factor-β (TGF-β), insulin like growth factor I (IGF-I), fibroblast growth factor (FGF), and platelet derived growth factor (PDGF).[126,139,140,146,147] Together, these growth factors aid at the target site by increasing mesenchymal stem cells and osteoprogenitor cells to enhance bone formation and participate in the regulation of bone-specific genes responsible for maintaining the osteoblastic phenotype and mineralization.[140,147] Furthermore, they can induce increased expression of the osteoblast phenotype including extracellular matrix molecules.[140] Specifically, TGF-β_1 is thought to increase differentiation and proliferation in osteoblasts, in addition to aid in increased bone formation in animals.[126] Furthermore, TGF-β_1 has been shown to play a role in bone graft incorporation.[148] IGF-I has demonstrated a chemotactic effect while increasing proliferation and differentiation of osteoblasts.[126,148] IGF-I is produced by osteoblasts and retained in the extracellular matrix.[147] Here it has been shown to promote proliferation and synthesis of type I collagen, and decrease collagenase synthesis to maintain collagen in bone microenvironments.[147] Furthermore, IGF-I is

known to activate osteocalcin expression, a marker for mature bone.[147] FGF has shown the ability to induce mesenchymal cell mitogenesis, and increase proliferation of osteoblasts.[126,139] However, it is thought to slow the differentiation of osteoprogenitors.[126] Additional studies have shown that FGF levels are increased during early stages of fracture healing, and that FGF upregulates osteocalcin expression.[147] PDGF is known to increase proliferation of osteoblasts.[126,148] In addition, it may also aid in recruiting bone cells during remodeling and repair.[148]

While there has been significant progress made in the field of bone tissue engineering with the use of growth factors, there are a number of concerns to working with these proteins. Specifically, a number of the growth factors have a very short biological half-life, which may be as short as 2 minutes.[146] This causes increased concern for the tissue engineer and the ability to deliver the appropriate dose to the target area. Furthermore, BMPs are known to be osteoconductive with a dose-response ratio and act locally.[138] Therefore, it is important to supply above a threshold level of BMP at the target site to induce bone formation. Thus far, in clinical settings rhBMPs have been used at concentrations 10 to 1000 fold higher than those of native BMPs.[138] In order to deliver BMPs, and ideally reduce the amount of BMP needed, it should be combined with a matrix to allow for slow release and area retention. When combined with a matrix, the BMP-matrix system allows for cell infiltration, retention of BMP at the site, and a substrate for cell growth and differentiation.[133] All of these concerns highlight the importance of an adequate delivery system for these growth factors to work. This is involved with the design of

the scaffold and the ability of the construct to the deliver the growth factor at a therapeutic level and rate.

3.5.3 Scaffold

Scaffold design is critical to the success of a tissue engineered construct. In orbital bone tissue engineering, scaffolds act as a temporary framework for cells to grow and produce new matrix and functional tissue. As the target tissue is regenerated, the scaffold should degrade to allow space for the new tissue to grow. There are several parameters involved in scaffold design, including polymer composition, biodegradation, biocompatibility, and mechanical strength.

Many strategies have been developed for bone tissue engineering using natural and synthetic polymers. Natural polymers may be advantageous because they are often biocompatible and easily degraded by the body. However, natural polymers tend to have a variable molecular structure. In addition, they generally do not possess adequate mechanical integrity. Synthetic materials have been widely investigated due to their reproducibility in the lab. In addition, these materials can be modified to have desired properties including mechanical stiffness and degradation by tailoring the fabrication methods. Furthermore, during synthesis, various bioactive molecules can be incorporated into the scaffolds through a number of techniques.

Many of the cells involved in bone tissue engineering are anchorage dependant, and therefore the scaffold should be engineered to aid in cell attachment. Scaffolds that have large accessible surface areas are generally more favorable as

cells can attach more easily. Furthermore, the surface has to be carefully designed as to how strongly cells attach. Studies have shown that strong cell adhesion promotes cell proliferation while a rounded morphology demonstrates their differentiation.[43] However, the most significant surface property of polymers is the ability to provide an environment for scaffold-host interaction. Advances in polymer synthesis allow for control of the polymer and side-chain architecture. This enables inclusion of functional groups at the surface in addition to within the material. The surface of the polymer can therefore be modified with short peptide sequences or long protein chains to promote interaction with the surrounding tissue.[89]

The scaffold macrostructure design is important to the success of a tissue construct as a highly porous scaffold allows cells to integrate into the porous void space. Specifically, it has been shown that human osteoblasts can penetrate pores with a diameter of 20 μm, however a larger diameter is better.[149] Migration studies with human mesenchymal stem cells have demonstrated that they can pass through 5 μm pores.[150] Other studies have demonstrated that interconnected pores with diameters greater than 50 μm are favorable to new bone formation.[98,149,151] In addition, it has been shown that the minimum pore size for osteoconduction is 80-100 μm.[149,152] Lastly, for the scaffold to support new vasculature, it has been shown that the minimum pore size is 45-100 μm; however, scaffolds with pore sizes of 100-150 μm resulted in a richer blood supply.[149,153] Therefore, from these above studies it appears that a minimum pore size of 100 μm is necessary for osteoconduction and vascularization.

As mentioned above, the ideal construct would degrade so that when the tissue is completely formed, the scaffold should be wholly degraded. For synthetic polymers, degradation occurs primarily by chemical hydrolysis of hydrolytically unstable polymer backbones.[41] Degradation can alter the mechanical properties of the construct, which subsequently can alter the effectiveness of the implant. This is critical in orbital bone engineering because if insufficient mechanical support is provided, delayed enophthalmos could occur. In addition, the degradation products can modify the surrounding environment of the implant. This is dependant on the biocompatibility of the degradation products and whether they are harmful to the adjacent tissue. Both of these properties are dependant on the structure, components, and fabrication techniques of the material. In addition, degradation is dependant on the location and geometry of the implant as well as the presence of catalysts, impurities and other additives.[41]

All implanted materials elicit a reaction from the host, but there is variation in the degree of response produced based upon the material. Reactions to injury include inflammation, wound healing, and foreign body responses.[99] A material may be considered to be biocompatible if it produces minimal inflammatory and immune response, and is able to function properly without significant harm to the host. The goal of designing a material for implantation is to minimize the magnitude of the response and response duration.

The immune response has a direct effect on bone tissue engineering. Specifically, degradation products are thought to be the cause of failure in many orthopaedic implants.[101] These degradation particles can be phagocytosed by

macrophages when less than 20 μm in diameter.[101] It is thought that these particles may indirectly affect bone cells through the secretory products of macrophages drawn to the area from the immune response.[101] Studies suggest that degradation particles directly interact with osteoblasts and affect their proliferation.[102] As mentioned above, biomaterial properties can affect the magnitude and duration of the host response. Characteristics of the material that can alter the immune response include the size, shape, and chemical and physical properties.[99]

Mechanical properties are of great importance in designing a scaffold for orbital floor regeneration. As the orbital floor acts as a natural crumple zone during trauma it is important to closely mimic the native tissue in order to restore this natural function. An experimental study was completed qualitatively analyzing the forces applied to the orbital floor in the two proposed traumatic defect mechanisms as a result of direct injuries to the globe or orbital rim by placing strain gauges beneath the orbital floor[114,115]. In conditions simulating the buckling mechanisms, anterior strains exceeded 3756 με and minimal strains detected posteriorly. In the hydraulic simulation, significant anterior strains were reported; however, posterior gauge readings all exceeded 3756 με. In addition, the average energy required to fracture the orbital floor for each of the mechanisms was 1.54 J and 1.22 J for buckling and hydraulic mechanisms, respectively. Other studies performed compared the orbital content weight and the load-resisting capabilities of common orbital reconstruction materials[154]. The investigation determined that the weight of the combined orbital contents was approximately 42.97 ± 4.05 g and all materials investigated provided adequate orbital support. Specifically, one material tested was dried calverium (1.5

mm) which exhibited a yield load of 11.93 ± 5.93 kg, a yield displacement of 1.70 ± 0.17 mm, a maximum load of 12.48 ± 6.13 kg, and a maximum displacement of 2.35 ± 0.77 mm. The scaffold designed should closely mimic the properties of orbital floor bone.

3.6 Current Tissue Engineering Progress

There has been significant progress made in the field of orbital bone tissue engineering; however a fully developed, ideal scaffold has yet to be created. This section reviews current progress achieved in orbital floor engineering and success in craniofacial engineering which may be applied to orbital floor regeneration (Table 2).

Scaffold	Cell Type	Growth Factor	Application	Reference
EH-PEG hydrogel	None	BMP-2	Orbital floor defects in rabbits	[155]
Porous PCL	Bone marrow aspirate	None	Orbital defects in pigs	[34]
Porous PGA	Periosteal	None	Calvarial defect in rabbit	[156]
Porous PCL with fibrin glue	Calvarial osteoblasts and mesenchymal progenitor cells	None	Calvarial defect in rabbit	[157]
Porous PPF	None	None	Cranial defect in rabbit	[54]
Porous PPF	None	Fibronectin, TGF-β_1	Cranial defect in rabbit	[42]
Solid PPF with bottom porous PPF layer	Bone marrow in porous PPF	TGF- β_2	Cranial defect in rabbit	[158]

Table 2: Craniofacial *in vivo* studies

3.6.1 EH-PEG Hydrogels

Investigators have developed a novel class of biomaterials based upon a cyclic acetal unit. These materials may be advantageous since the cyclic acetal unit degrades by hydrolysis into neutral primary degradation products of diols and carbonyls, and thus may not experience a change in local acidity associated with many synthetic biomaterials. The acidity of hydrogel degradation products may be a concern, for example, to the stable phenotypic function of encapsulated cell populations. Furthermore, acidic byproducts are thought to increase the inflammatory response and slow wound healing. In addition, an increase in acidity is associated with an increase in the degradation rate which may affect the mechanical support the construct is providing.

In order to create a cyclic acetal based hydrogel for cell encapsulation, the hydrophilic polymer poly(ethylene glycol) (PEG) was incorporated. Specifically, by including poly(ethylene glycol) diacrylate (PEGDA) within the radical polymerization of the cyclic acetal monomer 5-ethyl-5-(hydroxymethyl)-β,β-dimethyl-1,3-dioxane-2-ethanol diacrylate (EHD), a water swellable EH-PEG hydrogel has been produced[159]. This hydrogel can act as a platform for orbital floor repair by the integration of mesenchymal stem cells and osteoinductive signals such as BMPs.

Studies with these EH-PEG hydrogels have demonstrated that components required for gel crosslinking do not affect metabolic activity, viability or expression of osteogenic markers of bone marrow stromal cells (BMSCs).[160] Furthermore, BMSCs were shown to survive longterm in EH-PEG hydrogels while maintaining

viability.[160] In addition, when implanted in orbital floor defects *in vivo* the tissue surrounding the EH-PEG constructs showed a positive progression from 7 to 28 d indicating that constructs were not eliciting a chronic inflammatory response.[155] Lastly, the data shows the ability for EH-PEG gels to deliver BMP-2 *in vivo* as shown by the new bone growth in the area surrounding the constructs containing high concentrations of BMP-2 at 28 d (See Figure 3).[155] This demonstrates that EH-PEG constructs are a viable option for use *in vivo* of orbital floor repair.

Figure 3 : EH-PEG hydrogel in orbital floor defect from a control group at day 7.

3.6.2 Polycaprolactone Scaffolds

A study has been completed investigating orbital defects in pigs where they coated polycaprolactone (PCL) with bone marrow to aid in regeneration.[34] PCL is an advantageous material to work with because it has already been approved by the FDA as a bioresorbable polymer. Furthermore these investigators used fused deposition modeling to create a porous and highly interconnected network which should aid in the osteoconductive capacity of the scaffold and allow for vascular ingrowth. Scaffolds were implanted in medial wall defects and analyzed after three months using histology.

All scaffolds showed a thin layer of fibrous encapsulation indicating a mild inflammatory response with no additional signs of infection. PCL scaffolds without bone marrow were able to repair the defect and demonstrated the formation of new trabecular bone at the interface and within the scaffold, approximately 4.5%. While PCL scaffolds loaded with bone marrow aspirate reconstructed the defect and also showed significantly increased bone growth into the implant of 14.1%. In both conditions, the presence of giant cells was dismissed as not being clinically relevant, however; the researchers suggest that additional studies with more time points over an extended period might elucidate the foreign body reaction. This study demonstrates the importance of including a cell source as shown by the increased bone growth in PCL scaffolds with bone marrow aspirates. It is important to note that after three months, only 14.1% of the scaffold demonstrated new bone formation. Additional modifications to the scaffold may be necessary to improve bone regeneration however PCL is a viable option for orbital bone engineering.

3.6.3 Polyglycolic Acid Constructs

Other investigators have focused on craniofacial applications, and some of their findings can be applied to orbital bone engineering. Investigators harvested and expanded the periosteum *in vitro*.[156] The periosteum is of interest because it is easily harvested, has been shown to contain osteoprogenitor and chondroprogenitor cells, and contributes to osteogenesis in bone development and fracture healing. In this study, the periosteal cells cultured under osteogenic conditions were combined with resorbable polyglycolic acid (PGA) scaffolds and implanted in critical sized calvarial defects of rabbits.

Investigators demonstrated that the periosteal cells showed an osteoblast phenotype *in vitro* by expression of osteocalcin in osteogenic conditions. This corresponds with the literature that the periosteum contains osteoprogenitor cells. In addition, pre-implantation analysis demonstrated adherence of the periosteal cells to the PGA matrix which is important in tissue engineering. Furthermore, increased bone formation was found in groups with PGA scaffolds coated with periosteal cells as compared to untreated PGA implants *in vivo* by histology. This study again demonstrates the importance of delivering a cell population to the target site to aid in regeneration. While additional quantification of bone formation in the scaffolds may be beneficial in future studies, PGA is a promising scaffold for craniofacial tissue engineering.

3.6.4 Polycaprolactone Seeded Scaffolds

Other studies were performed using the polymer polycaprolactone (PCL) described above. However, this study focuses on calvarial defects. Here the investigators compared rabbit bone marrow derived mesenchymal progenitor cells (MPCs) and calvarial osteoblasts in *in vitro*[161] and *in vivo*[157]. Investigators demonstrated the 2-D differentiation potential of MPCs and then loaded both cell types onto 3-D porous interconnected PCL scaffolds fabricated using fused deposition modeling where their osteogenic differentiation was measured. Finally, the PCL scaffolds with a fibrin glue suspension were loaded with each cell type and implanted in critical-size calvarial defects in rabbits.

First, in the *in vitro* study, when seeded on 3-D PCL scaffolds MPCs were shown to have slightly higher alkaline phosphatase expression when compared to osteoblasts, however osteocalcin expression demonstrated no statistical differences. This demonstrates that both cell types show potential for use in craniofacial tissue engineering. In addition, continuous cell proliferation and homogenous cell distribution was seen throughout the PCL scaffolds. Homogenous cell distribution is a vital property of a tissue scaffold, but more importantly, measurable cell proliferation is a positive result showing PCL scaffolds are a promising tissue engineering construct. Further *in vivo* results demonstrated increased bone formation with cell-seeded scaffolds after three months, however there was no significant difference between scaffolds seeded with osteoblasts or MPCs as shown by histology and radiology. Therefore this study demonstrates that both cell types may be

successful in tissue engineering applications *in vitro* and *in vivo* and therefore it may be best to proceed with the cell type most easily harvested.

3.6.5 Poly(Propylene Fumarate) Scaffolds

Much progress has been made with poly(propylene fumarate) (PPF) for use in craniofacial tissue engineering. First, the soft and hard tissue responses to photocrosslinked PPF scaffolds were investigated in cranial defects using a rabbit model.[54] Results show an organized connective tissue at 8 weeks. Furthermore, the study demonstrated that PPF scaffolds elicit a mild immune response in both soft and hard tissues and that scaffold porosity and pore size did not significantly affect the tissue response as examined by histology. This study indicates that PPF may be an appropriate scaffold for craniofacial tissue engineering. Next, PPF scaffolds were treated with TGF-β_1 and implanted into subcritical-size cranial defects in rabbits.[42] Results show that constructs coated with TGF-β_1 had significantly higher bone growth when compared to other groups that were not coated with TGF-β_1 as demonstrated by analysis of histological images quantifying bone surface area, and bone area percentage. This indicates TGF-β_1 as an important growth factor in craniofacial tissue engineering. Further studies with PPF were performed by creating a construct that combined PPF with β-tricalcium phosphate.[158] In addition, these constructs were designed to contain a porous layer that was infused with bone marrow aspirate. This study examined the inclusion of TGF-β_2 to the constructs in a critical-size cranial defect in a rabbit model. Results show more bone formation found with constructs containing TGF-β_2 in addition to being the strongest bone when

compared to other groups as supported by mechanical testing. These above studies demonstrate that PPF scaffolds are a viable construct for use in craniofacial tissue engineering.

3.7 Summary

Orbital floor fractures can be a severe form of craniofacial trauma. In addition, the floor is the orbital wall most likely involved in orbital trauma. Unfortunately, the body's natural healing response to orbital floor fractures does not always restore proper function and facial aesthetics; therefore a clinical intervention is necessary. Current common clinical treatments include alloplastic implants and autologous grafts; however, each has associated disadvantages and sequelae. Orbital bone engineering offers solutions to the current clinical techniques and can aid in regeneration of natural bone tissue that is similar in both form and function to the native orbital floor. Tissue engineering utilizes cells, signals, and scaffolds, and this review has outlined necessary components for a successful construct for orbital floor repair. In addition, current successes and progress in the literature specific to orbital floors and craniofacial research have been reviewed.

Chapter 4: Objective

The goal of this project is to make use of tissue engineering strategies to regenerate orbital floor bone using a novel scaffold, known as a cyclic acetal biomaterial, utilizing an osteoprogenitor cell population and enhanced osteogenic cell signaling. Objectives of this work were to isolate bone marrow stromal cells and demonstrate their osteogenic differentiation through coculture with chondrocytes and standard media supplements. Next, bone marrow stromal cells were used to test the encapsulation potential of APS and TEMED as an initiator system for EH-PEG hydrogels. Further studies were completed where EH-PEG hydrogels were used to deliver BMP-2 to an orbital floor defect *in vivo*. To improve surrounding tissue interaction, macroporous EH-PEG hydrogels were created. These macroporous EH-PEG hydrogels were characterized using optical coherence tomography for porosity, pore size, and viability. Finally, the architecture of macroporous EH-PEG hydrogels was investigated for its effect on osteogenic signal expression of mesenchymal stem cells.

Chapter 5: Osteogenic Differentiation of Bone Marrow Stromal Cells[2]

5.1 Introduction

In recent years, the viability of tissue engineering approaches to treat bone defects and degenerative bone disease has been thoroughly demonstrated. The capacity of mesenchymal stem cells (MSCs) to differentiate into various cell types of the osteogenic lineage, defined here as osteoinduction, offers a potentially limitless source of donor cells with which these strategies could be executed.[128], [127] However, complete success remains contingent upon the illumination of a well-defined and fully understood protocol for guiding the differentiation of these progenitor cells destined for implantation into a defective site. The development of such a protocol would allow for the *in vitro* proliferation of the desired cell-types from a pool of harvested cells, and minimize the complications of differentiation toward undesired lineages following transplant.[162,163] To this end, a number of different strategies have been explored. Various groups have demonstrated the osteoinductive potential of chemical compounds such as prostaglandin E_2[164,165], 1,25-dihydroxyvitamin D_3 [166], as well as the often utilized pair of dexamethasone and Na-β-glycerolphosphate.[167] Biomaterial matrices fabricated from collagen and modified with calcium[168,169] or chondroitin sulfate[170] have also demonstrated osteoinduction. Reactive oxygen species[171-173] and even several forms of physical

[2] As Published in AD Thompson*, MW Betz*, DM Yoon, and JP Fisher. Osteogenic Differentiation of Bone Marrow Stromal Cells Induced by Coculture with Chondrocytes Encapsulated in Three-Dimensional Matrices. Tissue Engineering Part A. In Press. (Epub 2008 Oct 14)
* Contributed equally to the manuscript

stimuli[174,175] have been investigated for their osteoinductive effects. Finally, molecular signals from myeloma cells, vascular endothelial cells, and chondrocytes[176-178] have also been shown to have osteoinductive capabilities.

Of particular interest has been the application of coculture systems utilizing chondrocytes to control the differentiation of MSCs. The majority of *in vivo* bone formation, during both embryogenesis and postnatal fracture repair, occurs by way of a process known as endochondral ossification.[179,180] It begins as MSCs differentiate into chondrocytes and form a matrix template in the region of prospective bone. Then, as chondrocytes within this template progress through a spatially and temporally specific series of phases including proliferation, prehypertrophy, hypertrophy, and finally apoptosis, additional MSCs infiltrate the growth plate and begin to differentiate toward osteogenic lineages, replacing the cartilage template with ossified bone.[180] As the patterning and differentiation of chondrocytes within this matrix template seem to guide the recruitment and differentiation of the osteogenic precursors, the hypothesis then follows that chondrocytes produce some signaling factor, or some set of signaling factors, that elicit this response. Accordingly, studies have confirmed this hypothesis and identified a number of potentially relevant factors.[177,178,180-182] Within the generally osteoinductive subfamily of TGF-β signaling factors, known commonly as bone morphogenetic proteins[181,182], several have been identified as being highly expressed by chondrocytes during endochondral ossification.[180] Transglutaminase enzymes, known to be upregulated in chondrocytes found in the hypertrophic zone of the growth plate, have been implicated in the induction of osteoblastic markers by

preosteoblasts[178], and the expression of indian hedgehog, a potent inducer of osteogenic differentiation in MSCs[183], is upregulated by chondrocytes in the prehypertrophic zone of developing bone.[179]

Coculture methods have previously shown efficacy in inducing the differentiation of MSCs toward neuronal, cardiomyocytic, chondrocytic, as well as osteoblastic lineages.[176-178,184,185] These methods have been direct in nature, entailing cell-cell contact between the two populations being cocultured, or indirect in nature, wherein a permeable membrane may separate the populations. The physical contact of cells in direct coculture can lead to complications such as cell fusion[186], and ultimately necessitates separation of the two cell populations.[162] Indirect cocultures avoid these problems, but have typically been conducted in systems entailing two populations culturing in monolayer, with one in a well plate and another upon the surface of a transwell membrane. Unfortunately, this design imposes a spatial constraint on the mechanism of coculture limiting the number of cells that can be cultured to those that can adhere to the surface. As such, coculture systems in which one or both cell populations are suspended in three-dimensional matrices could potentially prove to be more efficient allowing more cells to be cultured within a limited area.

In this work, bone marrow stromal cells (BMSCs) in monolayer were cocultured with chondrocytes suspended in three-dimensional matrices, preventing direct cell-to-cell contact between the two cell populations. BMSCs are known to contain a population of MSCs and therefore have osteoprogenitor capabilities.[187] Prior to initiation of coculture, chondrocytes were suspended in alginate hydrogels

under the assumption that maintaining their natural morphology would be conducive to providing a more accurate simulation of an *in vivo* influence on bone formation.[188] The specific objectives of the study were (1) to determine whether chondrocytes cultured in alginate hydrogels could induce the osteogenic differentiation of BMSCs, (2) to compare the expression profiles of various osteoblastic markers for BMSCs cocultured with articular chondrocytes and BMSCs cultured in the presence of dexamethasone and Na-β-glycerolphosphate, and (3) to investigate the dependency of any osteoinductive effects observed upon the duration of coculture.

5.2 Methods

5.2.1 Materials

Alginic acid sodium salt from brown algae, HEPES, ascorbic acid, sodium bicarbonate, bovine serum albumin, Na-β-glycerolphosphate, dexamethasone, alizarin red S, and formaldehyde were obtained from Sigma-Aldrich (St. Louis, MO). Fetal bovine serum, penicillin/streptomycin, sodium pyruvate, α-minimal essential medium (α-MEM), and Dulbecco's modified eagle's medium: nutrient mixture F-12 ham (DMEM) were obtained from Gibco (Carlsbad, CA). Collagenase P was obtained from Roche (Indianapolis, IN). DNeasy isolation kits and RNeasy isolation kits were obtained from Qiagen (Valencia, CA). Quant-iT^{TM} picogreen dsDNA assay kits were obtained from Molecular Probes (Carlsbad, CA). All chemicals, reagents, and kits were used as delivered.

5.2.2 Bone Marrow Stromal Cell Isolation

BMSCs were obtained from young Wistar Hannover GALAS male rats weighing between 101 and 125g, following a University of Maryland approved IACUC animal protocol, as described previously.[189] Briefly, rats were euthanized with CO_2, and then both femurs and tibias were excised. Remaining soft tissue was removed from the bones prior to three ten-minute washes with 10 mL of control media (described below) containing 10% penicillin/streptomycin. Next, epiphysial plates were cleft and marrow was flushed out with control media using a syringe (18½ gauge). All marrow isolated from a single subject was then combined and homogenized by mixing with a syringe preceding filtration through a 70 μm cell strainer. The resultant solution was centrifuged for 5 minutes at 500g, and then resuspended in 5 mL of control media with 10% FBS and plated into a T-25 flask. After two days, a change of media isolated the adherent cells. BMSCs were precultured for two weeks, passaged when confluent, and then plated into six-well plates at a density of $4.5 X10^4$ per well.

5.2.3 Articular Chondrocyte Isolation and Encapsulation

Chondrocytes were obtained according to a protocol also described previously.[190] Briefly, cartilage was harvested from the metatarsal phalangeal joints of calves aged 15-18 weeks. Excised cartilage was washed thrice in control media, and then digested overnight in a 0.2% Collagenase P solution at 37°C and 5% CO_2. The following day, cells were filtered through a 70 μm cell strainer to rid the samples of undigested cartilage, and again washed three times in control media. Samples

were then pooled and centrifuged at 500g for 5 minutes. Alginate solution, prepared by heating 1.2% (w/v) alginic acid in a solution of 0.15M NaCl and 0.025 HEPES buffer, and filtered to achieve sterility (0.22μm pore size), was then used to resuspend the pelleted chondrocytes at a density of 2.25 x 10^6 cells/mL. Chondrocytes were encapsulated in three dimensional hydrogels by dropping this solution, via syringes (18½ gauge), into a beaker of stirring 100mM $CaCl_2$, which immediately crosslinked the alginate into beads. This produced spherical hydrogels measuring approximately 3 mm in diameter which contained chondrocytes at a density of 75,000 cells/bead. Cocultures were conducted with 20 beads/well, translating to a total density of 1.5 x 10^6 chondrocytes/well.

5.2.4 Cell Culture Conditions

Culture media for all five conditions consisted of a mixture of equal parts α-MEM and DMEM.[191] Prior to mixing, α-MEM was supplemented with 50 μg/mL ascorbic acid, 2.0 mg/mL sodium bicarbonate and 0.1% penicillin/streptomycin, while DMEM was supplemented with 50 μg/mL ascorbic acid, 1 mg/mL sodium bicarbonate, 0.1% penicillin/streptomycin, 1 mg/mL bovine serum albumin, and 0.1% sodium pyruvate. For the osteogenic control condition, this α-MEM/ D-MEM blend was additionally supplemented with 10 mM Na-β-glycerolphosphate and 10^{-8} M dexamethasone. Cells were cultured in six-well tissue culture plates at 37°C and 5% CO_2, and media containing 10% FBS was changed every two days. Controls did not contain any chondrocytes or alginate beads.

Cocultures were executed using Corning transwell inserts (0.4 μm size exclusion) to separate any chondrocytes that detached from the bead from the BMSC population. All three coculture conditions were conducted identically. At day 0, coculture was initiated for all experimental groups. For the 1-Day coculture condition, inserts along with chondrocytes were removed from the cultures after 1 day. For the 10-Day coculture condition, inserts were removed after 10 days, and for the 21-Day coculture condition, chondrocytes remained in the cultures until the final time point. Due to the fact that a small number of chondrocytes did detach from the hydrogels and settled on the transwell membranes as the cultures progressed, transwell inserts were replaced at day 10 in the 21-Day condition, in order to minimize the number of adherent chondrocytes culturing on the membrane. For the chondrocyte signaling study cocultures were initiated on day 0, and a control group with no BMSCs was also cultured.

5.2.5 DNA Quantification

In order to normalize the calcium deposition described below, DNA was isolated from BMSCs at each time point and quantified via picogreen assay. Briefly, samples were lifted in triplicate for each condition and DNA was isolated using the Qiagen DNeasy isolation kit according the manufacturer's protocol. DNA was then quantified using the Quant-iT picogreen kit by combining 100 μL of DNA isolate with 100 μL picogreen reagent, incubating at room temperature for 5 minutes, and then reading fluorescence at 480nm excitation and 520nm emission on an M5 SpectraMax plate reader (Molecular Devices, Sunnyvale, CA).

5.2.6 Quantitative rt-PCR

Chondrocytes were isolated from alginate beads by incubating in 0.1 M ethylenediamintetraacetic acid in PBS at 37^{o}C for 15 minutes, and then pelleted by centrifugation. RNA was isolated from BMSCs and chondrocytes at each time point using a RNeasy Mini Plus Kit, according to the manufacturer's protocol. This total RNA was reverse transcribed with a High Capacity cDNA Archive Kit, and then an ABI Prism 7000 Sequence Detector (Applied Biosystems, Foster City, CA) was utilized to determine the expression levels of the proteins of interest via quantitative rt-PCR.

BMSCs were analyzed for alkaline phosphatase (ALP), osteocalcin (OC), and bone morphogenetic-2 (BMP-2) mRNA with 18s ribosomal RNA served as an endogenous control in all samples, which were assayed in triplicate. The negative control at day 1 was used as a calibrator for each set of gene expression data, containing all groups at all time points. All primer and probe sequences were designed for rat species; the 18S sequences were designed for eukaryotic cells. Primer and probe sequences for OC and BMP-2 were designed as follows: GGCTTCCAGGACGCCTACA (OC forward primer), GGGCAACACATGCCCTAAAC (OC reverse primer), CGCATCTATGGCACCAC (OC probe), TGCCCCCTAGTGCTTCTTAGAC (BMP-2 forward primer), CCCGGCCACCATGGT (BMP-2 reverse primer), ACTGCGGTCTCCTAAA (BMP-2 probe). The primers and probes used for ALP and 18s were obtained from Applied Biosystems and are proprietary.

Chondrocytes were analyzed for transglutaminase 2 (TGM2), transforming growth factor-β2 (TGF-β2), and matrix metalloproteinase 13 (MMP13) with GAPDH as an endogenous control in all samples, which were assayed in triplicate. The negative control at day 1 acted as the calibrator for each set of gene expression data. All primer and probe sequences were designed for bovine species. Primer and probe sequences were designed as follows: CGAGAAACCCCTGTCCTAACC (TGM2 forward primer), CAGCATAGGCAACTAAGGCTATTG (TGM2 reverse primer), CAGTGCCTAGACGTC (TGM2 probe), TCTCCAACCCAGCGCTACA (TGF-β2 forward primer), TTCACCCTCTGCTCTGGTTTTC (TGF-β2 reverse primer), TGACAGCAAAGTCG (TGF-β2 probe), CCCTTGATGCCATAACCAGTCT (MMP13 forward primer), GCCGCCAGAAGAATCTGTCT (MMP13 reverse primer), CGCGGAGAAACACT (MMP13 probe).

5.2.7 Calcium Deposition Assay

The deposition of calcium by BMSCs was assayed following the method described by Gregory et al.[192] Cells were washed with phosphate buffered saline and fixed in 10% (wt/v) formaldehyde for 15 minutes at room temperature. Following a wash with excess water, 1 mL of 40 mM alizarin red S (ARS) (pH 4.1) was added to each well and cells incubated at room temperature, while shaking, for 20 minutes. A series of washes with excess water then removed unincorporated dye. Next, 800 μL of 10% (v/v) acetic acid was added to each well, and plates were allowed to incubate at room temperature for 30 minutes while shaking. Cells were then detached from wells using cell scrapers and transferred to 1.5 mL

microcentrifuge tubes, vortexed thoroughly, wrapped in parafilm and heated to 85°C for ten minutes, then transferred to ice for 5 minutes. After centrifugation at 20,000g for 15 minutes, 500 μL of supernatant was removed from each tube and combined with 200 μL of 10% (v/v) ammonium hydroxide. Finally, 150 μL of this solution was then read (in triplicate) on the M5 SpectraMax plate reader at 405 nm. A standard curve was created to determine ARS concentration. Previous work has demonstrated that ARS binds approximately 2 mol Ca^{2+} per mol ARS in solution[193,194].

5.2.8 Statistical Analysis

Data from all studies was analyzed using ANOVA single factor analysis and Tukey's multiple comparison test ($p \leq 0.05$). All results are reported as mean ± standard deviation. Please note that only pertinent statistical relationships are noted in the figures.

5.3 Results

Bovine derived chondrocytes were utilized in this study to induce the osteogenic differentiation of rat BMSCs. The interspecies nature of this coculture did not appear to significantly affect the response of rat BMSCs to the osteoinductive influence of bovine chondrocytes. Previous work has demonstrated that bovine BMP is osteoinductive when cultured in the presence of BMSCs derived from rats.[195] In

addition, rat osteoblasts and bovine chondrocytes have been shown to have reciprocal signaling effects in coculture.[191]

Qualitative micrographs were taken throughout the study to asses the cell populations. Images of the chondrocytes in the beads indicate morphological changes by the end of the coculture (Figure 4). In addition, the BMSCs were assessed to monitor morphological changes during the early stages of differentiation (Figure 5).

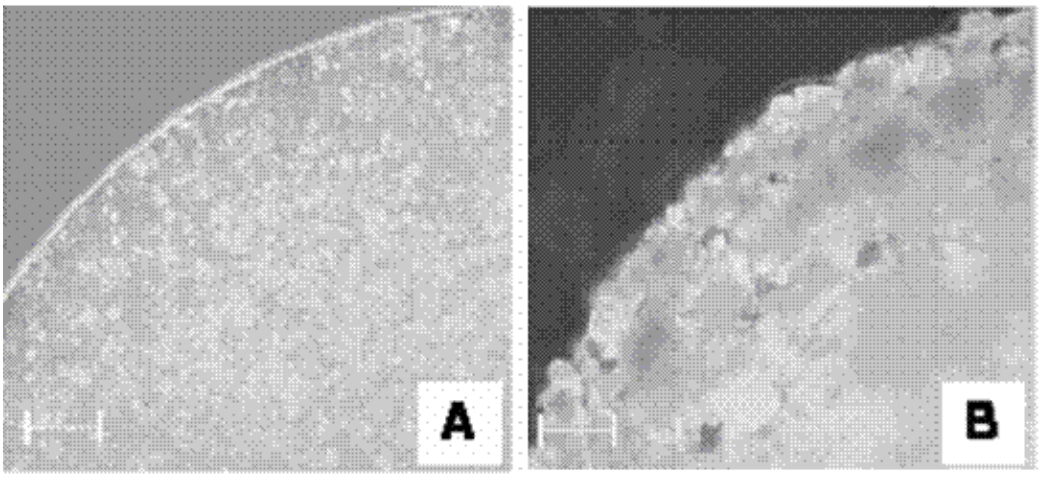

Figure 4: Phase contrast microscopy shows the chondrocytes culturing in alginate at (A) day 3, and (B) at day 19. The morphology of the chondrocytes can be seen to have changed by the end of the coculture. Scale bars denote 100 μm.

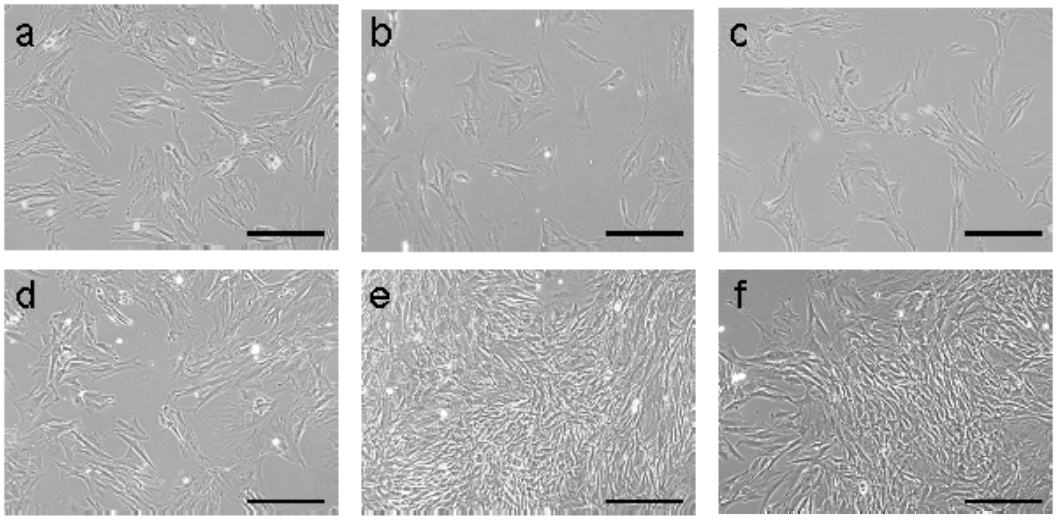

Figure 5: Phase contrast microscopy demonstrates the morphology of BMSCs at day 3 cultured in (a) control conditions, (b) continuous coculture with chondrocytes, (c) osteogenic conditions and at day 7 in (d) control conditions, (e) continuous coculture, and (f) osteogenic culture conditions. At day 3 the control condition morphology appears to be spindle-shaped, while the coculture and osteogenic conditions represent a more cuboidal population. Day 7 again shows the maintained spindle morphology of the control condition. The coculture and osteogenic conditions are more confluent, however it appears the populations demonstrate a cuboidal morphology. Scale bars denote 250 μm

At day 3 the control condition morphology appears to be spindle-shaped, while the coculture and osteogenic groups represent a more cuboidal population. Day 7 again shows the maintained spindle morphology of the control condition. The coculture and osteogenic populations are more confluent; however, it appears that they both demonstrate a cuboidal morphology. DNA quantification indicated that the populations were proliferating throughout the duration of the study. However, trends between examined groups were not observed. Specifically, at day 1 the 21-day coculture group and the osteogenic control were quantified to be 1.15 ± 0.01 and 1.35 ± 0.01 μg DNA/well, respectively. At day 21 the 21-day coculture group and the osteogenic control DNA levels were 20.31 ± 0.21 and 18.58 ± 0.14, μg DNA/well respectively.

In order to quantify the changes in expression by the BMSCs, quantitative rt-PCR was performed. By isolating mRNA from the BMSCs, and using primers and probes designed for rat mRNA, only fold-changes that developed in the BMSC population were measured. Many *in vitro* studies utilize protein assays; however, protein levels in the cocultures described in this study may be confounded with both chondrocyte protein expression and exogenous FBS proteins. Therefore, the expression of osteoblastic markers was only studied through quantitative rt-PCR analysis and detection of mineralization.

The expression of alkaline phosphatase mRNA was quantified at each time point as a marker for early stages of osteogenic differentiation. Expression was upregulated most immediately in cells cultured in osteogenic medium, showing a significant increase over the other conditions at days 1, 8, and 14 (Figure 6). All three of the coculture conditions demonstrated a statistically significant increase in expression over the negative control at day 8 and at day 14. Similar levels of expression were exhibited by all three coculture conditions at both the onset of upregulation at day 8, as well as the peak expressions at day 14. However, while cells cultured in the osteogenic medium demonstrated continued upregulated ALP expression at day 21, BMSCs in the coculture conditions demonstrated a marked decrease in ALP expression between day 14 and day 21.

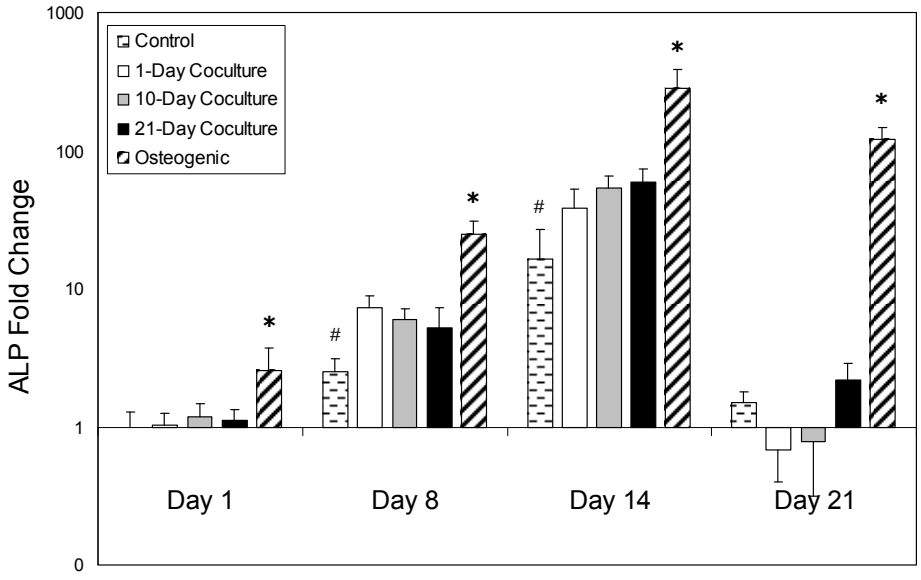

Figure 6: Alkaline phosphatase expression levels of BMSCs as determined by quantitative rt-PCR analysis at days 1, 8, 14, and 21. At days 8 and 14, the three coculture conditions have induced a significantly higher level of expression than the negative control, but a similar level of expression is observed in all three experimental conditions. (*, #) indicate statistical difference from all other groups within timepoints. (Values reported as mean ± standard deviation, n = 3)

Similar trends were observed with BMP-2 expression as those seen with ALP. However, the upregulation of this marker in the osteogenic control condition was not as immediate; at day 1 all five conditions were at similar levels of expression. Nevertheless, the osteogenic control again demonstrated the quickest response, showing a significantly greater increase in expression over all other groups by day 8 (Figure 7). The three different coculture conditions also exhibited significantly increased expression over the negative control at day 8, but by day 14 all conditions had peaked at similar levels of expression. Once again, the osteogenic control maintained nearly the same expression at day 21 as at day 14, whereas the experimental conditions all evinced decreased expression at the final timepoint.

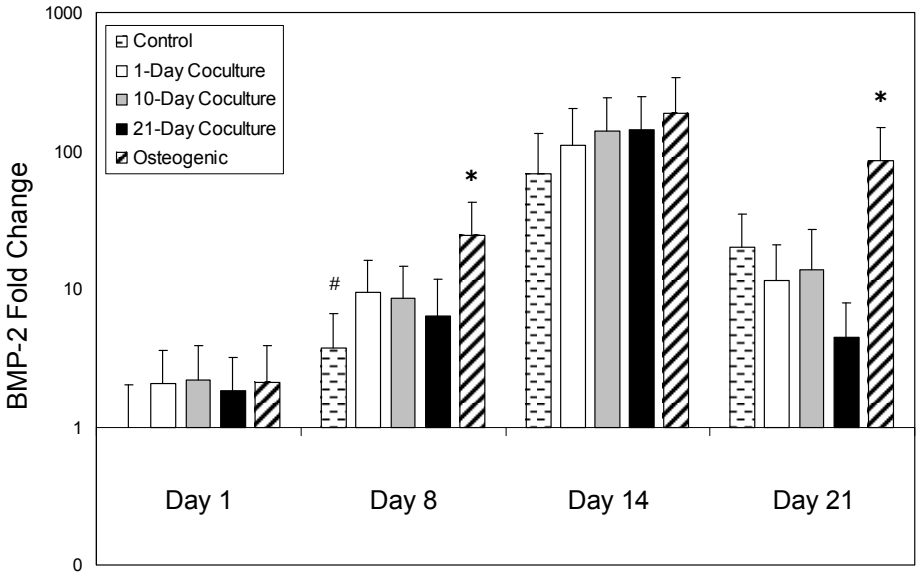

Figure 7: Bone morphogenetic protein-2 expression levels of BMSCs as determined by rt-PCR analysis at days 1, 8, 14, and 21. The experimental conditions induced higher levels of expression at days 8 and 14 compared to the negative control, but similar to that of one another. (*, #) indicate statistical difference from all other groups within timepoints. (Values reported as mean ± standard deviation, n = 3)

Osteocalcin mRNA was quantified at all time points in order to assess the progression of BMSCs through later stages of osteogenic differentiation. At days 1 and 8, the expression of OC transcripts fluctuated variably at low levels, but by day 14 significant upregulation was observed (Figure 8). Again, the osteogenic control group elicited the strongest response, showing a significant increase over all other groups at both days 14 and 21. However, for this marker, variable responses were observed within the three experimental groups. At day 14, the 10-day and 21-day coculture conditions had induced significantly greater levels of OC expression compared with the 1-day coculture and the negative control. At day 21, the 21-day coculture maintained a significantly increased level of OC expression, while the abbreviated coculture conditions had dropped to a level similar to that of the negative control.

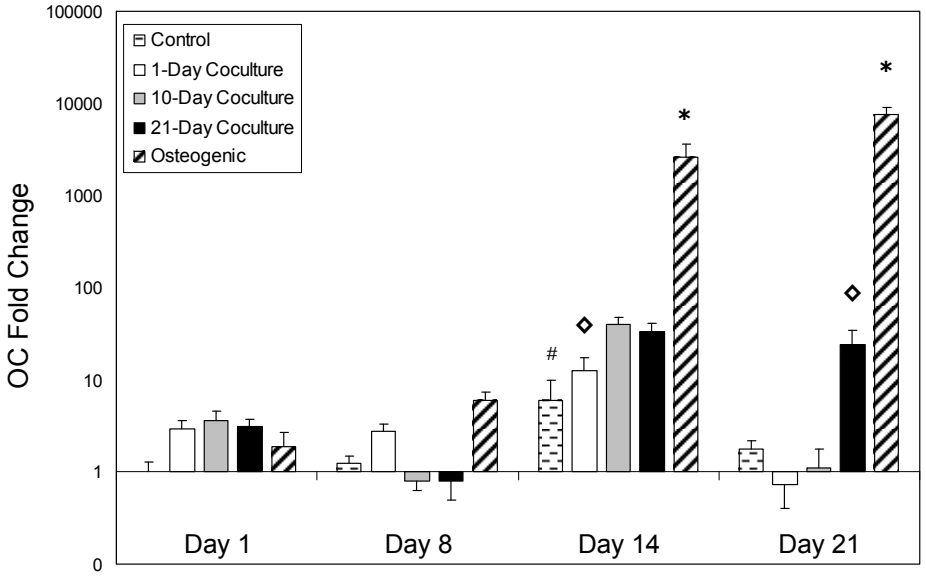

Figure 8: Osteocalcin expression levels of BMSCs as determined by rt-PCR analysis at days 1, 8, 14, and 21. By day 14, all experimental conditions had induced a higher level of expression than the negative control, but the two extended coculture conditions had also induced a significantly higher level of expression than the single-day coculture. Additionally, at day 21, the 21-Day coculture condition maintained an upregulated expression, while the 1-Day and 10-Day conditions had dropped to baseline levels. (*, ◊, #) indicate statistical difference from all other groups within timepoints. (Values reported as mean ± standard deviation, n = 3)

Calcium deposition was measured throughout the study as a means to ascertain the density of mature osteoblasts. After 8 days, a significant increase was observed in the 10-day and 21-day cocultures (Figure 9). By day 14, the 21-day coculture condition and the osteogenic control had shown a much higher level of calcium deposition compared with the negative control and the 1 and 10-day coculture groups. This difference expanded by day 21, with the osteogenic control and the 21-day coculture condition having accumulated significantly more calcium than the other three groups. Micrographs were taken of the wells before quantitative measurement to qualitatively assess the calcium deposition (Figure 10). The images demonstrate minimal staining in all groups at day 1. Day 8 shows an increase in intensity from day 1, and also significantly more staining for the continuous coculture

and osteogenic groups. Day 21 exhibits even staining for both groups, however it appears that the coculture and osteogenic groups have stained more intensely.

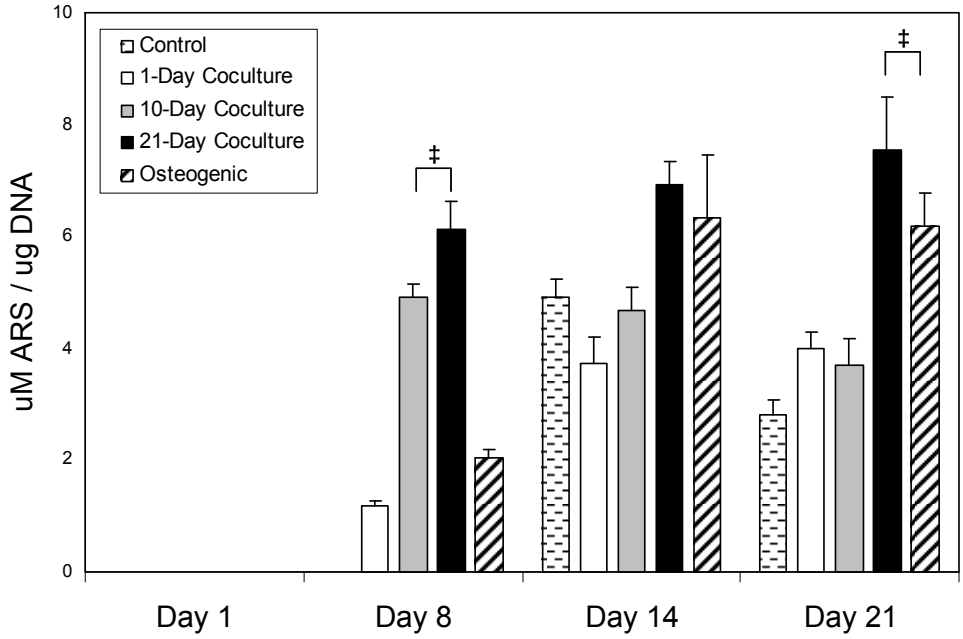

Figure 9: Calcium deposition by BMSCs after days 1, 8, 14, and 21, normalized to DNA at each time point. At day 8, calcium levels were significantly higher in the extended coculture conditions than in both controls and the 1-Day coculture. By days 14 and 21, the 21-Day coculture condition had accrued more calcium than the 10-Day coculture, and the osteogenic control increased to levels of deposition greater than the 10-Day coculture and near those of the 21-Day coculture. (‡) indicates no statistical difference between groups at each timepoint. (Values reported as mean ± standard deviation, n = 3)

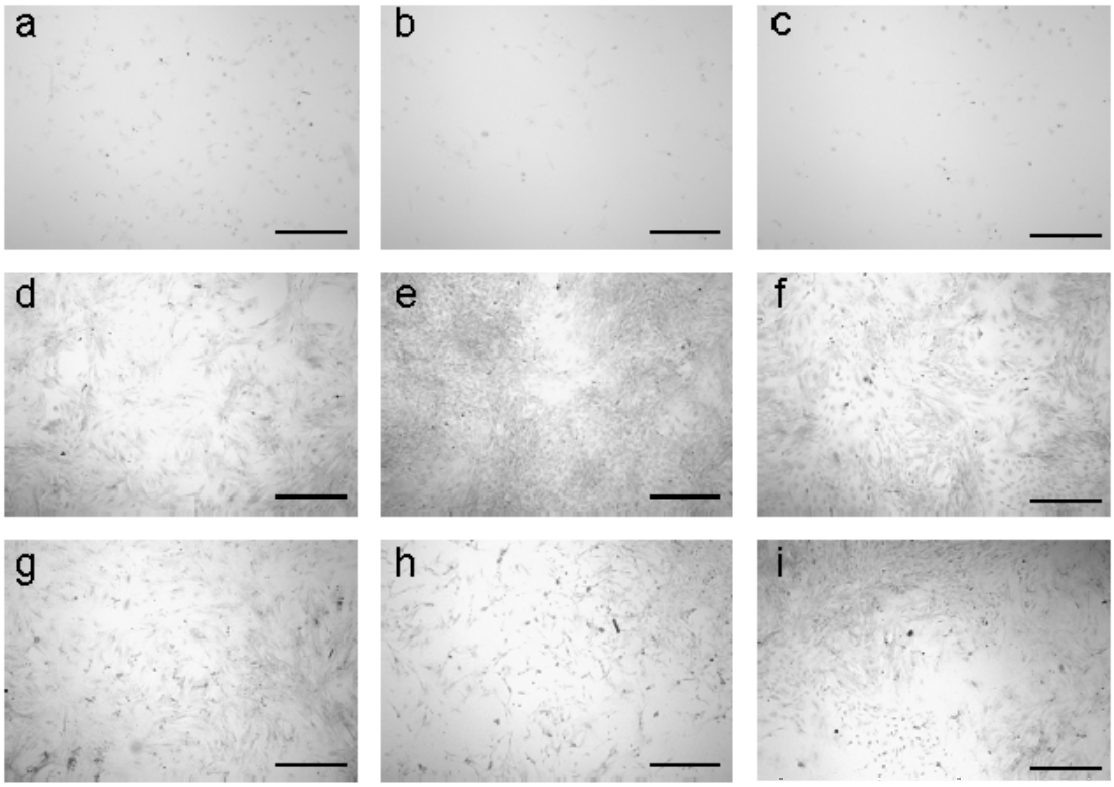

Figure 10: Phase contrast microscopy qualitatively demonstrates calcium deposition by BMSCs at day 1 (a) control, (b) continuous coculture, (c) osteogenic control, day 8 (d) control, (e) continuous coculture, (f) osteogenic control, and day 21 (g) control, (h) continuous coculture, (i) osteogenic control. Day 1 depicts minimal levels in all groups. Day 8 demonstrates an increase in intensity from day 1, and also significantly more staining for the continuous coculture and osteogenic groups. Day 21 shows even staining for both groups, however it appears that the coculture and the osteogenic groups have stained more intensely. Scale bars denote 500 μm

A culture was also conducted in order to analyze the expression of transforming growth factor-β2, matrix metalloproteinase 13, and transglutaminase 2 in chondrocytes cocultured with BMSCs (Figure 11). TGF-β2 demonstrated an increase in mRNA expression at day 8 which then decreased to initial levels at day 14 (Figure 11a). MMP-13 showed steady levels at days 1 and 8 and a large increase at day 14 (Figure 11b). TGM-2 displayed decreasing levels throughout the study with minimal expression at day 14 (Figure 11c).

(a)

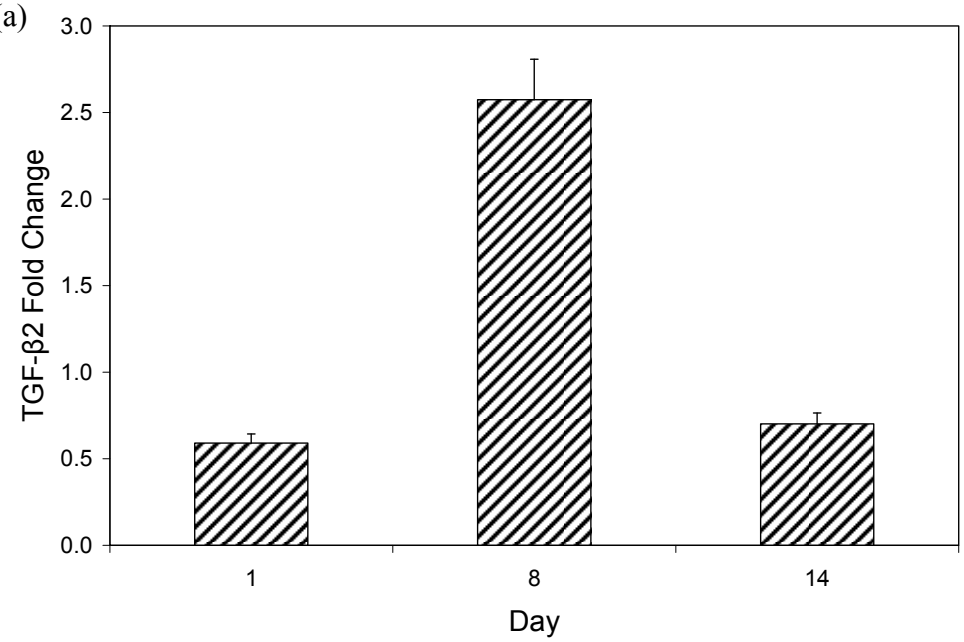
3.0
2.5
2.0
1.5
1.0
0.5
0.0
TGF-β2 Fold Change
1
8
14
Day

(b)

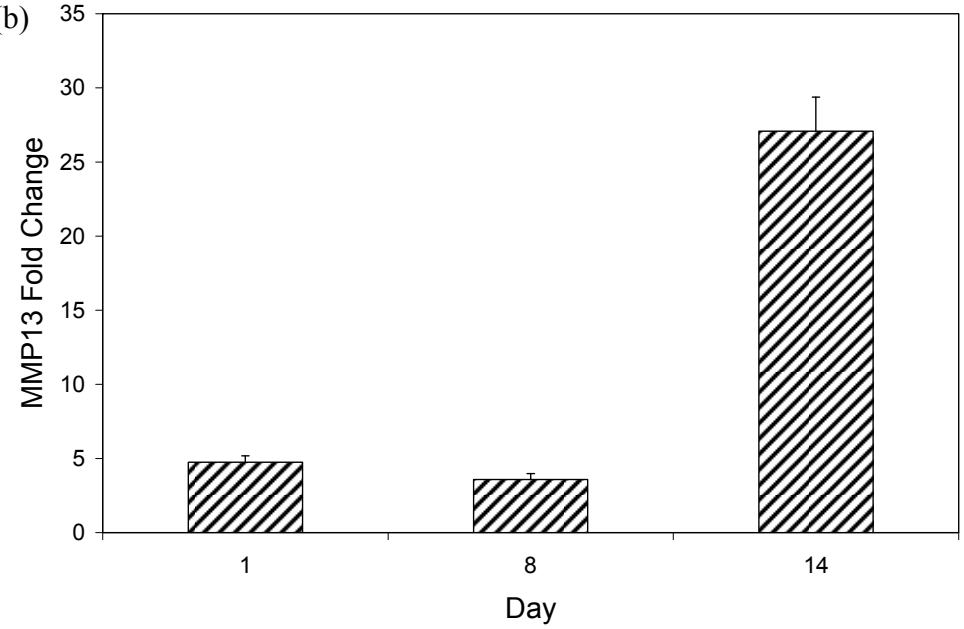
35
30
25
20
15
10
5
0
MMP13 Fold Change
1
8
14
Day

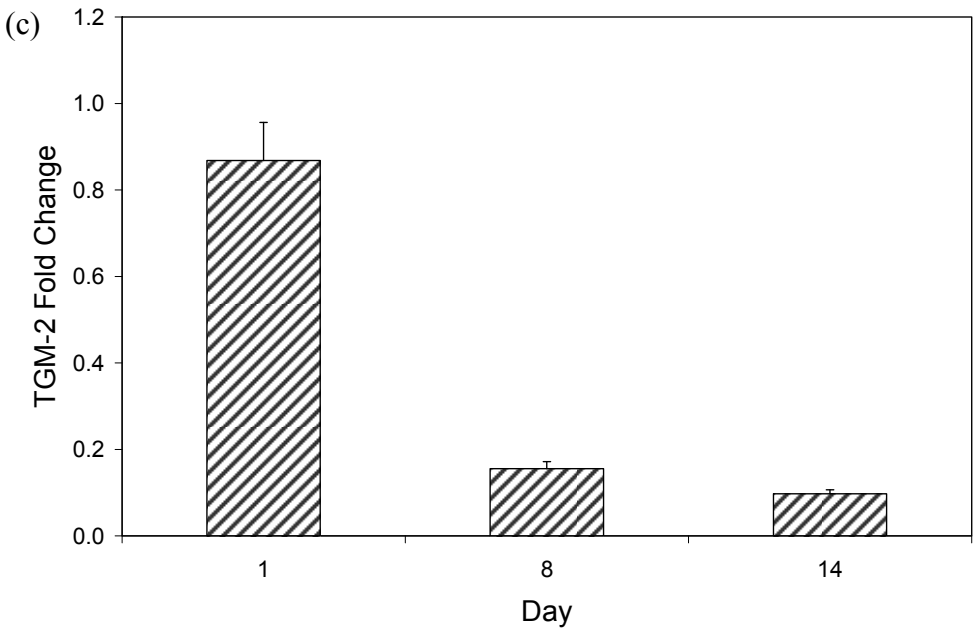

Figure 11: (a) transforming growth factor-β2, (b) matrix metalloproteinase 13, and (c) transglutaminase-2 in chondrocytes cocultured with BMSCs. TGF-β2 demonstrated an increase in mRNA expression at day 8 which then decreased to initial levels at day 14. MMP-13 showed steady expression levels at days 1 and 8 and a large increase at day 14. TGM-2 displayed decreasing levels throughout the study with minimal expression at day 14.

5.4 Discussion

Previous coculture investigations in this field demonstrate the ability of chondrocytes to induce the osteogenic differentiation of mesenchymal stem cells through continuous coculture[176,177]. This work further investigates the relationship between chondrocytes and the differentiation of BMSCs by varying the length of coculture time of chondrocytes with BMSCs. Furthermore, this work cultures the chondrocytes in a three-dimensional environment to maintain phenotypic function and slow dedifferentiation of the cells which can occur in monolayer. Specifically, the objectives of this of work were to demonstrate the potency of encapsulated articular chondrocytes in promoting the osteogenic differentiation of BMSCs, to elucidate the similarities and differences between this mechanism of induction and

the medium supplements Na-β–glycerolphosphate and dexamethasone, and to determine the dependency of this induction on the duration of coculture.

The osteoinductive capability of chondrocyte signaling was apparent throughout this study. Qualitatively the micrographs depicting BMSC morphology transition from spindle to cuboidal was on the time scale presented in the literature.[196] Previous reports had shown morphological changes by day 4, and this study demonstrated initial transitions by day 3 and a more complete cuboidal population by day 7. Further quantitative data from differentiation markers assayed in this study supported the effects of chondrocytes on BMSCs. The early markers ALP and BMP-2 were upregulated faster and peaked higher in the coculture conditions as compared with the negative control, and the later markers of OC expression and calcium deposition also showed increased differentiation in coculture conditions over the negative control. Quantitative rt-PCR results indicate that the level of osteogenic differentiation seen in BMSCs cocultured with chondrocytes was not as great as that seen in BMSCs cultured in osteogenic control media. Two alternatives may account for these results. On the one hand, while encapsulating the chondrocytes in a three-dimensional hydrogel preserved the native morphology of these cells, the system of coculture executed in this study remains a simplified recreation of the naturally occurring process of bone formation. For example, the forces acting upon a population of MSCs within developing or repairing bone are likely mediated not just by chondrocytes, but also by the mineralizing matrix surrounding these cells, blood vessels that begin to arborize as hypertrophic chondrocytes apoptose and initiate vascularization, and even additional cell types

such as osteoclasts and haematopoetic stem cells.[179] On the other hand, osteoinduction by Na-β-glycerolphosphate and dexamethasone may induce an artificially high response, and the coculture response described here might better reflect *in vivo* conditions. Further studies are required to confirm one of the two alternatives. Nevertheless, the results presented here do demonstrate the osteoinductive effects of hydrogel embedded chondrocytes.

The next objective of this experiment was to compare the two mechanisms of osteogenic induction examined in this study. The glucocorticoid dexamethasone and Na-β–glycerolphosphate are widely used in cell culture experimentation as medium supplements intended to induce the osteogenic differentiation of BMSCs. In this study, the similarities between chondrocyte-induced differentiation and supplement-induced differentiation were readily apparent. The onset of upregulation and the peak expression of various markers assayed were similar in the extended coculture condition and the osteogenic media condition, but an interesting difference appeared in the final stages of expression. In cells cocultured with chondrocytes, the presence of transcripts for the early markers ALP and BMP-2 dropped off significantly, while cells cultured in osteogenic media decreased minimally. Previous work has demonstrated that early markers for differentiation, such as ALP, peak between days 8 and 12.[196,197] Our study corresponds with a later peak expression for ALP and BMP-2; however due to experimental design the peak expression may have occurred between the measured timepoints at 8 and 14 days. The variation between the coculture groups and the osteogenic control indicates a possible flaw of the osteogenic control model. The probable cause being that the influence exerted on

BMSCs by the supplemented media is constant over the course of the experiment. As media is replenished throughout the study, cells are subject to the same exact set of external stimuli from day 1 of the culture through day 21, resulting in continuous increased expression of factors that might only peak briefly during natural differentiation. By comparison, the influence exerted on BMSCs by chondrocytes may be dynamic, where the chondrocytes act in a coordinated manner with the BMSCs to induce the expression of varying genes at different times. Furthermore, as endochondral ossification involves several cell types in addition to MSCs and chondrocytes, the milieu of a differentiating MSC during *in vivo* osteogenesis can only be more complex by comparison. For this reason alone, an awareness of the limitations of dexamethasone and Na-β–glycerolphosphate induced osteogenic differentiation should be maintained.

In order to investigate the temporal nature of the chondrocyte signaling that induces osteogenic differentiation of BMSCs, cocultures were carried out for three different lengths of time. Results showed that early stages of differentiation would progress regardless of the length of coculture; a single day of chondrocyte signaling was sufficient to induce upregulated expression of ALP and BMP-2 through day 14 of the study (Figures 6, 7). One possible implication of this data is that signals produced by the chondrocytes within the first 24 hours of coculture initiate the process of differentiation in BMSCs that continues via autocrine and/or paracrine signaling among the BMSCs themselves. As such, ALP and BMP-2 expression remain increased in the 1-Day coculture condition even after culturing from day 1 through day 14 in the absence of the original stimulus. Alternatively, the progression

of BMSCs through later stages of osteogenic differentiation was dependent upon extended periods of coculture with chondrocytes. Specifically, the only coculture condition that maintained an increased OC expression at day 21 was the 21-Day coculture condition (Figure 8). Osteocalcin, a protein produced by mature osteoblasts during mineralization, is thought to signal bone turnover.[198] Therefore, the failure of the 1-Day and 10-Day conditions to maintain osteocalcin expression through day 21 indicates that continuous exposure to morphogenetic signals from chondrocytes is necessary for BMSCs to continue expression of mature bone phenotype and indicators of late stage osteogenic differentiation. This is supported by the fact that mineralization observed in 21-day coculture was significantly higher than that of the abbreviated coculture conditions at day 21 (Figure 9).

The dependency of BMSC osteogenic differentiation on extended chondrocyte coculture can be interpreted in several ways. One possible explanation is that articular chondrocytes constitutively express the factors responsible for inducing the later stages of osteogenic differentiation, but differentiating BMSCs require prolonged exposure to these factors in order to benefit from their effects. There may also be an issue of competence, such that BMSCs exposed to these factors during the early stages of differentiation may not be capable of responding to them. However, the possibility also exists that the signaling factors in question are not expressed constitutively. Their production may in fact be a result of interaction with the BMSCs. If this were the case, the BMSCs in the 1-Day coculture condition may not have been exposed to these signals, and the cells in the 10-Day coculture condition were likely only exposed to them briefly. As described earlier, chondrocytes are

known to progress through a series of phases during endochondral ossification. Indeed, the morphological appearance of the chondrocytes in this study changed drastically over the course of the 21-day coculture (Figure 4). As chondrocyte morphology has been shown to be intimately linked to gene expression[188], then the inductive effects exerted by the chondrocytes may be changing throughout the coculture. Comparing the osteogenic differentiation of BMSCs cocultured with articular chondrocytes and BMSCs cultured in chondrocyte-conditioned media might clarify this ambiguity.

As signaling is an aspect of this study, chondrocytes exposed to BMSCs were analyzed for signaling and hypertrophic factors. TGF-β2 is secreted by chondrocytes and known to be involved in mesenchymal stem cell and chondrocyte proliferation as well as stimulate bone healing in fracture repair.[199] In this study the chondrocytes demonstrated a 5-fold increase from day 1 to day 8 in TGF-β2 mRNA expression (Figure 11a) which may have caused increased proliferation in the cell populations. MMP-13 is expressed by chondrocytes and is known to be present during endochondral ossification[200] and also to be a hypertrophy-associated marker as it promotes the resorption of hypertrophic cartilage.[201,202] In this study, MMP-13 showed steady levels at the initial timepoints, with a significant increase at day 14 (Figure 11b) which may be caused by a need to resorb surrounding collagen. Lastly, TGM-2 was analyzed which is a marker of hypertrophic chondrocytes via the MAPK pathway and is involved in matrix calcification.[203] The data demonstrates a decrease of TGM-2 expression over time (Figure 11c) suggesting the chondrocytes may not be hypertrophic through this pathway.

5.5 Conclusions

Regenerative techniques aimed at repairing bone defects rely heavily on the ability to induce a population of progenitor cells to differentiate toward osteogenic lineages. Ideally, the method employed to induce this differentiation would be identical to that which occurs *in vivo*, a mechanism inextricably tied to chondrocyte signaling. In the study presented here, we demonstrate that coculturing chondrocytes encapsulated in alginate hydrogels with BMSCs can effectively induce differentiation in these osteoprogenitor cells, in a mechanism distinct from that of the media supplements dexamethasone and the Na-β–glycerolphosphate. Furthermore, we characterized this interaction as having separate temporal components, with brief exposure proving sufficient to induce early stages of differentiation, but extended exposure necessary for mature osteogenic development.

Chapter 6: Cyclic Acetal Hydrogel System for Cell Encapsulation[3]

6.1 Introduction

Many biomaterials, both natural and synthetic, have been developed for use in tissue engineering applications. A number of laboratories have developed strategies utilizing natural polymers such as agarose[204,205], alginate[206,207], chitosan[208-210], collagen[211,212], hyaluronic acid[213,214], and silk[215,216]. However, natural polymers have a variable molecular structure and often do not possess sufficient mechanical rigidity, especially when exposed to significant compressive force. Synthetic biomaterials have been investigated due to their reproducibility and modification capability. These biomaterials can often be engineered to have desired properties, including mechanical stiffness and biodegradability, by tailoring both the component monomers and the material fabrication technique. To this end, a number of synthetic polymers have been developed, including poly(D,L-lactic acid-co-glycolic acid)[45,46], poly(ε-caprolactone)[51], poly(propylene fumarate)[42,54], and poly(vinyl alcohol)[217]. While a number of polymers are currently under investigation for biomedical applications, an ideal biomaterial has not been developed.

Our laboratory has recently developed a novel class of biomaterials based upon a cyclic acetal unit. These materials may be advantageous since the cyclic acetal unit degrades by hydrolysis into primary degradation products of diols and carbonyls, and thus may not experience a change in local acidity associated with

[3] As published in MW Betz, PC Modi, JF Caccamese, DP Coletti, JJ Sauk, and JP Fisher. Cyclic Acetal Hydrogel System for Bone Marrow Stromal Cell Encapsulation and Osteodifferentiation. Journal of Biomedical Materials Research, Part A. 86: 662-670 (2008).

many synthetic biomaterials. The acidity of hydrogel degradation products may be a concern, for example, for the stable phenotypic function of encapsulated cell populations. A cyclic acetal biomaterial in the form of a rigid plastic may be fabricated from the radical polymerization of the monomer 5-ethyl-5-(hydroxymethyl)-β,β-dimethyl-1,3-dioxane-2-ethanol diacrylate (EHD).[218] This biomaterial has been shown to have controllable physical properties and can support the surface adhesion of bone marrow stromal cells (BMSCs). However, many applications of biomaterials, including tissue engineering and cell-based sensors, may prefer the encapsulation of the cell population within the matrix of the material in order to deliver and/or maintain the population to a specific site based upon the degradation characteristics of the material. As has been repeatedly demonstrated, cell encapsulation within biomaterials, especially biomaterials based upon synthetic polymers, poses a significant challenge.

In order to create a cyclic acetal based hydrogel for cell encapsulation, we followed the well described route of incorporating the hydrophilic polymer poly(ethylene glycol) (PEG). Specifically, by including poly(ethylene glycol) diacrylate (PEGDA) within the radical polymerization of the EHD monomer, a water swellable EH-PEG hydrogel has been produced.[219] However, further studies are required to extend this material for cell encapsulation applications.

To this end, a water soluble radical initiation system based on ammonium persulfate (APS) and N,N,N',N'-tetramethylethylenediamine (TEMED) was chosen for the fabrication of EH-PEG hydrogels for bone marrow stromal cell encapsulation. APS is an acidic initiator and when combined with TEMED, a basic accelerator, at

low equimolar concentrations the pH remains within a reasonable range for cell encapsulation.[220] Specifically, TEMED is known to accelerate the homolytic scission of APS yielding sulfate ($SO_4^{\cdot-}$), hemiTEMED ($(CH_3)_2NCH_2CH_2(CH_3)$-$NCH_2^{\cdot}$), and hydroxyl ($^{\cdot}OH$) radical species which initiate crosslinking.[221-223] In addition, the APS-TEMED system has also been used in hydrogel systems as a thermal initiator with high molecular weight polymers for osteogenic applications.[224,225]

In order to develop the EH-PEG hydrogel for cell encapsulation, this paper examines the APS-TEMED initiation system and its effect on bone marrow stromal cells in order to optimize the concentration to be used to initiate crosslinking of EH-PEG hydrogels. Bone marrow stromal cells have the ability to replicate as undifferentiated cells and also the potential to differentiate into a number of lineages such as bone, cartilage, adipose, tendon, ligament, and marrow stroma.[127,128] Due to this property, BMSCs have application in the field of bone tissue engineering which is of interest to our laboratory. Specific objectives of this work were to determine (1) the effect of continuous exposure of the initiator system on the metabolic activity and viability of bone marrow stromal cells, and (2) the effect of short term exposure on expression of osteogenic differentiation markers, and (3) encapsulation potential of bone marrow stromal cells in EH-PEG hydrogels.

6.2 Methods

6.2.1 Materials

α-minimal essential medium, fetal bovine serum (FBS) penicillin-streptomycin antibiotics, Trypsin/EDTA were obtained from Gibco (Carlsbad, CA). Collagenase P was purchased from Roche (Indianapolis, IN). Wistar Hannover rats were purchased from Taconic (Hudson, NY). Ascorbic acid Na-β-glyerophosphate, dexamethasone, ammonium persulfate (APS), N,N,N',N'-tetramethylethylenediamine (TEMED), MTT kit, p-nitrophenyl phosphate liquid substrate system, PEGDA Mn~ 700, 5-ethyl-5-(hydroxymethyl)-β,β-dimethyl-1,3-dioxane-2-ethanol diacrylate (EHD) were purchased from Sigma (St. Louis, MO). The Live/Dead assay and Quant-iT PicoGreen Kit were ordered from Molecular Probes (Carlsbad, CA). The DNeasy Tissue kit and RNeasy Mini Plus Kit were purchased from Qiagen (Valencia, CA). The M-per Mammalian Protein Extraction Reagent was ordered from Pierce (Rockford, IL). The High Capacity cDNA Archive Kit and TaqMan Gene Expression assays were purchased from Applied Biosystems (Foster City, CA).

6.2.2 Bone Marrow Stromal Cell Isolation and Culture

Bone marrow stromal cells were isolated from young Wistar Hannover GALAS male rats weighing 101-125g following NIH guidelines for the care and use of laboratory animals and under a University of Maryland approved IACUC animal protocol (R-04-61). Rats were euthanized with CO_2 and the femurs as well as tibias excised and cleaned of soft tissue. The femurs and tibias from each rat were washed

three times in 10mL of control media (without FBS) with 10% penicillin/streptomycin (v/v) under sterile conditions. The epiphyseal plates were clipped and the bone marrow was flushed from the bone using 10 mL of control medium (without FBS) and filtered from a syringe, homogenized by mixing with the syringe, and passed through a 70 μm cell strainer. After centrifugation at 300g for 8 minutes, the pellet was resuspended in 10 mL of control media and plated in a T-75 flask, with each flask containing BMSCs from only one subject. The media was changed every 2 days and non-adherent cells were washed away after two media changes.

Cell culture control media consisted of α-minimal essential medium supplemented with 10 % (v/v) FBS, 0.2 mM ascorbic acid, and 1% (v/v) penicillin-streptomycin antibiotics. Osteogenic media was control media further supplemented with 10 mM Na-β-glyerophosphate and 10^{-8} M dexamethasone. Cell cultures were maintained in an incubator at 37^{o}C with 5% CO_2 and passaged every 5-7 days using Trypsin/EDTA and 2.0% w/v Collagenase P.

6.2.3 Metabolic Activity

Bone marrow stromal cells were harvested and cultured as described above. Cells were lifted, pooled, and plated at 1 x 10^5 cells/well in a 24-well plate and allowed to attach for 24 hours. At this time, the media was removed and cells were then exposed to the initiator system consisting of APS and TEMED at 10 mM, 15 mM, and 20 mM (final concentration of each initiator in control media) for 30 min, 1 hr, and 3 hr in the incubator with a control at each timepoint consisting of control

media and 0 mM initiators. Metabolic activity was then assessed using a dimethylthiazolyldiphenyltetrazolium bromide (MTT) based *in vitro* toxicology kit following standard protocols. Briefly, 100 µL of MTT reconstituted in control media (without FBS) was added to the cultures and returned to the incubator. After 2.5 hr, the formazan crystals were solubilized and read at 570 nm using a GENESYS10 spectrophotometer (Thermo Electron). The study was completed with four replicates (n = 4).

6.2.4 Viability

Bone marrow stromal cells were harvested and cultured as described above. Cells were lifted and plated in 96-well plates at 4 x 10^4 cells/cm^2 and allowed to attach for 24 hours. The media was then removed and cells were then exposed to APS and TEMED at 10 mM, 15 mM, and 20 mM (final concentration of each initiator in control media) for 30 min, 1 hr, and 3 hr in the incubator with a control at each timepoint consisting of control media and 0 mM initiators. Viability was assessed using the Live/Dead assay according to standard protocols. The media was removed, the Live/Dead reagents were added (4µm ethidium homodimer-1 and 2 µm calcein AM) and incubated at room temperature for 30 min. Micrographs were then taken using a fluorescent microscope (Axiovert 40 CFL with filter set 23, Zeiss, Thornwood, NY) equipped with a digital camera (Diagnostic Instruments 11.2 Color Mosaic, Sterling Heights, MI). The study was completed with three replicates (n = 3).

6.2.5 Differentiation

In order to simulate the initiator exposure the cells would experience during the encapsulation process, bone marrow stromal cells were exposed in monolayer to increasing concentrations of the initiator system for the approximate time it takes the gels to form. However, it is important to note that during encapsulation the cell population may be exposed to an initiator concentration less than the initial concentration, due to the fact that the initiator is being used in the crosslinking reaction. After exposure, the flasks were then washed with PBS to remove any residual initiator, similar to the procedure utilized after a gel is formed and before it is cultured.

Bone marrow stromal cells were then harvested and cultured as describe above, and passaged once. Cells were exposed to APS and TEMED at 10, 15, and 20 mM, final concentration of each initiator in control media, in T-75 flasks for 1 min. (The 1 min exposure time was based upon the approximate gelation time of the EH-PEG hydrogel using the APS/TEMED system. Gelation time was characterized by creating a 1 mL gel in a 15 mL Falcon tube using a 1:50 molar EHD:PEGDA with an initiator concentration of 15 mM. Gelation was then determined to be complete when the Falcon tube could be inverted and the gel components remained at the tip of the tube.) After exposure, the cells were washed three times with 10 mL of PBS. All flasks were then returned to the incubator with control media for 2 d. At this time, the cells were lifted, and plated in 6-well plates at 1.5×10^5 cells/well. All experimental groups and a positive control, which did not contain any initiator chemicals, were cultured using osteogenic media described above. A negative

control consisted of control cell culture media and no initiator chemicals. At 1, 4, and 8 d BMSCs were lifted and analyzed using the assays described below.

6.2.5.1 Deoxyribonucleic Acid Quantification

Deoxyribonucleic acid (DNA) was isolated from all samples to normalize the alkaline phosphatase assay described below. Specifically, DNA was isolated using the DNeasy Tissue kit following standard protocols into 400 μL of eluate. DNA was then quantified using the Quant-iT PicoGreen Kit following standard protocols for a 200 μL sample volume. Samples were incubated at room temperature for 5 minutes and read using the M5 SpectraMax plate reader (Molecular Devices, Sunnyvale, CA) with excitation/emission of 480/520 nm. All samples were completed in triplicate (n = 3).

6.2.5.2 Alkaline Phosphatase Assay

BMSCs were lifted and centrifuged at 2,500g for 10 min to form a pellet. Protein was extracted using the M-per Mammalian Protein Extraction Reagent following standard protocols. Briefly, 50 μL of M-per was added to each cell pellet, and shaken for 10 min. Cell debris was removed by centrifugation at 14,000g for 15 min and the supernatant was used for analysis. A p-nitrophenyl phosphate liquid substrate system (pNPP) was used to analyze intracellular alkaline phosphatase (ALP) concentrations from the extracted protein. Briefly, the extracted protein sample was suspended in PBS and added to 100 μL of pNPP and incubated at room temperature for 30 min. The reaction was stopped by adding 50 μL of 2M NaOH. The

absorbance was read using a M5 SpectraMax plate reader at 405 nm and normalized by the PicoGreen assay. All samples were completed in triplicate (n = 3).

6.2.5.3 Gene Expression

BMSCs were lifted and RNA was isolated using the RNeasy Mini Plus Kit following standard protocols. The isolated total RNA was reverse transcribed using High Capacity cDNA Archive Kit. The expression of 18S, ALP, and osteocalcin was then investigated by quantitative real time polymerase chain reaction (qrt-PCR) on an ABI Prism 7000 sequence detector (Applied Biosystems). The primer and probe sequences, designed by our laboratory, used for osteocalcin included GGCTTCCAGGACGCCTACA (forward primer), GGGCAACACATGCCCTAAAC (reverse primer), and CGCATCTATGGCACCAC (probe). A TaqMan Gene Expression assay was used to analyze ALP, while a predeveloped 18s rRNA was used as the endogenous control. The sequences for the 18s and ALP primers and probes are proprietary. All samples were completed in triplicate (n = 3).

6.2.6 EH-PEG Hydrogel Encapsulation

To determine the effect of the encapsulation process on the viability of bone marrow stromal cells, cells were encapsulated, cultured, and analyzed using the LIVE/DEAD assay. Specifically, the EH-PEG hydrogel constructs were prepared in a sterile environment using aseptic technique. The two components used were EHD and PEGDA Mn~ 700 at 1:50 molar EHD to PEGDA. APS and TEMED solutions were prepared and sterile filtered, a final concentration of 15 mM was used in the

gels, with a component to solvent ratio of 1:2 (water was used as the solvent). BMSCs were suspended in the gel solution at 2 x 10^6 cells/mL. All components were vortexed together and a 12-well plate was used as a mold to create gels 2 mm thick. The crosslinking reaction was complete in approximately 1 min, smaller gel disks were punched out with a cork borer to create gels that were 6 mm in diameter. The disks were washed in PBS for 15 minutes. Gels were cultured in control media and analyzed immediately after encapsulation and 7 d post-encapsulation. On d 7, the gels were soaked in PBS for 1 hr to remove FBS from the gel which can interact with the Live/Dead reagents. The gels were incubated with the Live/Dead reagents (2.5 μm ethidium homodimer-1 and 2.5 μm calcein AM) and incubated at room temperature for 30 min. Micrographs were then taken using a fluorescent microscope equipped with a digital camera. Viability of the gels was then determined using ImageJ (v1.37) cell counter plugin available from the National Institutes of Health. All samples were completed in triplicate. (n=3)

6.2.7 Statistical Analysis

Data from all studies was analyzed using ANOVA single factor analysis and Tukey's multiple comparison test ($p \leq 0.05$). All results are reported as mean ± standard deviation. In order to confirm the reproducibility of the observed trends, two identical and independent studies were performed. Statistical analysis was performed within studies, but not across studies to elucidate trends and differences between groups. Results and overall trends from the two studies were similar;

however, data was not pooled as the primary cell populations were used in these studies are variable in nature. Therefore, only data from the second study is reported.

6.3 Results

6.3.1 Metabolic Activity and Viability

Bone marrow stromal cells were exposed continuously to the initiator system for 30 min, 1 hr, and 3 hrs to determine whether there was an effect on cell metabolic activity (Figure 12). After 30 min and 1 hr of exposure, the 10 mM and 15 mM initiator experimental groups showed a metabolic activity that was not statistically different ($p<0.05$) from the control. At the longer time point of 3 hr, the 10 mM and 15 mM groups were still not statistically different ($p<0.05$), however they were significantly less than the control. In all cases the metabolic activity of the 20 mM group was significantly less than the control and the 10 mM and 15 mM initiator concentrations. Across all timepoints, the groups with higher initiators concentrations had lower metabolic activity than those with lower concentrations of initiator or the control groups.

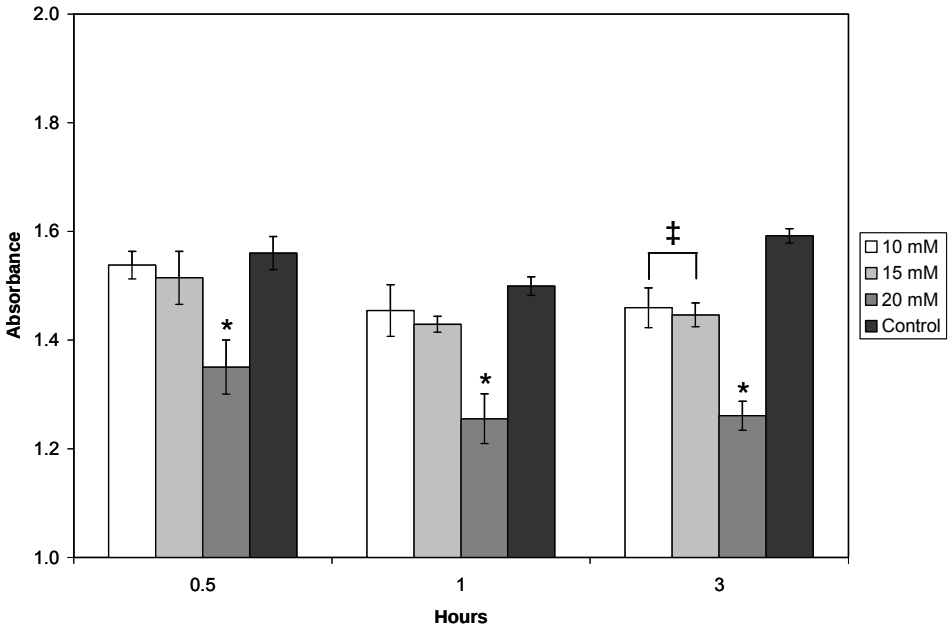

Figure 12: Metabolic activity of BMSCs assessed after 30 min, 1 hr, and 3 hr with initiator system concentrations of 10 mM, 15 mM, and 20 mM. Results indicate that over the shorter time points the metabolic activity of BMSCs exposed to initiator concentrations of 10 mM and 15 mM did not differ from the control group. * indicates statistical difference, ‡ indicates no statistical difference. (Values reported as mean ± standard deviation, n = 4.)

Similarly, the viability of bone marrow stromal cells was also assessed in monolayer after exposure to the initiator system. Results qualitatively showed that after 30 min and 1 hr of initiator system exposure, BMSCs viability appeared similar across all initiator concentrations (See Figures 13 and 14; note that 1 hr images are not presented for brevity). For all time points, some non-viable cells are apparent in the experimental groups, with higher numbers apparent in the higher concentrations, and there are morphological changes in the exposed cells. However, in all groups, the majority of the cells are still viable. At the later time point (3 hr), the LIVE dye, calcein, appears to be localized in certain areas within the cells, although they still appear viable.

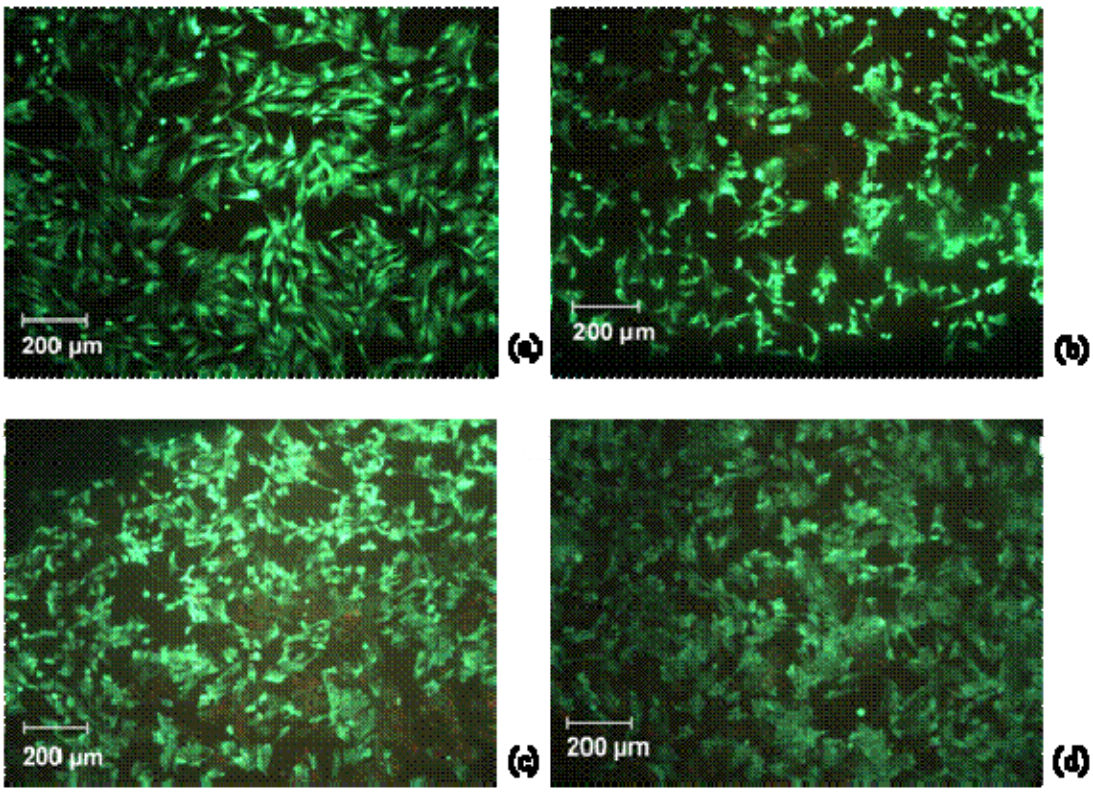

Figure 13: Viability of bone marrow stromal cells assessed after 30 min exposure to initiator system concentrations of (a) 0 mM, (b) 10 mM, (c) 15 mM, and (d) 20 mM by LIVE/DEAD assay. The microscope images qualitatively demonstrate that a 30 min continuous exposure to the initiator system appears to have little effect on the bone marrow stromal cells, and demonstrate viability similar to the control group. (n = 3)

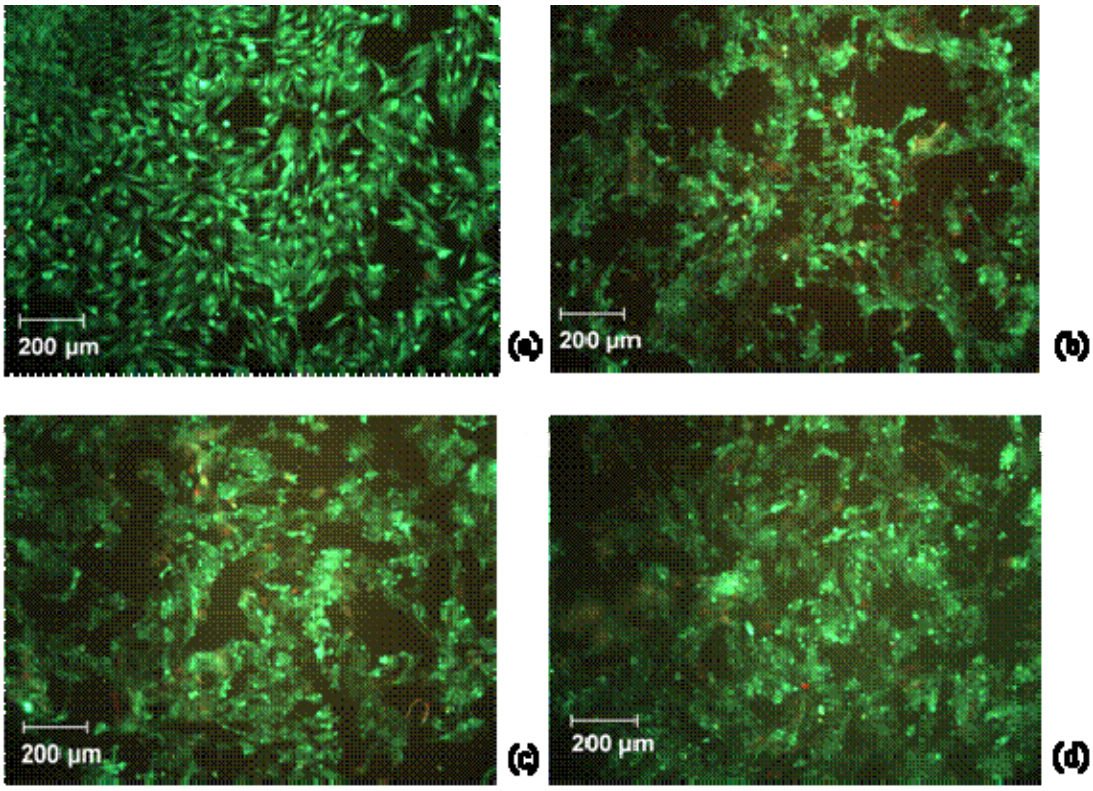

Figure 14: Viability of bone marrow stromal cells assessed after 3 hr with initiator system concentrations of (a) 0 mM, (b) 10 mM, (c) 15 mM, and (d) 20 mM by LIVE/DEAD assay. The microscope images qualitatively demonstrate that continuous exposure to the initiator system for 3 hr appears to have a minimal effect on the bone marrow stromal cell viability. (n = 3)

6.3.2 Osteodifferentiation

Bone marrow stromal cells were exposed to the initiator system for 1 min to simulate the encapsulation process. Differentiation was initiated and the early osteogenic marker alkaline phosphatase was measured to determine if the encapsulation process had an effect on osteodifferentiation (Figure 15). Results showed that after 1 d, the ALP expression of the osteogenic control was not statistically different ($p<0.05$) from the 10 mM experimental group. However, the ALP expression of the 15 mM and 20 mM groups were significantly less than that of the osteogenic control. For this early time point, the higher initiator concentrations

had lower expressions of ALP when compared to experimental groups with lower initiator concentrations. After 4 and 8 d, the ALP expression of the osteogenic control was not statistically different ($p<0.05$) from all experimental groups.

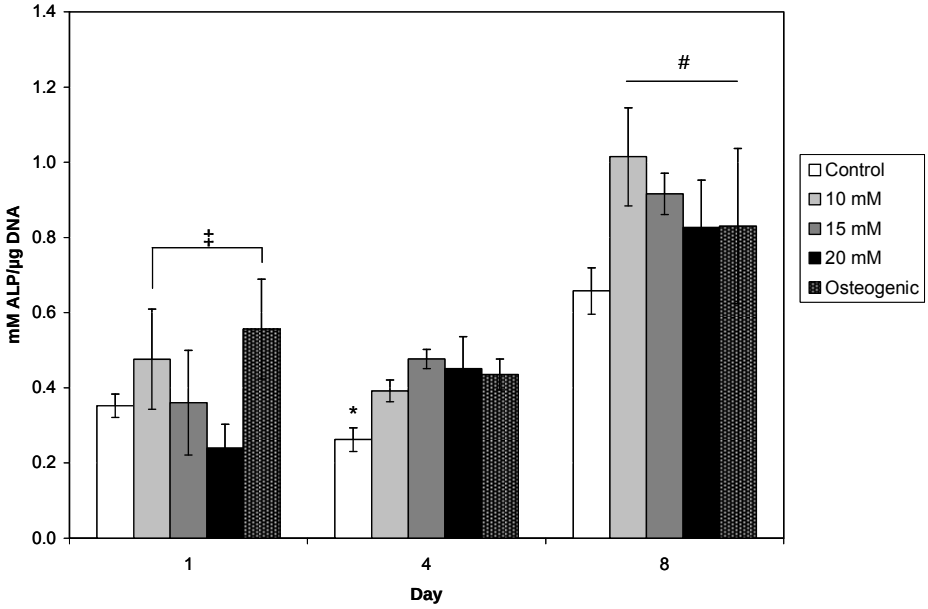

Figure 15: Alkaline phosphatase expression of cells after 1 d, 4 d, and 8 d, normalized by DNA. After 1 d, there was an early effect from the initiator system at higher concentrations on differentiation. However, after 4 d and 8 d all experimental groups are similar to the osteogenic groups indicating that there are no long term effects for alkaline phosphatase activity on this time scale. * indicates statistical difference, ‡, # indicate no statistical difference. (Values reported as mean ± standard deviation n = 3)

To further asses the effect of the encapsulation process on differentiation, osteogenic markers alkaline phosphatase and osteocalcin were also measured at the mRNA level after exposure to the initiator system. Results demonstrated that after 1 d, all the experimental groups had an ALP expression that was not statistically different ($p<0.05$) from the osteogenic control (Figure 16). After 4 d, the ALP expression of the osteogenic control is not statistically different ($p<0.05$) from the 10 mM and 15 mM groups, while the ALP expression of the 20 mM experimental group is statistically higher than the osteogenic control. After 8 d, the ALP expression of the 20 mM group was not statistically different ($p<0.05$) from the osteogenic control,

while the 10 and 15 mM groups had significantly higher expression than the osteogenic control. In regards to the osteocalcin marker (Figure 17), after 1 d the osteogenic control was not statistically different ($p<0.05$) from the osteocalcin mRNA expression as the 15 mM group. However, the 10 mM and 20 mM group's osteocalcin expression was significantly higher than the osteogenic control at this timepoint. After 4 d, all experimental groups had significantly higher osteocalcin expression than the osteogenic control. Finally after 8 d, osteocalcin expression was significantly higher for all experimental groups compared to the negative control.

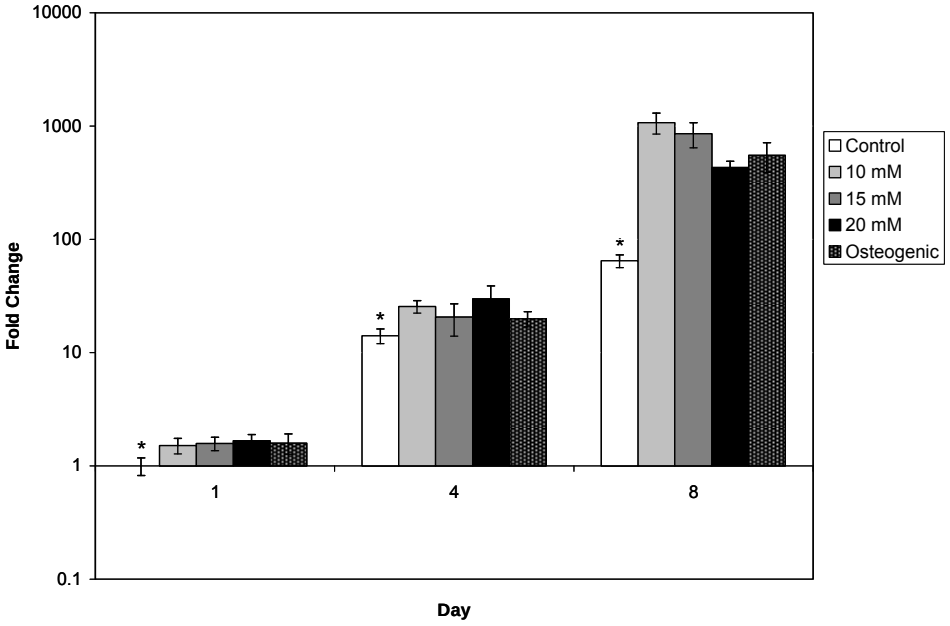

Figure 16: Quantitative rt-PCR analysis of alkaline phosphatase expression after 1 d, 4 d, and 8 d. At all concentrations tested the initiator system did not have a negative effect on the expression of alkaline phosphatase. * indicates statistical difference. (Values reported as mean ± standard deviation n = 3)

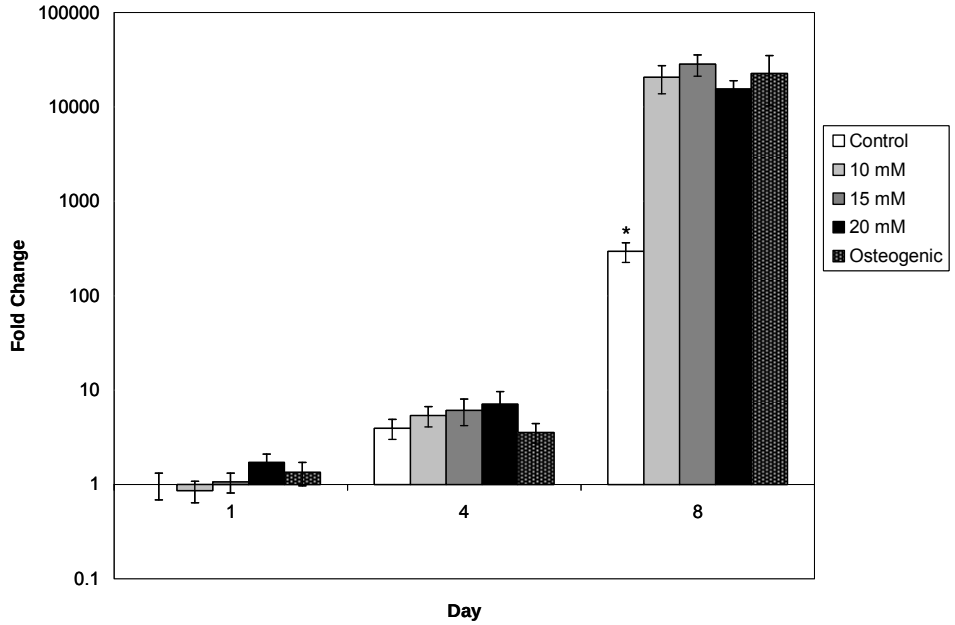

Figure 17: Quantitative rt-PCR analysis of osteocalcin expression after 1 d, 4 d, and 8 d. All experimental groups were higher than the negative control, indicating that exposure to the initiator system allows osteodifferentiation as demonstrated by osteocalcin levels. (Values reported as mean ± standard deviation n = 3)

6.3.3 EH-PEG Hydrogel Encapsulation

To determine the encapsulation potential of bone marrow stromal cells, cells were suspended in sterile liquid gel components and crosslinked using an initiator concentration of 15 mM (Figure 18). Micrographs were quantified and the viability of the encapsulated cells immediately after crosslinking was 86.3% ± 2.6 demonstrating that they are able to withstand the encapsulation process. After 7 d, the viability slightly decreased to 80.2% ± 1.2; however, the majority of the cells were still viable.

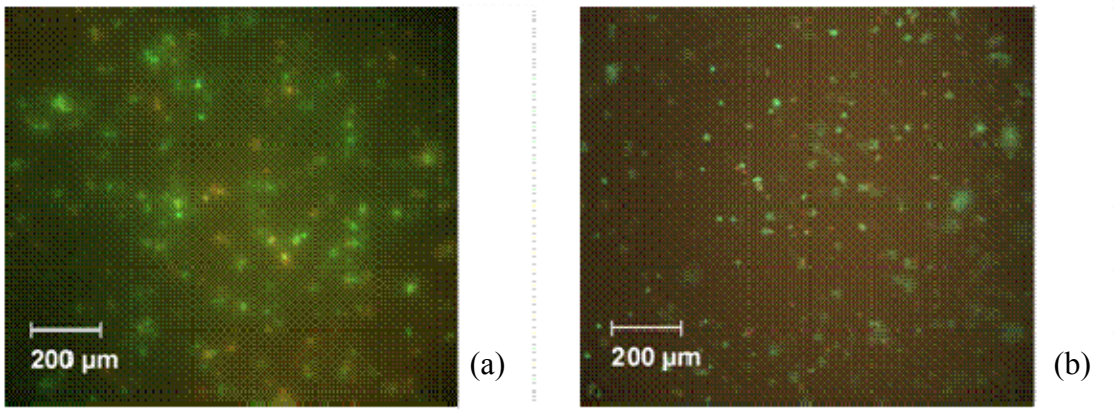

Figure 18: Viability of EH-PEG hydrogel encapsulated BMSCs immediately after encapsulation (a) and after 7 d of culture by LIVE/DEAD assay. Immediately after encapsulation, the image qualitatively shows that the majority of the cells are alive, (quantified to be 86.3% ± 2.6) demonstrating that many of the cells can survive the encapsulation process. After 7 d of culture, the images qualitatively demonstrate that the majority of the cells are still viable (quantified to be 80.2% ± 1.2) within the EH-PEG hydrogels. (n = 3)

6.4 Discussion

The objectives of this work were to determine (1) the effect of continuous exposure of the initiator system on the metabolic activity and viability of bone marrow stromal cells, and (2) the effect of short term exposure on expression of osteogenic differentiation markers. From these first two objectives, we anticipated that the results would indicate an appropriate initiator concentration to encapsulate bone marrow stromal cells in our EH-PEG hydrogel system. Therefore, we finally aimed to demonstrate the encapsulation potential of bone marrow stromal cells in EH-PEG hydrogels.

Results indicate that over the shorter time points the metabolic activity of bone marrow stromal cells exposed to initiator concentrations of 10 and 15 mM did not differ from the control group (Figure 12). This continuous exposure is

considerably longer than the length of time required to form a hydrogel using this initiation system and components (approximately 1 min). Furthermore, the optimal concentration chosen to form the hydrogels (see discussion below) was 15 mM which did show significantly different metabolic activity from the control group until continuous exposure of 3 hr. Furthermore, microscope images of the Live/Dead assay qualitatively demonstrate that bone marrow stromal cells remain viable after continuous exposure to increasing concentrations of the initiator system. A few non-viable cells were apparent at all timepoints, although the majority of the cells remained viable. The morphology of the cells did appear to change slightly over the longer timepoints indicating the continuous exposure to the initiator system was having an effect on the cells. Specifically, it appears the calcein is being compartmentalized within the membrane-enclosed structures of the cells due to an increase of the dye within the cell. This could be an indication of a compromised cell membrane allowing more dye into the cells. Furthermore, the integrity changes of the membrane could be responsible for altering cell morphology in cells exposed to the initiator system. However, overall the data indicates that the initiation system at the desired concentration does not have a detrimental effect on the metabolic activity or viability of the cell population in monolayer.

The osteodifferentiation of bone marrow stromal cells in monolayer was then assessed after a 1 min exposure to the initiation system, again chosen to simulate the length of time it takes for the EH-PEG hydrogels to crosslink using an initiator concentration of 15 mM. Alkaline phosphatase levels were first assayed. Results demonstrated that high initiator concentrations may have some initial affects upon

ALP expression (Figure 15). However, on d 4 and d 8 all experimental groups are similar to the osteogenic groups indicating that these effects may be transitory. The data does not specifically indicate whether this recovery is achieved on an individual or population basis. The micrographs generally indicate a uniform response by the cell population, so there is some small evidence that the BMSC population may recover without individual cell death on a significant level.

Osteodifferentiation was also assayed by alkaline phosphatase mRNA level using qrt-PCR. This data reported that after 1 d, all experimental groups were not statistically different ($p<0.05$) from the osteogenic control (Figure 16), in contrast to trends measured at the protein level. This result implies that while mRNA production is minimally affected by the initiator system, downstream protein expression may be more sensitive to the initiator system. As described above, after 4 and 8 d all experimental groups were not statistically different ($p<0.05$) from the osteogenic control, suggesting that the recovery described above may be realized in mRNA translation or further downstream processing. Also, there is an apparent trend where the experimental groups express ALP at higher levels than the osteogenic control; however this difference is significantly less than that compared to the negative control. Finally, osteocalcin results from the later stage of osteodifferentiation largely support the trends described by the ALP expression data that exposure to the initiator system allows osteodifferentiation as demonstrated by mRNA levels.

The objective of the first part of this work was to optimize the concentration to crosslink EH-PEG hydrogels. Continuous exposure of BMSCs to the initiator system at concentrations of 10 mM and 15 mM demonstrated cell viability and

metabolic activity at levels similar to the control group. In addition, the protein and gene expression data collectively shows that BMSC exposure to the initiator system at concentrations of 10 mM and 15 mM groups performed similarly to the osteogenic control group for all time points and all genes. From these results, we concluded that future studies could be achieved using an initiator system concentration ranging from 10 mM to 15 mM. However, as hydrogel gelation time generally decreases with an increase in initiator concentration, we chose to proceed using an initiator system with a 15 mM concentration.

Using this system, the viability of BMSCs was assessed after EH-PEG hydrogel encapsulation. Results indicate that immediately after encapsulation, the majority of the cells are viable and therefore a large percentage of the encapsulated BMSC population can remain viable after exposure to the radical polymerization of the EH-PEG network. After 7 d, the BMSCs still demonstrate significant cell viability within the EH-PEG hydrogel. Published literature on short-term culture studies of adult human mesenchymal stem cells encapsulated within hydrogels indicate cells within Collagen-Agarose maintained viability within the range of 75-90% for 8d[226], and exhibited a viability of approximately 75% after 7d within PEGDA with RGD.[227] Our data from 7d appears to lie within the acceptable range of what has been published and what may be expected of a tissue engineered construct.

Previous work in this field has demonstrated that the APS-TEMED system can be used to crosslink hydrogels for bone tissue engineering applications through histological and biochemical assays for differentiation markers while varying

polymer components.[224,225] However, this work investigates the effect the initiator system will have on the encapsulated cell population, and elucidates that the downstream ALP protein expression may be more sensitive to the initiator system as shown by the difference between the biochemical assay and the qrt-PCR data. This study determined the optimal concentration of the initiator system to use for encapsulation to minimize differentiation effects, specifically for use with the EH-PEG hydrogel developed in our laboratory. This hydrogel is advantageous over other hydrogel systems because it is based upon a cyclic acetal unit which primary degradation products should not affect local acidity unlike most synthetic hydrogels.

6.5 Conclusions

The objective of this study was to determine whether EH-PEG hydrogels, and their fabrication components, permit bone marrow stromal cell viability, metabolic activity, and osteodifferentiation. The results demonstrate that the metabolic activity and viability of bone marrow stromal cells in monolayer are minimally affected by the APS-TEMED initiator system for extended time periods. In addition, it shows that on the time scale required for encapsulation, the initiator system does not significantly affect expression of osteogenic markers, measured both at the mRNA and protein level. From these results, an optimal initiator concentration can be chosen to crosslink EH-PEG hydrogels. Finally, encapsulated bone marrow stromal cells were shown to survive in EH-PEG hydrogels crosslinked using the optimal APS-TEMED concentration for 7 d. This demonstrates that EH-PEG hydrogels are a viable option for encapsulation and osteodifferentiation of bone marrow stromal cells.

Chapter 7: Tissue Response and Orbital Floor Regeneration Using Cyclic Acetal Hydrogels[4]

7.1 Introduction

Orbital floor injuries, most commonly caused by assault and traffic accidents, are a devastating form of craniofacial trauma.[110,111] In addition, they account for approximately 60-70% of all orbital fractures.[113,228] Orbital bone fractures, if left untreated, may not heal adequately through standard primary and secondary bone healing mechanisms. In orbital fractures, only small and thin bone fragments might be present and there are generally few bony edges to conduct bone formation. Instead, a fibrous scar forms, lacking the support, architecture, and load bearing properties of bone. Therefore, the endogenous response to orbital fractures, in contrast to many other bone fractures, is not sufficient for proper healing. Furthermore, a number of sequelae are associated with orbital floor injuries, the most common being unsatisfactory facial aesthetics, enophthalmos (sunken eye), and diplopia.[112,124,229]

The orbital floor is composed of portions of three bones, the maxilla, zygomatic, and palantine[107,108]. The main purpose of the floor is to separate the orbital contents from the maxillary sinus and it is therefore very thin, approximately 0.5 mm[107,230]. The thinness of this structure makes it an excellent model for *in vitro* tissue engineering as experiments are able to be performed without the need for

[4] As Published in MW Betz, JF Caccamese, DP Coletti, JJ Sauk, and JP Fisher. Tissue Response and Orbital Floor Regeneration Using Cyclic Acetal Hydrogels. Journal of Biomedical Materials Research, Part A. In Press. (Epub 2008 Jul 9)

bioreactors and additional attention to diffusion which is necessary in larger tissue engineered constructs.

Various reconstructive clinical treatments have been employed for orbital floor repair including poly (tetrafluoroethylene) (Teflon)[231], poly(ethylene) sheets (Medpor)[232-234], titanium mesh[235,236], and bone grafts[118,119,122]; however, these have been associated with lifelong risk of infection, loss of function, extrusion, as well as poor aesthetics[237]. The ideal implant would be resorbable, encourage bony healing of the orbital floor, and not threaten the globe in subsequent orbital trauma. For this reason, and the above mentioned complications with current strategies, tissue engineering methods employing polymers may be a promising strategy for the treatment of orbital floor defects. Many tissue engineering strategies utilize natural polymers such as agarose[204,205], alginate[206,207], chitosan[149,208,210], collagen[211,212], hyaluronic acid[213,214], and silk[215,216]. However, natural polymers tend to have variable composition between batches and often do not possess sufficient mechanical strength in hard tissue engineering applications.[238] Synthetic biomaterials have been investigated due to their reproducibility and modification capability. These biomaterials can often be engineered to preferred properties, including mechanical stiffness and biodegradability. To this end, synthetic polymers have been developed, including poly(D,L-lactic acid-co-glycolic acid)[45,46], poly(ε-caprolactone)[51], poly(propylene fumarate)[42,54], and poly(vinyl alcohol).[217] While a number of polymers are currently under investigation for tissue engineering applications, an ideal biomaterial with favorable tissue response and cellular interactions, mechanical strength, degradation and degradation products, has not been developed.

Our laboratory has developed a class of biomaterials based upon a cyclic acetal unit. These materials may be advantageous since the cyclic acetal unit degrades by hydrolysis into primary degradation products of diols and carbonyls, and thus may not experience a change in local acidity associated with many degradable synthetic biomaterials. The acidity of hydrogel degradation products may be a concern, for the stable phenotypic function of embedded cell populations, or surrounding tissue when implanted *in vivo*. A cyclic acetal biomaterial in the form of a rigid plastic may be fabricated from the radical polymerization of the monomer 5-ethyl-5-(hydroxymethyl)-β,β-dimethyl-1,3-dioxane-2-ethanol diacrylate (EHD) (Figure 19b).[218] This biomaterial has been shown to have controllable physical properties and can support the surface adhesion of bone marrow stromal cells (BMSCs).[218]

To create a cyclic acetal based hydrogel that could be used for cell embedding and also growth factor delivery, we used the well described route of incorporating the hydrophilic polymer poly(ethylene glycol) (PEG). Specifically, by including poly(ethylene glycol) diacrylate (PEGDA) (Figure 19a) within the radical polymerization of the EHD monomer, a water swellable EH-PEG hydrogel has been produced.[159] A water soluble radical initiation system based on ammonium persulfate (APS) and N,N,N',N'-tetramethylethylenediamine (TEMED) was chosen for the fabrication of EH-PEG hydrogels. Previous work with this system has demonstrated that the metabolic activity, viability, and osteodifferentiation of BMSCs are minimally affected by APS and TEMED.[239] In addition, BMSCs were shown to

maintain viability in EH-PEG hydrogels for 7 d indicating this is a viable bone tissue engineering system.[239]

The overall objective of this work is to examine the utility of EH-PEG hydrogels in orbital bone repair. To this end, we broadly investigated the tissue response to an unmodified EH-PEG hydrogel as well as an EH-PEG hydrogel loaded with bone morphogenetic protein-2 (BMP-2). BMP-2 is well known to facilitate formation of bone *in vivo*[240] , and induces bone regeneration after injury[144] which is thought to be due to the fact that BMP-2 can direct the differentiation of mesenchymal stem cells into osteoblasts.[241] However, BMP-2 is known to have a limited half-life requiring a carrier or high doses to maintain activity and therapeutic levels.[242,243] Previous work has combined BMP-2 with the glycosaminoglycan heparin[244], and dextran-based polysaccharides[243]. Our laboratory will investigate BMP-2 adsorption onto EH-PEG hydrogels to prolong activity in an aqueous environment. Therefore, specific objectives of this work were to (1) investigate the tissue response surrounding EH-PEG gels *in vivo*, (2) examine the release of a BMP-2 from EH-PEG gels, and (3) investigate the ability of EH-PEG hydrogels to deliver BMP-2 *in vivo* and facilitate bone formation.

7.2 Methods

7.2.1 Materials

Ammonium persulfate (APS), N,N,N',N'-tetramethylethylenediamine (TEMED), PEGDA Mn~ 700, 5-ethyl-5-(hydroxymethyl)-β,β-dimethyl-1,3-dioxane-2-ethanol diacrylate (EHD), bovine serum albumin (BSA) were purchased from

Sigma (St. Louis, MO) Recombinant human BMP-2 (containing BSA as a carrier), and a Quantikine BMP-2 immunoassay ELISA kit were purchased from R&D Systems (Minneapolis, MN). OCT embedding compound and SuperFrost glass slides were purchased from Fisher Scientific (Pittsburgh, PA).

7.2.2 Hydrogel Formation

The EH-PEG hydrogel constructs were prepared in a sterile environment using aseptic technique. The two components used were EHD and PEGDA (Figure 19) at 1:50 molar EHD to PEGDA with a total 10% w/v in water. APS and TEMED solutions were prepared and sterile filtered, a final concentration of 15 mM was used in the gels. All components were vortexed and a large Petri dish was used as a mold to create gels 2 mm thick. The crosslinking reaction was complete in approximately 1 min, and PBS was used to wash the surface of the gel. Smaller gel disks were punched out with a sterile cork borer to create gels that were 12 mm in diameter. The gels were then stored in PBS at 4^{o}C until use.

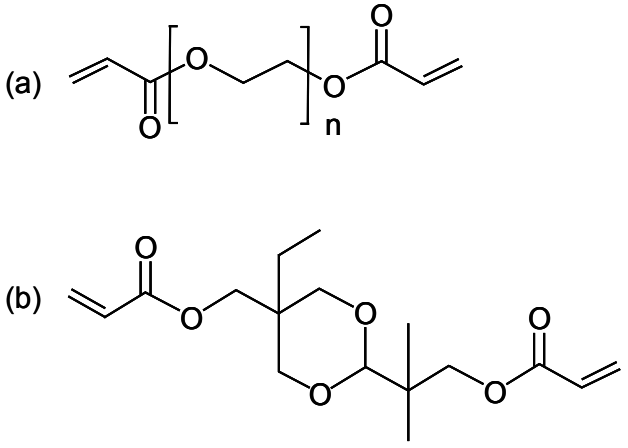

Figure 19: Chemical structures of (a) PEGDA where average Mn ~ 700 and (b) EHD.

7.2.3 BMP-2 Loading

The hydrogels were loaded with BMP-2 in a sterile environment approximately 12 hours before use. Specifically, hydrogels were patted dry to remove surface PBS. Next, to load each hydrogel, a concentrated solution containing a final concentration of 0, 0.25, or 2.5 μg BMP-2/implant resuspended in 4 mM HCl with 0.1% BSA was added to the top of the hydrogel. Each implant received the same amount of suspension solution to minimize effects that may be caused by BSA. Gels were then left in the biosafety cabinet for 30 minutes to evaporate the majority of the suspension solution. Gels were then placed in falcon tubes overnight at 4^{o}C.

7.2.4 BMP-2 Release Study

Hydrogel constructs were created and loaded with BMP-2 as described above. The constructs were then placed in 1.5 mL of PBS at 37^{o}C and assayed at 0.25, 0.5, 0.75, 1, 2, 4, 6, and 12 h for BMP-2 using a quantikine ELISA kit according to the manufacturer's instructions and read using a M5 SpectraMax plate reader (Molecular Devices, Sunnyvale, CA). Percentage of BMP-2 released was calculated as (ng BMP-2 released/ng BMP-2 loaded) x 100. (n=5)

7.2.5 Rabbit Orbital Defect Model

All work was performed following animal protocols approved by the University of Maryland Medical School IACUC as well as the University of Maryland College Park IACUC. In addition, all work was performed in AAALAC approved animal

facilities at the University of Maryland Medical School and under veterinary supervision. Briefly, adult male, New Zealand White rabbits (3.0 – 3.5 kg) were anesthetized with intramuscular injection (0.6 ml/kg) of a solution of 91% ketamine hydrochloride (100 mg/ml; Ketaset, Aveco Co.) and 9% xylazine (20 mg/ml; Rompun, Mobay Corp.). A 0.1 ml dose of the anesthesia cocktail was injected intramuscularly as needed for continued anesthesia. The animals were placed on their side and covered with sterile drapes. The surgical site was prepped and draped in the usual sterile/surgical fashion. An infraorbital surgical approach was performed to access the orbital floor. Using a rotary instrumentation and round burs, the perimeter of the socket floor was cut, thus releasing the socket floor. An 8 mm defect, approximately 50% of the surface area of the socket floor, was then removed (Figure 20).

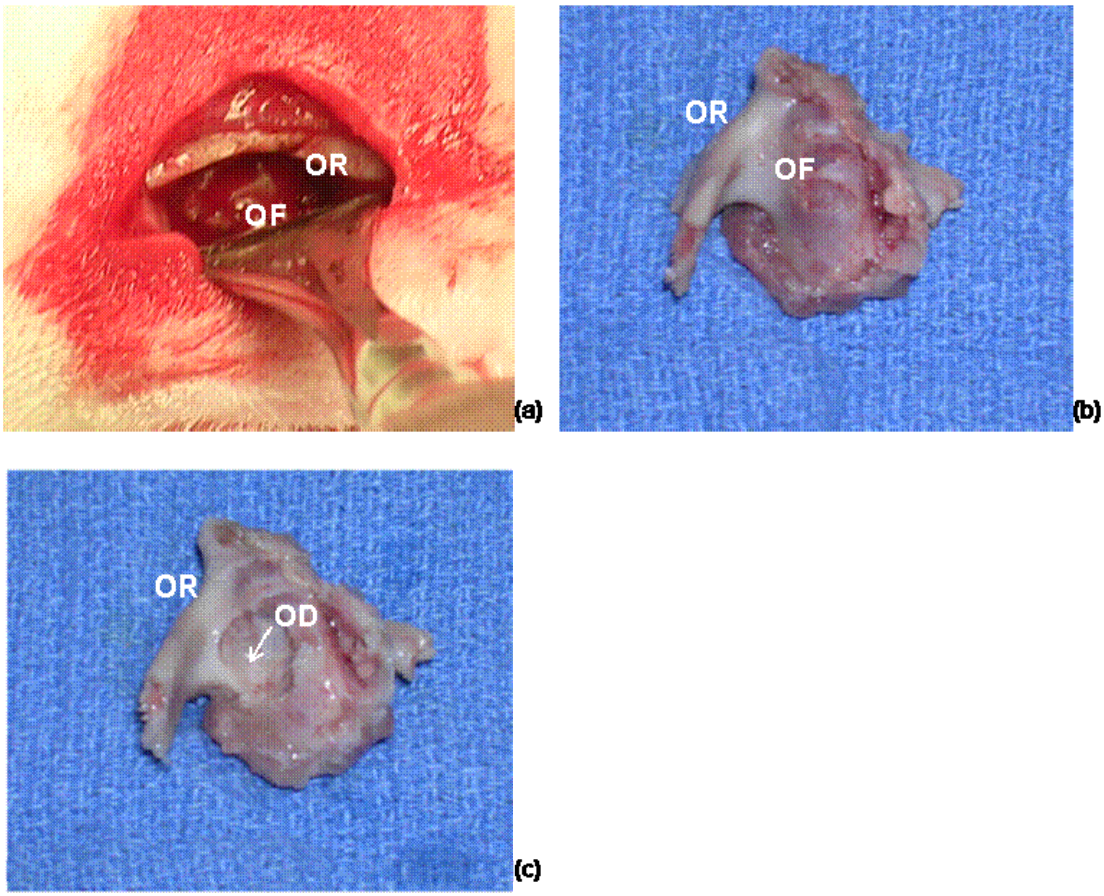

Figure 20: Surgical field (a), intact orbital floor (b), and orbital floor defect (c). OR: orbital rim, OF: orbital floor, OD: orbital defect.

Copious saline irrigation was administered as needed to prevent adjacent tissue necrosis. For the experimental group and the control groups, the defect was closed by implanting the hydrogel construct along the orbital floor with the top of the gel facing the globe. Following current clinical procedures with many biomaterial implants, no fixation device was utilized to keep the implant in place. Soft tissue was replaced and sutured as necessary. The total length of the surgery was approximately 10 minutes. The animals were allowed to recover on a water heating pad and covered with a blanket. Once ambulatory, the animals were given 0.03 mg/kg of buprenorphine HCl subcutaneously for pain, returned to their cages, and allowed to move and feed freely.

The following day during routine follow-up, the animals were given an additional 0.03 mg/kg of buprenorphine HCl subcutaneously. The rabbits were observed post-operatively twice daily until the end of the experiment.

7.2.6 Euthanasia and Tissue Harvest

The animal subjects were then euthanized to allow for tissue harvest. Briefly, a dose of a ketamine, acepromazine cocktail was first given for deep sedation. After sedation, an intravenous injection of an overdose of a pentobarbital preparation (100 mg/kg) was given to euthanize the animal. The sample and surrounding bone tissue were then dissected intact using a surgical saw and scalpel.

7.2.7 Tissue Preparation

The harvested tissues were immediately placed into 120 ml of freshly prepared paraformaldehyde-lysine-phosphate (PLP) fixative solution at a pH of 7.4 for 48 hours. Samples were removed from the PLP fixative, and rinsed 5 times in 0.01M PBS (pH 7.4). A 5% (v/v) formic acid solution was used as the decalcifying agent for the bone tissue. Samples were removed from the PBS and placed into the 5% formic acid decalcifying solution. The solution was changed daily until the decalcification process was complete (approximately 4 and 6 days). The end point was reached when confirmed by ammonium hydroxide/ ammonium oxalate testing and the samples were easily cut with a razor blade. Samples were then removed from the 5% formic acid solution, and rinsed 5 times in 0.01M PBS (pH 7.4). Next the samples

were equilibrated in 30% sucrose in 0.01M PBS at 4°C and then washed for 1-2 hours in 1:1 of 30% sucrose in PBS:OCT on a shaker plate at low speed. Then, the tissue samples were placed into plastic molds filled with OCT compound. The samples embedded in OCT were quick frozen with liquid nitrogen and stored at -80°C until sectioning. Frozen sections were cut in the coronal plane on a HM 550 Microm cryostat system at 12-16 μm and placed on Superfrost glass microscope slides. The sections were stored at -20°C until staining. Sections from each sample were stained using hematoxylin and eosin.

7.2.8 Semi-Quantitative Histological Scoring

After staining, each sample was semi-quantitatively scored[54,245] in a blinded study for tissue response, capsule thickness, and bone growth as outlined in Tables 3, 4, and 5, respectively. To remove bias, a predetermined scheme was developed to determine the location of each scoring region (Figure 21b). In particular, each sample was scored at the interface between the sample and surrounding tissue, with one region located at the interface midline and two regions located lateral to both sides of the midline. Furthermore, each sample was scored on the globe side of the implant as well as the orbital floor side of the implant. Thus, each sample was scored six times.

Score	Description
0	Cannot be evaluated due to infection or other factors not necessarily associated with the implant
1	Interface contains inflammatory cells with little or no signs of organized connective tissue
2	Capsule tissue is dense, containing both fibroblasts and many inflammatory cells
3	Capsule tissue is fibrous, but immature organization into a capsule, less inflammatory cells
4	Capsule tissue is fibrous, mature, little to no inflammatory cells surrounding capsule

Table 3: Scoring method used for semi-quantitative analysis of tissue response surrounding the implant.

Score	Capsule Cell Layers
0	N/A
1	1-4
2	5-9
3	10-30
4	>30

Table 4: Scoring method used for semi-quantitative analysis of capsule thickness surrounding implant.

Score	Description
0	Inflammation
1	Fibrous tissue capsule
2	Localized fibrous tissue not arranged as a capsule
3	Remodeling lacuna with osteoblasts and/or osteoclasts at the surface of the bone, near the gel
4	Remodeling lacuna with osteoblasts and/or osteoclasts at the surface of the bone, adjacent to the gel

Table 5: Scoring method used for semi-quantitative analysis of bone growth surrounding implant.

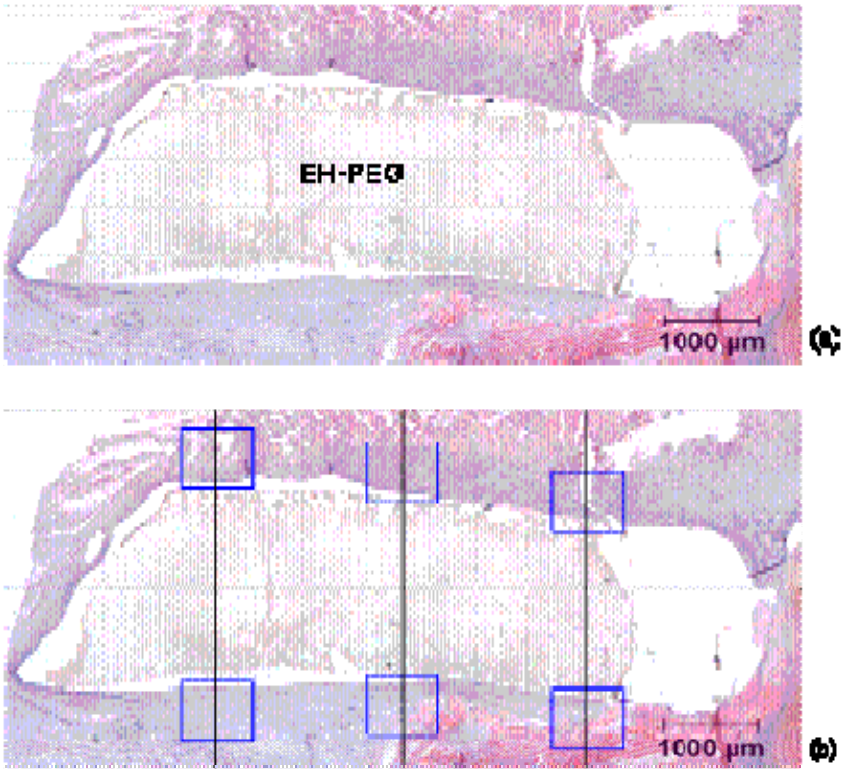

Figure 21: Stained section demonstrating the scoring scheme for each slide. Figure (a) shows the orientation of an example slide, while (b) demonstrates where the slide would be scored under higher magnification.

7.2.9 Histomorphometric Analysis

Each sample was examined at locations using the predetermined scheme outlined above. Micrographs were taken using a digital camera and analyzed using SpotSoftware (Diagnostic Instruments Inc) and the measurement function. Bone percent was determined by (bone area/(total tissue area))x100. Each slide analyzed was approximately 750 μm by 560 μm.

7.2.10 Statistical Analysis

Data from all studies was analyzed using ANOVA single factor analysis and Tukey's multiple comparison test ($p \leq 0.05$). All results are reported as mean ± standard deviation.

7.3 Results

The rabbit orbital defect was found to be a functional model for the *in vivo* evaluation of tissue engineered constructs. The rabbit orbital floor is readily accessible, as each surgical procedure lasted approximately ten minutes; however, the defect location is somewhat inhibited by the height of the orbital rim as well as the size of the orbital floor. Furthermore, in the rabbit, the globe is supported by both soft and hard tissue. In this model, construct implantation was easily achieved; although it should be noted that the limited amount of soft tissue sometimes caused migration of the implant.

An initial microscopic inspection of all the sample slides after histological processing demonstrated that the EH-PEG was easy to identify (as shown in Figure

21a). The EH-PEG stained a light purple, whereas the surrounding tissue stained a darker purple and pink color. In addition, the tissue-implant interface was easy to identify. Lastly, construct shape was observed to be similar to the original implantation shape, and rarely were minimal deformations present. It should be noted that degradation studies have not been completed on EH-PEG hydrogels. However, similar hydrogels composed of a copolymer of EHD and PEG had approximately 80% remaining mass after one month under physiological conditions.[246]

The overall tissue response to the implanted EH-PEG hydrogels appeared to be mild. In addition, there was minimal cellular invasion around the edges of the implant. Furthermore, the implants had initial masses surrounding the tissue which are likely to be fibrin clots. The experimental implants showed a mild inflammatory response, as evidenced by a lack of significant number of macrophages and foreign body giant cells. At the later timepoints, some implants were surrounded by a moderate amount of fibrous encapsulation. Lastly, new bone formation was present in the BMP-2 loaded implants at the later timepoint with increasing amounts present with higher concentrations of BMP-2.

In order to provide a semi-quantitative description to the implanted EH-PEG hydrogels, the tissue response to the surrounding area was scored according to Table 3 and shown in Figures 22 and 23. The control constructs showed an initial response at 7 d of little surrounding connective tissue and then a statistically significant improvement in surrounding tissue quality to fibrous encapsulation by 28 d. In addition if analyzed more closely, there appeared to be a spatial disparity present in the control group at 28 d: the globe surface of the gel scored tissue similar to dense

levels of fibroblasts, while the orbital floor surface of the gel presented tissue more similar to fibrous encapsulation.

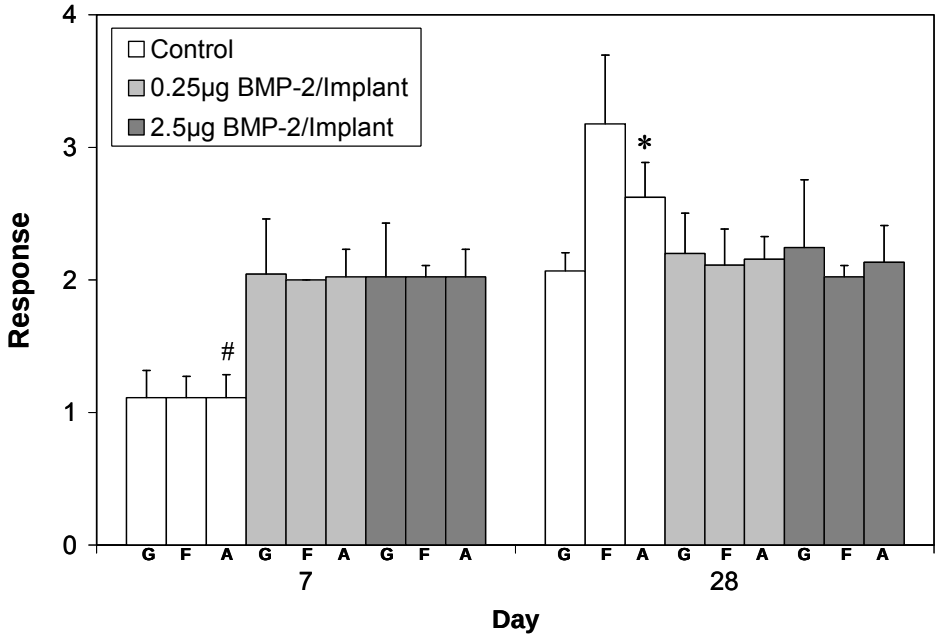

Figure 22: Response of surrounding tissue to EH-PEG constructs with 0, 0.25 and 2.5 µg BMP-2 /implant at 7 and 28d scored according to Table 3 and Figure 21b. The control constructs showed an initial response of no connective tissue at 7 d and then progressed to fibrous encapsulation at 28 d which was statistically higher than all groups. There was a spatial disparity noted with the control constructs. The BMP-2 loaded constructs were surrounding by fibroblasts at the initial timepoint and only increased slightly at 28 d. However, the tissue response surrounding all BMP-2 loaded constructs were not statistically different throughout the study. (*, #) indicate statistical difference among averages across both timepoints. G: Globe surface, F: Orbital floor surface, A: Average of globe and floor surfaces (n = 15).

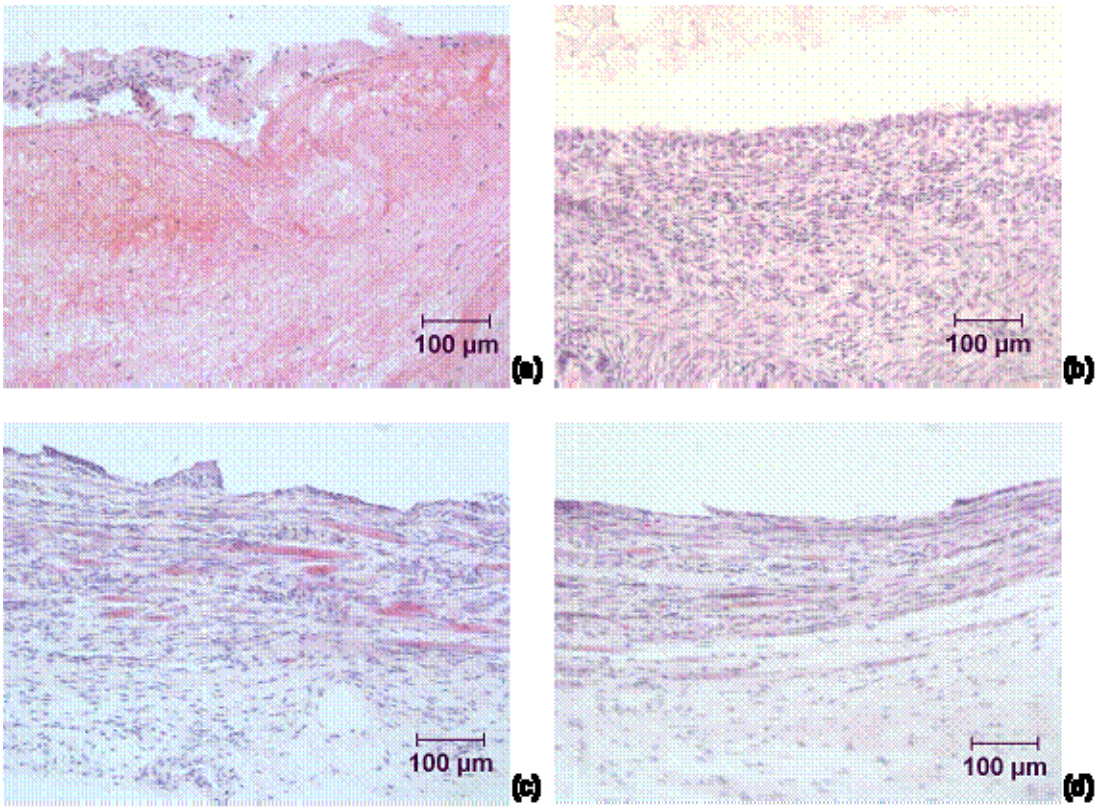

Figure 23: Hematoxylin and eosin staining of samples demonstrating the scores for Table 3. (a): a score of 1 demonstrating some inflammatory cells with no connective tissue, (b): a score of 2 showing dense surrounding tissue containing both fibroblasts and inflammatory cells, (c): a score of 3, representing fibrous but immature tissue, and (d): a score of 4 showing mature, fibrous tissue.

The EH-PEG constructs were further analyzed for capsule thickness according to Table 4 and shown in Figures 24 and 25. At 7 d there was very minimal capsule formation; however, by 28 d, there was a significant increase in the control constructs. Furthermore, it was again apparent that there was a spatial difference and that the orbital floor surface of the gel had a higher degree of fibrous encapsulation than the globe surface.

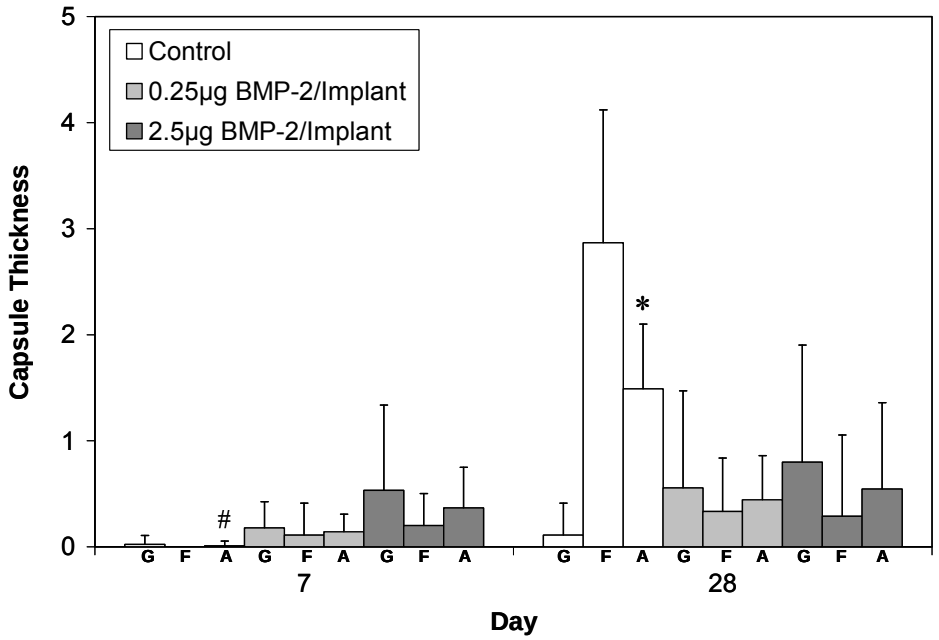

Figure 24: Capsule thickness surrounding EH-PEG constructs with 0, 0.25 and 2.5 µg BMP-2/implant at 7 and 28d scored according to Table 4 and Figure 21b. At 7 d all groups showed minimal capsule formation. There was a slight increase in the BMP-2 loaded groups at 28 d, but the most significant increase was with the control groups. All BMP-2 loaded groups were not statistically different during the study, and the control group showed significantly higher capsule formation than all groups. The spatial disparity was also present with the capsule thickness. (*, #) indicate statistical difference among averages across both timepoints. G: Globe surface, F: Orbital floor surface, A: Average of globe and floor surfaces (n = 15).

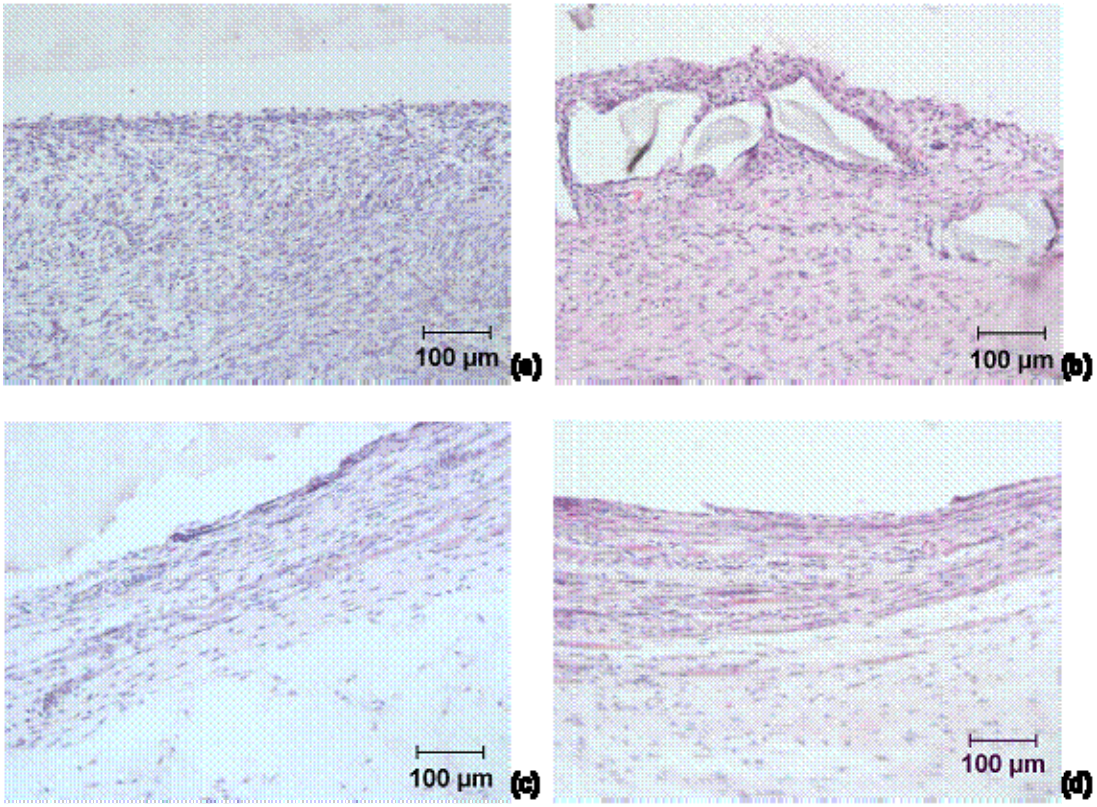

Figure 25: Hematoxylin and eosin staining of samples demonstrating scores for Table 4. (a): a score of 1 showing 1-4 cell layers, (b): a score of 2 showing 5-9 cell layers; here pieces of the EH-PEG gel were encapsulated by the surrounding tissue, (c); a score of 3 representing 10-30 cell layers, and (d): a score of 4 demonstrating >30 cell layers.

In addition, the area surrounding the EH-PEG gels was analyzed for bone growth according to Table 5 and is shown in Figures 26 and 27. At 7 d all groups had scores close to zero representing inflammation. However, by 28 d, there was an increase in scoring averages of all groups. However, the control group increase was due to fibrous capsulation located near the orbital floor surface edge of the EH-PEG construct rather than bone formation.

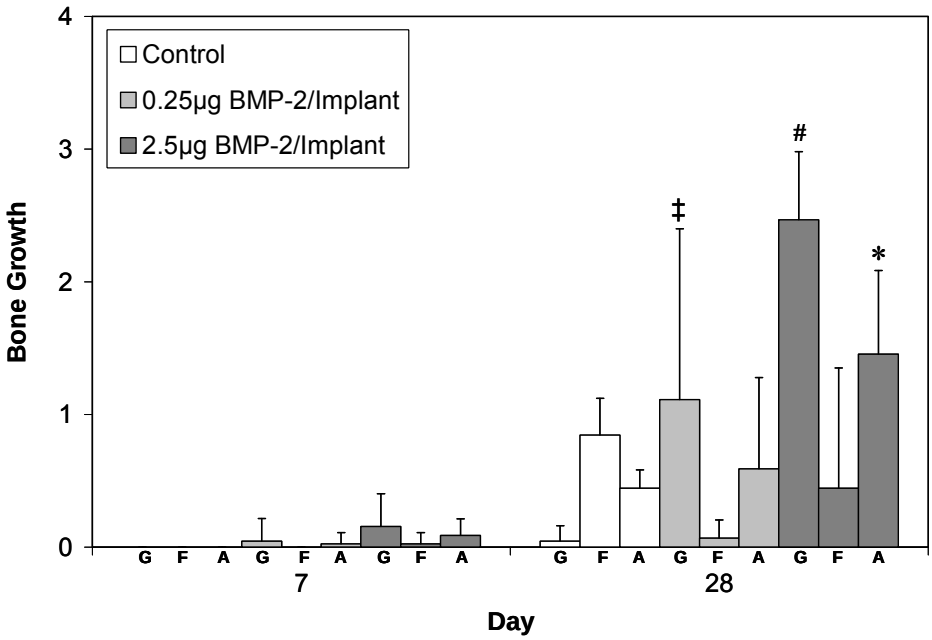

Figure 26: Bone growth surrounding EH-PEG constructs loaded with 0, 0.25 and 2.5 µg BMP-2 /implant at 7 and 28d scored according to Table 5 and Figure 21b. Results show that at 7 d all groups showed inflammation, however there was an increase at 28 d. Here the control constructs showed fibrous tissue capsule formation in the control group, some bone growth in the 0.25µg BMP-2 group, and significant bone growth in the 2.5µg BMP-2 group. (*) indicates statistical difference among averages across both timepoints, (‡, #) indicate statistical differences among globe surfaces at 28 d. G: Globe surface, F: Orbital floor surface, A: Average of globe and floor surfaces (n = 15).

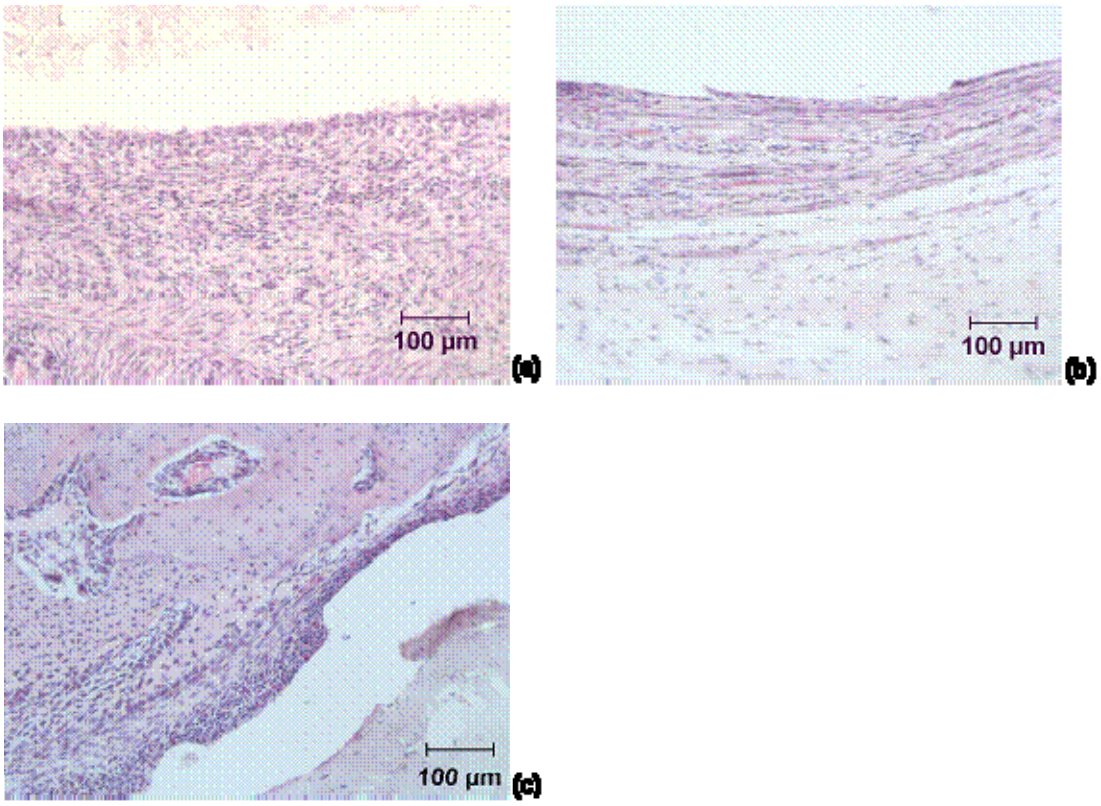

Figure 27: Hematoxylin and eosin staining demonstrating scores for Table 5. (a) a score of 0 showing inflammation, (b) a score of 1 showing a fibrous tissue capsule, and (c) a score of 3 showing new bone growth near the gel. Please note that scores of 2 and 4 were not observed in this study.

As one objective of the study was to determine the efficacy of growth factor release from EH-PEG hydrogels for the initiation of bone formation, it was therefore necessary to characterize growth factor release profile for the EH-PEG hydrogels. To this end, BMP-2 was released *in vitro* over a period of 12 hours and assayed using an ELISA kit (Figure 28). The constructs loaded with 0.25 µg BMP-2/implant showed a steady release over the first 4 hours and then leveled off to a 10% final release. Therefore, the 0.25 µg BMP-2/implant constructs had a final release of approximately 25 ng. Furthermore, the 0.25 µg/implant construct showed no statistical difference in BMP-2 release at 4, 6, and 12 hours, indicating that release occurred in the first 4

hours. The 2.5 µg BMP-2/implant constructs showed a slight, increasing release trend up to 2 hours and held level with a total release of approximately 25%, or 625 ng. In addition, the final percent released was significantly different between the 0.25 µg BMP-2/implant constructs and the 2.5 µg BMP-2/implant constructs.

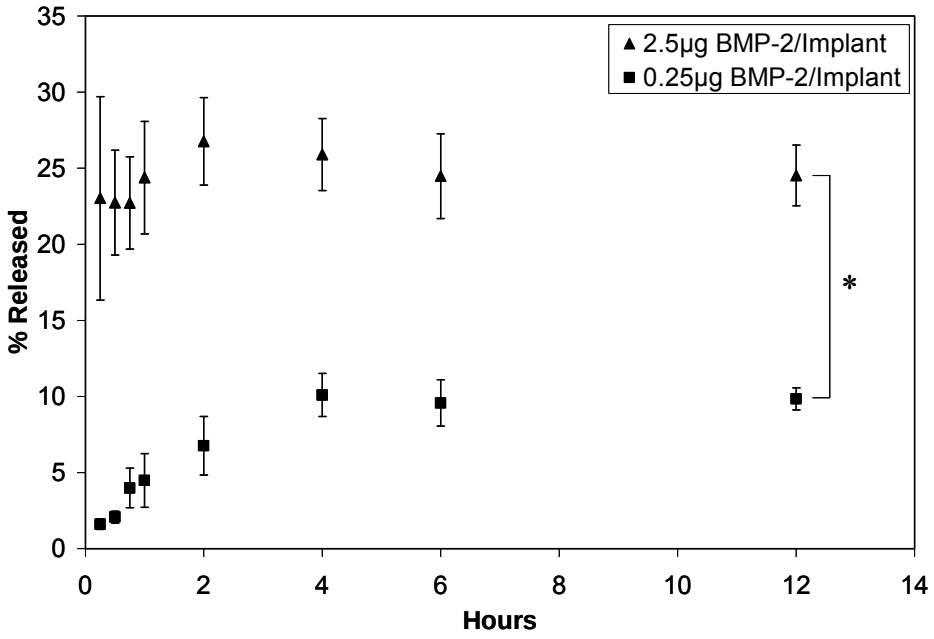

Figure 28: Release of BMP-2 from EH-PEG hydrogels. Hydrogels were loaded with 0.25 and 2.5 µg BMP-2/implant and the amount of BMP-2 was assayed using an ELISA kit over 12 hours. Approximately 25 % of the amount loaded was released from the 2.5 µg/implant construct as compared to 10 % for the 0.25 µg/implant constructs. The final percent released was significantly different between groups. In addition, the 0.25 µg/implant construct showed no statistical difference when compared at 4, 6, and 12 hours indicating that release occurred in the first 4 hours. (*) indicates statistical difference. (n = 5).

The tissue response to the BMP-2 loaded EH-PEG hydrogels was also scored according to Table 3 and is shown in Figure 22. The BMP-2 loaded groups were mostly surrounded by fibroblasts and did not show much increase in semi-quantitative scoring between the timepoints. The EH-PEG constructs were further analyzed for capsule thickness (Table 4, Figure 24). At 7 d there was slight capsule formation for both experimental groups, and by 28 d there was an increase across all

groups. However, for both tissue response and capsule thickness, all BMP-2 groups were not statistically different throughout the study. In addition, the spatial disparity that was present in the control group for tissue response and capsule thickness was not present in the BMP-2 loaded constructs. The area surrounding the EH-PEG gels was also analyzed for bone growth (Table 5, Figure 26). It is important to note that scores 2 and 4 were not found in this data set. At 7 d all groups had scores close to zero representing inflammation. However, by 28 d, there was an increase in the averages of all groups. The 0.25 μg BMP-2/implant group had a significant increase on the globe surface when compared to the control at 28 d, due to new bone growth near the construct. Furthermore, the 2.5 μg BMP-2/implant group had significantly higher levels of new bone growth on globe surface when compared to the 0.25 μg BMP-2/implant group at 28 d. Histomorphometric analysis (Figure 29) at day 28 demonstrates significant increases in bone percentages in the 2.5 μg BMP-2 group both at the globe interface and average of globe and floor surfaces compared to the control and the 0.25μg BMP-2 group.

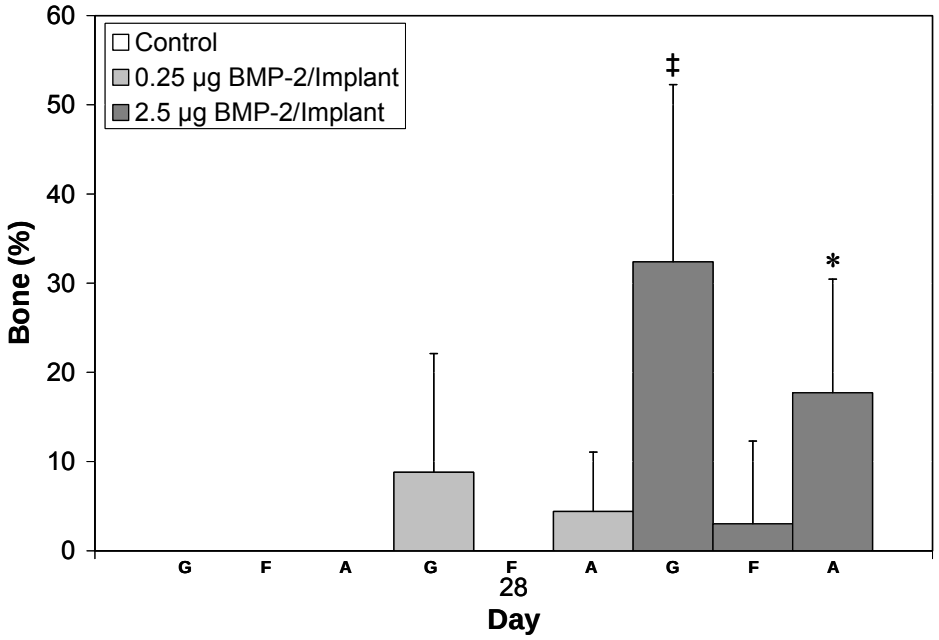

Figure 29: Histomorphometric analysis surrounding EH-PEG constructs loaded with 0, 0.25 and 2.5 µg BMP-2 /implant at 28d showing bone percent. Results demonstrate significant increases in bone percentages in the 2.5 µg BMP-2 group both at the globe interface and average of globe and floor surfaces compared to the control and the 0.25µg BMP-2 group. (*) indicates statistical difference among averages, (‡) indicates statistical differences among globe surfaces. G: Globe surface, F: Orbital floor surface, A: Average of globe and floor surfaces (n = 15).

7.4 Discussion

Orbital floor injuries are a devastating form of facial trauma and when left untreated often do not heal properly and form nonfunctional scar tissue. Many clinical methods have been employed to treat orbital floor defects; however these are associated with a number of sequelae. Therefore, our laboratory proposes a tissue engineering strategy utilizing EH-PEG hydrogels.

Our first objective was to describe the tissue response surrounding EH-PEG hydrogels implanted into a rabbit orbital defect. To this end, constructs were examined 7 and 28 d after implantation and scored using Tables 3 and 4 (see Figures

23 and 25). Results indicated an initial mild response to the control constructs as well as a low level of fibrous encapsulation. Furthermore, Figure 22 presents an increase in semi-quantitative scoring for these implants from 7 to 28 d, indicating that the surrounding tissue has a favorable response to the EH-PEG constructs over time and, more specifically, do not appear to induce a chronic inflammatory response.

An interesting development was the spatial disparity that was present between the tissue surrounding the globe surface and the orbital floor surface of the control constructs. For example, in Figure 24 capsule thickness was analyzed and showed minimal levels for all groups at all timepoints, however an increased thickness at 28 d for the orbital floor edge of the control group was observed. We speculate this response may be due to the differences in vascularization, where the tissue adjacent to the orbital floor surface of the construct is likely more vascularized than the tissue adjacent to the globe surface. In particular, the latter would require vascular development due to the creation of the defect which may have disrupted vascular support to the globe surface, in addition to the EH-PEG construct acting as a barrier to vascular growth from the orbital floor side. We must also note that while the constructs are uniform, the control groups did also receive a control solution loaded with BSA on the globe surface, and this experimental procedure may contribute to the differences in tissue response.

In order to examine our second objective, the *in vitro* release of BMP-2 from EH-PEG gels, BMP-2 was loaded onto the gels and the concentration of BMP-2 in the surrounding PBS was measured over time (Figure 28). The 0.25 μg/implant had a total release of 10%, significantly lower than the 25% release by the 2.5 μg/implant.

The difference in release percentages could be due to the stability of the BMP-2 at different concentrations, where BMP-2 is more stable when at a higher concentration (R & D Systems). This concentration effect upon stability could therefore be realized both during the loading process and during the release process. Alternatively, the surface loading process may have allowed the high concentration implants to minimize BMP-2's interactions with the hydrogel, as BMP-2 molecules accumulate on each other on the surface of the hydrogel. This phenomenon would likely allow the high concentration implants to demonstrate quicker release, as some BMP-2 molecules need only to solubilize rather than diffuse through the surface of the EH-PEG hydrogel, as well as a higher percentage release, as BMP-2 molecules observe less physical interactions during the release process. Indeed, both quicker and increased BMP-2 released was observed by the high concentration implants (Figure 28). Nevertheless additional studies, beyond the scope of this work, are required to fully address the relationship between loading concentration and release profile. Finally, we do note that the use of an ELISA to detect BMP-2 concentrations allows for not only the detection of the growth factor, but also some confidence that the growth factor remains in a biologically active form. It is also important to note that in both conditions 100% protein recovery was not observed. This may be due to BMP-2 degradation, as proteins tend to be unstable at low concentrations, and also the ELISA assay's specificity to protein structure.

Lastly, our third objective was to investigate the ability of EH-PEG hydrogels to deliver BMP-2 to an orbital defect in a rabbit model and facilitate bone formation. Results first showed that BMP-2 delivery augmented the tissue response to the

implant as well as the capsule thickness surrounding the implant (Figures 22 and 24). In addition, results showed that BMP-2 delivery was associated with increased bone formation (Figure 26) and bone percentage (Figure 29). Here the 2.5 μg BMP-2/construct had the most significant bone growth at 28 d, demonstrating the ability of EH-PEG gels to deliver biologically active BMP-2 to a rabbit orbital defect. Furthermore, it was apparent in both of the BMP-2 loaded groups that the majority of bone growth appeared on the globe surface of the construct. As described in the methods section, BMP-2 was loaded on the top of the gel, and this side was placed facing the globe during surgery. We predicted that diffusion as well as the relatively small defect size would allow BMP-2 to be adequately transported throughout the defect volume; however, the results indicate that the majority of the growth was immediately adjacent to the BMP-2 loaded surface. We do note that in the 2.5 μg BMP-2/implant group at 28 d, there were some instances of new bone growth near the orbital floor surface of the gel, although these were not as common as those near the globe surface.

7.5 Conclusions

The objectives of this study were to investigate the tissue response to EH-PEG hydrogels, characterize the release of BMP-2 from EH-PEG hydrogels, and analyze their ability to deliver BMP-2 *in vivo* and facilitate bone formation. The results indicate that the tissue surrounding the EH-PEG constructs showed a positive progression from 7 to 28 d indicating that constructs were not eliciting a chronic response. In addition the release of BMP-2 from the construct was complete in 2-4

hours, and happened more quickly at the higher concentration. Lastly, the data shows the ability for EH-PEG gels to deliver BMP-2 as shown by the new bone growth in the area surrounding the constructs containing high concentrations of BMP-2 at 28 d. This demonstrates that EH-PEG constructs are a viable option for use *in vivo* and for delivery of BMP-2 *in vivo*.

Chapter 8: Characterization of Macroporous Cyclic Acetal Hydrogels

8.1 Introduction

An important aspect of tissue engineering is the scaffold which can act as a support medium to deliver cell populations or induce surrounding tissue ingrowth. The construct typically acts as a template which facilitates cell attachment and matrix deposition. Scaffold properties directly determine the success in tissue engineering and must be designed for each purpose. In many applications, including bone regeneration, porosity, pore size, and interconnectivity are key parameters as they allow for improved cell migration, proliferation and vascularization.

A number of polymers are currently under investigation for tissue engineering applications; however an ideal biomaterial has not been developed. Our laboratory has developed a class of biomaterials based upon a cyclic acetal unit. These materials may be advantageous for tissue engineering applications as they degrade hydrolytically to form primary degradation products of diols and carbonyls, and thus should not affect the local acidity of the implant or phenotypic function of the delivered cell population. A cyclic acetal biomaterial in the form of a rigid plastic may be fabricated from the radical polymerization of the monomer 5-ethyl-5-(hydroxymethyl)-β,β-dimethyl-1,3-dioxane-2-ethanol diacrylate (EHD).[218] Here, the EHD monomer and PEGDA polymer were fabricated into a macroporous EH-PEG hydrogel by radical polymerization using porogen-leaching.

Macroporous biomaterials have been created using a number of techniques including porogen-leaching as a common method for use with non-water soluble polymers. However, to create macroporous water-swollen hydrogels, freeze drying, stereolithography, and gas-foaming are frequently used.[20-22,24,25,247,248] Using porogen-leaching to create a macroporous hydrogel is not an established technique even though it may be easily implemented. Here, the EHD monomer and PEGDA polymer were fabricated into a macroporous EH-PEG hydrogel by radical polymerization using porogen-leaching. In this study, saturated salt was used as the water component of the gel to slow the dissolution of the salt and maintain porogen integrity during crosslinking.

There are a number of methods available for measuring porosity within scaffolds, each with associated advantages and disadvantages. Mercury intrusion porosimetry is a technique that has been commonly used, and is based upon the infusion of mercury within the scaffold under increasing pressure to determine the porosity and estimate pore sizes.[249-252] While this technique may give reasonable estimate of porosity and pore size, the use of mercury is not ideal. The liquid displacement method is a technique that is also frequently used. Here the construct is submerged in a volume of liquid and is brought through a series of evacuation-repressurization cycles to force liquid into the pores.[249] The porosity can be estimated from the amount of liquid that was taken up into the construct.[253-255] However, it can be difficult to find a proper solvent that will not affect the biomaterial and can be forced into the pores. In addition, sensitive biomaterials may compress and alter their structure when exposed to varying pressures indicating these above

techniques may not be appropriate. Image analysis has also been used to measure porosity and more frequently, pore size. In particular, scanning electron microscopy is a commonly used technique.[255-257] The sample has to be dried and the surfaced coated, commonly with gold-palladium, which limits the type of biomaterial that can be analyzed by this method. Other imaging techniques such as microcomputed tomography have been used to analyze bone morphology, and are beginning to be used to determine porosity and pore sizes in scaffolds where 2D images are reconstructed to generated 3D images.[258] It is important to note, that many of these above techniques are invasive, discrete methods of analysis. Therefore, an optimal method is not widely available for analysis of engineered tissues.

Optical coherence tomography (OCT) is a promising technique that overcomes many of the negative aspects of the previous techniques. This method allows for noninvasive cross-sectional imaging of material architecture by measuring optical reflections.[259] OCT is based upon the idea of optical ultrasound.[260] For this technique near-infrared light is shone upon a sample, and the morphological features can be elucidated from the variations in their corresponding refractive index.[260,261] Specifically, the intensity of the backreflected light is measured using interference.[259,260,262] OCT has been used previously *in vivo* to image microstructures of various tissues including the eye, skin, gastrointestinal tract, and the nervous system.[261-263] However, OCT is still an emerging technology for the *in vitro* analysis of tissue engineered scaffolds.

OCT is an ideal technique for imaging tissue engineered scaffolds for many reasons. The primary advantage is the ability to image to a depth of 2-3 mm with a

resolution of 3-15μm which is significantly improved over other techniques.[260] This allows for analysis at the cellular level and visualization of the extracellular matrix.[260] Furthermore, OCT does not rely on exogenous agents such as fluorescent dyes to provide contrast which allows for maintained cell viability during imaging and repeated analysis. OCT eliminates the needs for specimen fixation and processing which reduces any artifacts that can occur during these procedures, and allows for real-time imaging. Specifically, when compared to histology, OCT is capable of demonstrating the same morphological features in tissue without the extensive processing necessary for histological sample preparation.[259] In addition, OCT is capable of performing repeated observations within the same sample for a time-lapse analysis. Lastly, OCT is relatively low cost when compared to other imaging techniques.[262]

In this work, for the first time, macroporous EH-PEG hydrogels were characterized using OCT. Objectives of this study were to (1) create water-swollen macroporous EH-PEG hydrogels using porogen-leaching, (2) use optical coherence tomography to characterize EH-PEG hydrogel architecture, specifically for pore size and porosity, and (3) combine OCT with confocal microscopy to demonstrate viable cells within the scaffolds.

8.2 Methods

8.2.1 Hydrogel Formation

Macroporous EH-PEG constructs were crosslinked using ammonium persulfate and N,N,N',N'-tetramethylethylenediamine at 15 mM using a sodium chloride-leaching technique. A saturated salt solution was used as the water component of the gel to slow the sodium chloride crystals from dissolving into the gel solution. The constructs were prepared using EHD and PEGDA Mn~ 700 at 1:10 molar EHD to PEGDA with 30 wt% initial monomer components. Sieves were used to sort sodium chloride to specified sizes. Gels were created in Petri dishes by spreading the salt evenly and dispersing the gel solution over the salt before cross linking. Gels were allowed to crosslink and smaller gels were cut to 8 mm diameter with a cork borer. The sodium chloride was leached out over 2 days in water with multiple washes while on an orbital shaker. Gels were sterilized in 70% ethanol, washed four times in PBS and presoaked in control media plus FBS for four hours before cell loading. EH-PEG hydrogels were created with the following formulations: 100 μm/65%, 100 μm/70%, 250 μm/70%, 250 μm/75% where 100 μm hydrogels were fabricated with salt that had been collected between sieves of 106-150 μm and 250 μm hydrogels between 250 and 300 μm and the reported porosities are based upon mass.

8.2.2 Optical Coherence Tomography (OCT)

This study is performed with a Fourier-domain OCT system.[264] The fiber-based high-speed, high-resolution OCT system utilizes a wavelength-swept laser as the light source. It generates a broadband spectrum of 100 nm at 1300 nm, which provides an axial resolution of 8 μm in the tissue. The laser operates at a sweep rate of 16 kHz (equivalent to an imaging speed of 15 frames per second for a 1024 axial-line image) with an average output power of 12 mW. The system sensitivity is 95 dB. A Michelson interferometer composed of one circulator and a fiberoptic 50/50 splitter is used to generate the Fourier-domain OCT signal. The OCT interference signal returned from the sample and reference arms is detected by a balanced photodetector. A Mach-Zehnder interferometer (MZI) with a fixed path difference is used to generate an optical frequency clock. Data acquisition is triggered by the zero-crossing points of the MZI fringes, which are evenly spaced in optical frequency (k). Discrete Fourier transform (DFT) is performed on the data to generate an axial depth profile. Three-dimensional (3D) images were acquired using a pair of galvanometer mirrors.

8.2.3 OCT Image Processing and Analysis

The 3D OCT volumetric images of the hydrogel measured 2.5 mm x 2.5 mm x 2.5 mm with 512 x 512 x 512 pixels. The image processing was performed on the *en face* OCT images. First, the *en face* images were segmented with MATLAB based on the different back-scattering intensities of the porous and mass regions. The segmentation process formed a binary image. Next, the pore size and the porosity were quantified based on the segmented images. The pore sizes were determined by

the average between the longest and shortest lengths that could be measured on a pore. The porosity was expressed in the ratio of volume divided by the total volume. Multiple measurements were performed and the means and standard deviations of those measurements were obtained.

8.2.4 Combined OCT/Confocal Microscopy System

In order to detect cells within the scaffolds, OCT was combined with fluorescence confocal microscopy (FCM). The FCM system is combined with the OCT system using a dichroic filter which passes through the visible and near-infrared light used for FCM, and deflect the 1.3 μm light used in OCT. The FCM system uses a continuous-wave laser diode as the excitation source. Different excitation wavelengths can be chosen depending on specific fluorescence marker under investigation. The excitation light is focused by a microscope objective. The fluorescence light is collected back by the objective and directed into the emission filter by another dichroic filter which separates the excitation light from the fluorescence emission light. The fluorescence signal is then collected by a multimode fiber, and detected by photomultiplier tubes. To generate an *en face* confocal fluorescence image, the illumination point is raster-scanned by a resonance scanner and a galvanometer mirror to achieve a real-time speed of 8-10 Hz.

We performed combined OCT/FCM imaging of scaffolds containing hMSCs. Cells can be stained with the Live/Dead assay. Due to the current laser source only one dye can be imaged at a time. In this study the co-registered OCT/FCM provides qualitative information demonstrating scaffold structure and hMSC distribution.

8.2.5 Human Mesenchymal Stem Cell Culture

hMSCs were purchased from Lonza and cultured according the manufacturer's specifications and as described in the literature.[265] Prior to the study, the hMSCs were cultured in control media composed of high glucose DMEM with 4 mM L-Glutamine, 0.1 mM non-essential amino acids, 1% penicillin/streptomycin (v/v) and 10% MSC qualified FBS. hMSCs were added to sterile, presoaked hydrogels in a concentrated cell solution. The cells were allowed to attach for 4 hours before filling the well with media.

8.2.6 Viability

Gels were cultured and analyzed using the LIVE/DEAD assay. Before analysis, the gels were soaked in PBS for 1.5 hrs to remove FBS from the gel which can interact with the Live/Dead reagents. As only one dye can be read at a time due to the microscopy setup, the gels were incubated with the Live reagents (2.5 μm calcein AM) at room temperature for 30 min.

8.2.7 Statistical Analysis

Data from all studies was analyzed using ANOVA single factor analysis and Tukey's multiple comparison test ($p \leq 0.05$). All results are reported as mean ± standard deviation. Please note that only pertinent statistical relationships are noted in the figures.

8.3 Results

EH-PEG hydrogels with varying pore sizes and porosities were created, imaged using OCT, and analyzed with image processing. Three-dimensional reconstruction was performed from binary images to visualize the pores (Figure 30). From both the cross-sectional and *en face* images, results qualitatively show a difference in pore size between the 100 μm and 250 μm EH-PEG hydrogels. Furthermore, the 3D view of the cell pores demonstrates limited interconnectivity of the scaffolds.

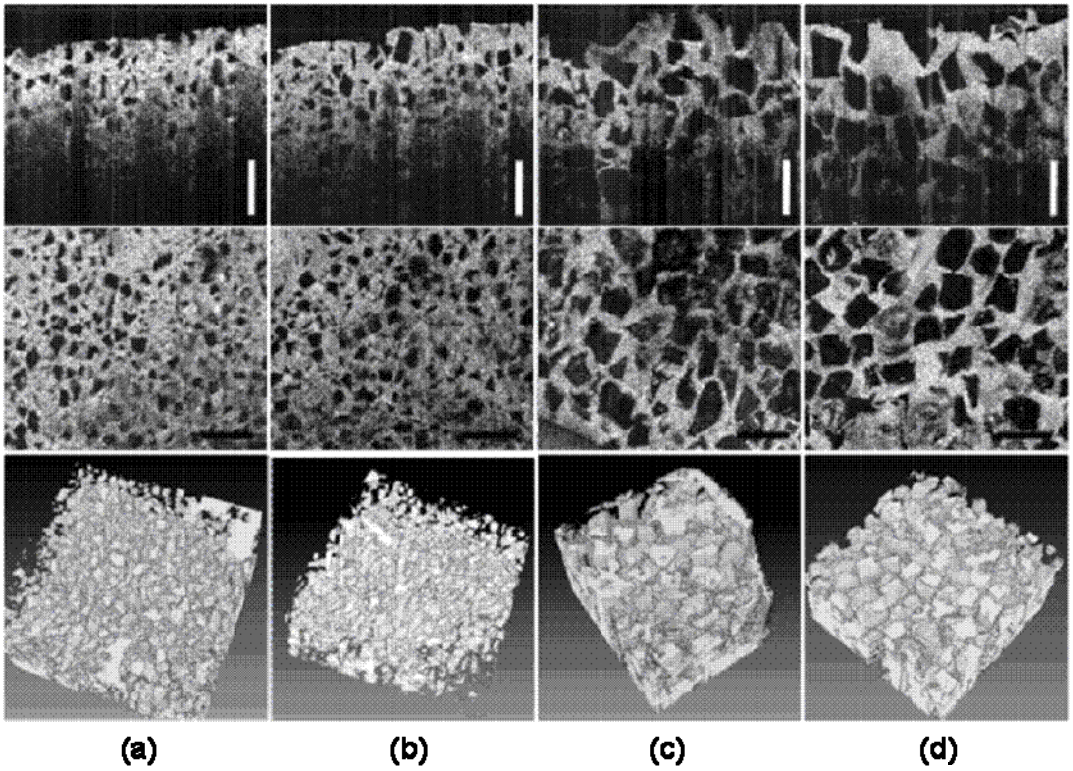

Figure 30: Cross-sectional OCT (top row) and *en face* OCT (middle row) images of cell scaffolds with varying pore sizes and porosities: (a) 100 μm/65%, (b) 100 μm/70%, (c) 250 μm/70%, (d) 250 μm/75%. Bottom row of images depicts 3D visualization of pores from segmented OCT images. Scale bar denotes 500 μm.

Figure 31 shows the quantified pore sizes as measured from the average between the longest and shortest lengths in the pore. For the 100 μm pore size, the measured sizes were 132 ± 22.5 μm and 144 ± 31.2 μm for 65% and 70%, respectively and are not statistically different. These two values both lie within the range of expected values dependant on the starting size of the salt used to create these hydrogels. For the 250 μm pore size, the quantified pore sizes were 295 ± 63.9 μm and 239 ± 54.3 μm for 70% and 75%, respectively which are again within the expected range and are not statistically different. When comparing between the 100 μm and 250 μm hydrogels the results indicate that the pores sizes are statistically different.

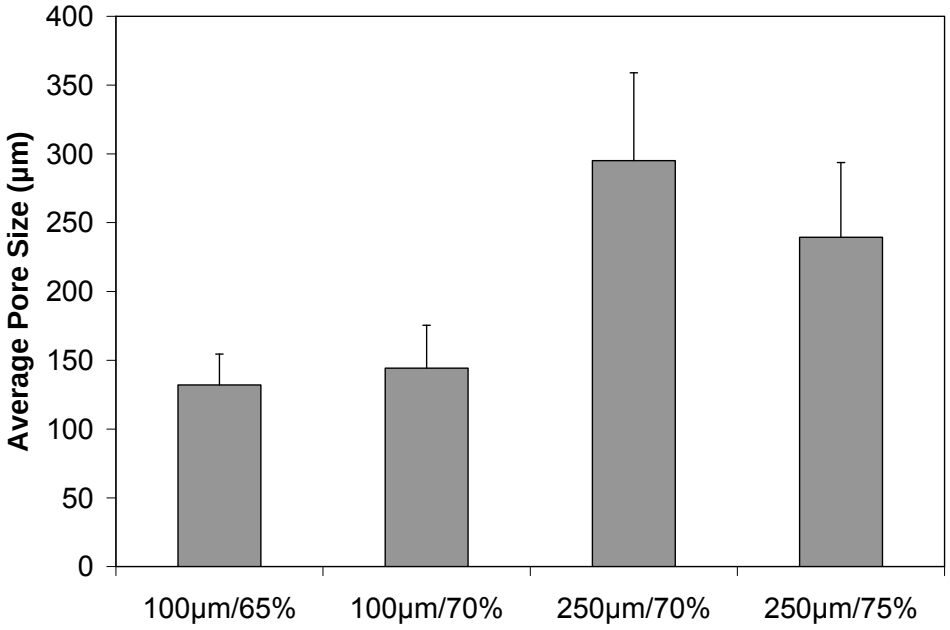

Figure 31: Average pore size of EH-PEG hydrogels was quantified using OCT images. Measured pore sizes fall in the predicted ranges for all experimental groups.

Porosity was also analyzed based upon the three-dimensional reconstructions. As the original porosities are based upon mass, we expect the calculated porosities to

be different as they are derived from volume. For the 100 μm pore size, calculated volume porosities were 70.2 ± 11.6 % and 73.7 ± 10.7% for the mass porosities 65% and 70%, respectively (Figure 32). The 250 μm pore size hydrogels demonstrated calculated volume porosities of 51.7 ± 9.4 % and 62.7 ± 8.9% for the mass porosities 70% and 75%, respectively. It is important to note that there is a trend between groups of the same pore sizes in that hydrogels with a higher mass porosity demonstrated higher volume porosity both for the 100 μm and 250 μm pore size hydrogels. When comparing between hydrogels of different pore sizes, the 100 μm 70% hydrogel showed higher volume porosity than the 250 μm 70%, however they are not statistically different.

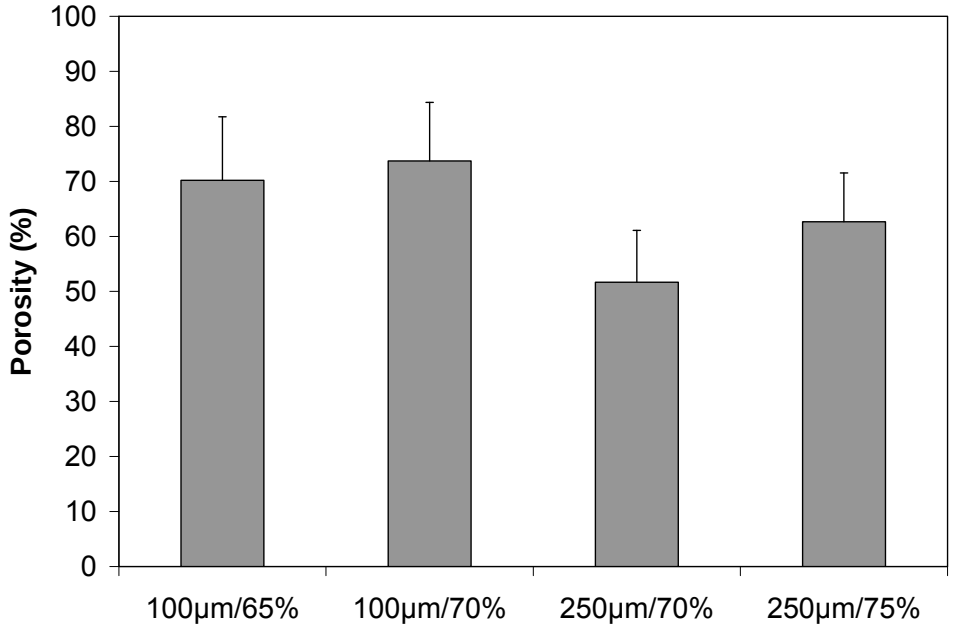

Figure 32: Measured volume porosity of EH-PEG hydrogels quantified from OCT images. Within gels of the same pore size, gels with a higher predicted porosity demonstrated a higher porosity. In addition, both gels with 70% mass porosity demonstrated volume porosities that were not statistically different.

Fluorescence confocal microscopy (FCM) was also combined with OCT to image live cells within the scaffolds (Figure 33). The 2D image is of the top face of the scaffold and can be used to qualitatively visualize cell distribution and viability. For all the scaffolds, viable cells can be seen spread across the surface and within the pores.

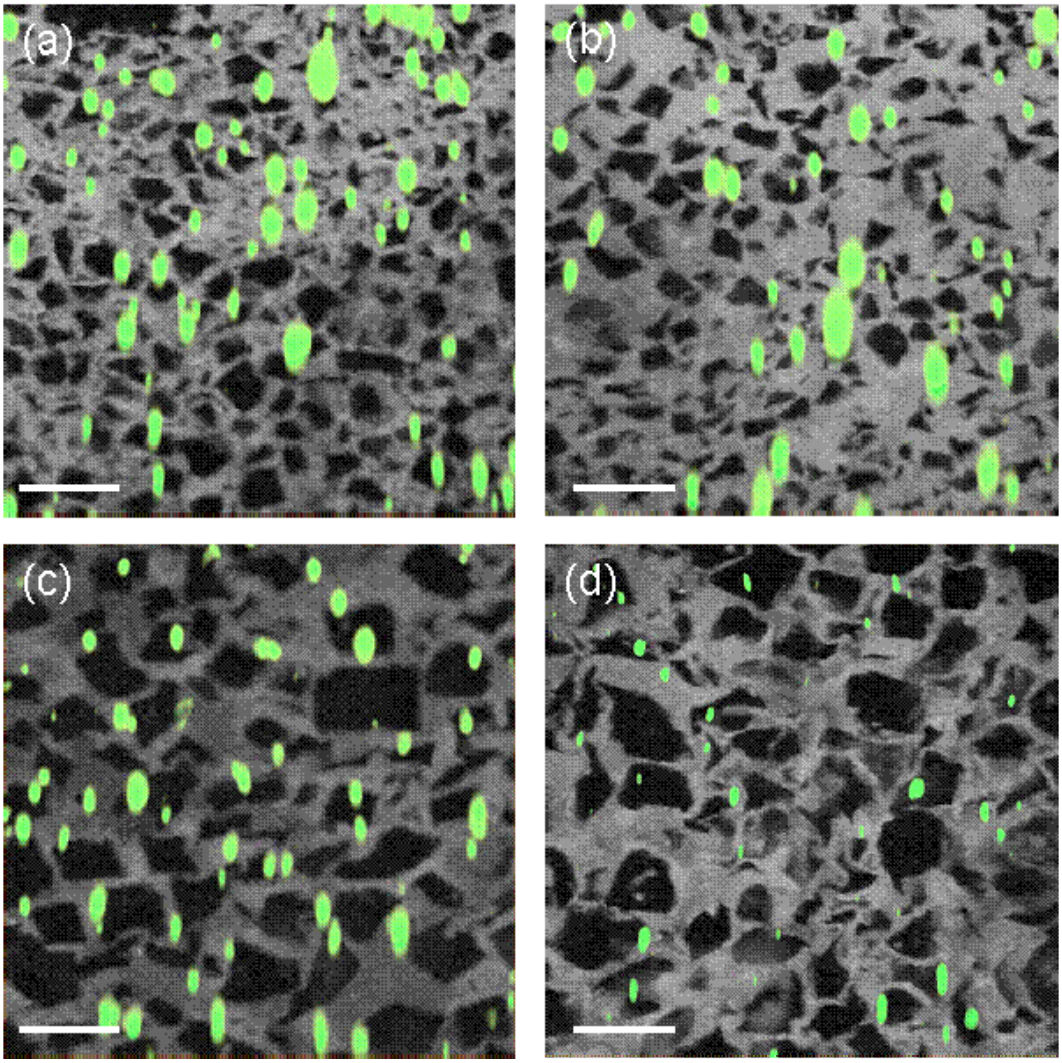

Figure 33: OCT/FCM images of hMSCs stained with LIVE dye within EH-PEG hydrogels. Results show the top view of the scaffolds and demonstrate viable cells spread across the constructs and within the pores. (a) 100 μm/65%, (b) 100 μm/70%, (c) 250 μm/70%, (d) 250 μm/75%. Scale bar denotes 250 μm.

8.4 Discussion

Objectives of this study were to (1) create water-swollen macroporous EH-PEG hydrogels using porogen-leaching, (2) use optical coherence tomography to characterize EH-PEG hydrogel architecture, specifically for pore size and porosity, and (3) combine OCT with confocal microscopy to demonstrate viable cells within the scaffolds.

This study demonstrates the use of porogen-leaching to create macroporous water-swollen hydrogels. Other methods have been employed to create macroporous hydrogels; however each has associated disadvantages. Freeze drying uses temperature changes to create porous structures.[20] Pore size is controlled by altering the freeze rate, however better success occurs when combined with porogen-leaching.[38] Gas foaming is also commonly used with hydrogels where pores result from bubbles created in a chemical reaction or gasses under pressure.[24] Variations in pore size are controlled by altering gas volume, rate of gas nucleation, and diffusion.[25] Again, to improve pore size control, gas foaming can be combined with porogen-leaching.[25] Laser stereolithography is also employed to create porous structures. Here complex internal structures can be produced through computer aided design.[266] While this technique allows for excellent repeatability between scaffolds, it requires the use of a computer and intricate machinery. The simple porogen-leaching method presented in this paper allowed for the creation of macroporous hydrogels in a simple technique and produced pores of the desired size.

OCT was used to analyze EH-PEG hydrogel architecture, specifically for pore size and volume porosity. The results indicate that OCT is capable of elucidating

pore size and demonstrated the EH-PEG hydrogels had pores in the expected range. This indicates that the fabrication method succeeded in slowing the dissolution of sodium chloride into the aqueous gel solution before crosslinking. Further analysis allowed for the quantification of volume porosity, which is an important parameter in tissue engineering scaffolds. The volumes reported were low for the 250 μm pore sizes indicating that they might not be optimal for use as tissue engineering constructs. However, the 100 μm EH-PEG hydrogels reported volume porosities in the range of 70% which is reasonable for tissue engineering applications.

OCT was also combined with FCM demonstrating the capability of the system to visualize cells within the scaffolds. These results qualitatively show viable cells across the surface and within the pores of the constructs. Further image reconstruction will allow for 3D rendering to demonstrate a global view of viable cells within the construct. This will allow for elucidation of cellular interactions with the scaffold. As OCT is a non-invasive imaging technique, long term migration studies could be completed with this system to better understand the proliferation of a cell population over time as well as long term viability within the scaffolds.

8.5 Conclusions

Scaffold properties are important parameters in the success of tissue engineering applications. In this work, macroporous EH-PEG hydrogels were produced using porogen-leaching demonstrating a simple technique for fabrication. OCT was used to quantify pore size and volume porosity. Reported pore sizes were within the expected range, as estimated from the starting materials, demonstrating the

ability of OCT analysis to quantify pore size. In addition, OCT image analysis was able to be used to characterize volume porosity, a parameter not previously known. Further work combined OCT with FCM where viable cells were visualized within the scaffolds.

Chapter 9: Macroporous Cyclic Acetal Hydrogels for Orbital Floor Repair

9.1 Introduction

Orbital floor injuries are a devastating form of craniofacial trauma and account for approximately 60-70% of all orbital fractures.[113,228] Injury to the orbit is commonly caused by blunt force through assault and traffic accidents.[110,111] Orbital bone fractures, if left untreated, may not heal adequately. Generally, only small bone fragments and few bony edges are present to conduct bone formation and restore orbital volume. Instead, a fibrous scar forms which lacks the support, architecture, and load bearing properties of bone. Therefore, the endogenous response to orbital fractures, in contrast to many other bone fractures, is not sufficient for proper healing. In addition, when treated inadequately, a number of sequelae are associated with orbital floor injuries including unsatisfactory facial aesthetics, enophthalmos (sunken eye), and diplopia.[112,124,229]

The orbital floor is composed of portions of three bones, the maxilla, zygomatic, and palantine.[107,108] The orbital floor is a very thin plate, approximately 0.5 mm, and its main purpose is to separate the orbital contents from the maxillary sinus.[107,267] Given that the orbital floor is a thin structure, it is an excellent model for *in vitro* tissue engineering as experiments are able to be performed without the need for bioreactors and additional attention to diffusion which is necessary in larger tissue engineered constructs.

Bone morphogenetic proteins (BMPs) are some of the most promising growth factors involved in bone tissue engineering. BMPs are members of the TGF-β superfamily and are known to be secreted signaling molecules.[133] The family of BMPs is known to induce formation of cartilage, bone, and other tissues of the skeleton.[133] Specifically, BMP-2 is known to increase mesenchymal stem cell proliferation and differentiation into osteoblasts.[144] In addition, it has chemotactic effects on human osteoblasts.[143] The BMP receptors play an important part in the signaling ability of the molecule. There are two types of BMP receptors, Type I and Type II, and both are able to bind the ligand.[133] It is thought that signal transduction requires the formation of a complex between the Type I and Type II receptors before ligand binding, and binding initiates a signal cascade within the cell.[133,135,268] Furthermore, BMP signaling has been shown to be involved in a number of functional osteoblast pathways including bone matrix proteins, osteogenic regulatory genes, BMP inhibitory factors, and osteogenic transcription factors.[268]

Current alloplastic implants that are available for clinical use in orbital floor repair include Teflon, silicone, Gelfilm, Medpor (high-density polypropylene), and titanium.[107,111,116,117] However, an ideal biomaterial with favorable cellular interactions, mechanical strength, degradation and degradation products, is not available. To this end, our laboratory has developed a class of biomaterials based upon a cyclic acetal unit. Cyclic acetals may be preferred for tissue engineering applications as they hydrolytically degrade to form diol and carbonyl primary degradation products, which should not affect the local acidity of the implant or phenotypic function of a delivered cell population. A cyclic acetal biomaterial in the

form of a rigid plastic may be fabricated from the radical polymerization of the monomer 5-ethyl-5-(hydroxymethyl)-β,β-dimethyl-1,3-dioxane-2-ethanol diacrylate (EHD).[218] The hydrophilic polymer poly(ethylene glycol) (PEG) was incorporated to create a cyclic acetal based hydrogel that could be used to deliver cell populations and growth factors.[219] Previous work has demonstrated that EH-PEG hydrogels support long term viability of encapsulated bone marrow stromal cells.[269] In addition, EH-PEG hydrogels were able to deliver bone morphogenetic protein-2 in an orbital floor defect model supporting new bone growth indicating EH-PEG hydrogels are a viable craniofacial bone tissue engineering system.[155]

In order to improve bone regeneration and tissue integration, the scaffold should mimic bone morphology, structure, and function.[249] An important aspect of bone morphology is the pores which facilitate both molecular diffusion and cell migration. Furthermore, scaffold porosity allows vascularization as well as improves mechanical stability between the implant and surrounding native bone.[270] There are a number of studies in the literature reporting minimum pore sizes for osteogenesis. It has been demonstrated that interconnected pores with diameters greater than 50 μm are favorable to new bone formation, while the minimum pore size for osteoconduction is 80-100 μm.[98,151,152,209] Lastly, for the scaffold to support new vasculature, it has been shown that the minimum pore size is 45-100 μm; however, scaffolds with pore sizes of 100-150 μm resulted in a richer blood supply.[153,209] While studies have been completed on scaffolds with micropores (<10 μm) and in macroporous 500 μm pores structures, the above results indicate that a minimum pore size of 100 μm is necessary for osteoconduction and vascularization.[75,249,271]

Many techniques have been utilized to create porous scaffolds for tissue engineering applications. Porogen-leaching has been implemented frequently with non-water soluble polymers. While to create macroporous water-swollen hydrogels, freeze drying, stereolithography, and gas-foaming are commonly used.[20-22,24,25,247,272] However, using porogen-leaching to create macroporous water-swollen hydrogels is not an established technique even though it may be easily implemented. The EHD monomer and PEGDA polymer may be fabricated into a macroporous EH-PEG hydrogel by radical polymerization using salt-leaching. Here, saturated salt was used as the water component of the gel to slow the dissolution of salt and maintain porogen integrity.

Macroporosity within hydrogels may facilitate both molecular diffusion and cell migration. This environment should promote cellular interactions and signaling, and as a result, differentiation. However, high porosity scaffolds can be associated with poor mechanical integrity. Engineering these properties to allow for appropriate diffusion and mechanical strength are important challenges in the construction of bone tissue engineering scaffolds. In this work, for the first time, the effect of scaffold architecture in macroporous EH-PEG hydrogels on osteogenic signaling of hMSCs was investigated. Specifically, the objectives of this work were to (1) investigate the effects of scaffold architecture, through porosity and pore size, in EH-PEG hydrogels on osteogenic signal expression, (2) examine the effect of adhesion through incorporating the extracellular matrix protein fibronectin in EH-PEG hydrogels on osteogenic signal expression, and (3) investigate the strength of EH-PEG scaffolds with varying pore size and porosity.

9.2 Methods

9.2.1 Materials

Ammonium persulfate (APS), N,N,N',N'-tetramethylethylenediamine (TEMED), PEGDA M_n~ 700, benzoyl peroxide, N,N-Dimethyl-p-toludine, ascorbic acid Na-β-glyerophosphate, dexamethasone, trizol, Isobutyraldehyde, formaldehyde (37% aqueous solution), trimethylolpropane, triethylamine, hydroquinone and acryloyl chloride were purchased from Sigma (St. Louis, MO). Potassium carbonate, sodium sulfate, ethyl ether, silica gel (60-200 mesh) and stainless steel sieves in the appropriate sizes were purchased from Fisher Scientific (Pittsburg, PA). Human fibronectin and Quantikine BMP-2 immunoassay ELISA kit were purchased from R&D Systems (Minneapolis, MN). The DNeasy Tissue kit and RNeasy Mini Plus Kit were purchased from Qiagen (Valencia, CA). The Live/Dead assay and Quant-iT PicoGreen Kit were ordered from Molecular Probes (Carlsbad, CA). High-glucose DMEM, MSC-qualified fetal bovine serum (FBS), penicillin-streptomycin antibiotics, L-glutamine, and non-essential amino acids were obtained from Invitrogen (Carlsbad, CA). The M-per Mammalian Protein Extraction Reagent was ordered from Pierce (Rockford, IL). The High Capacity cDNA Archive Kit and TaqMan Gene Expression assays were purchased from Applied Biosystems (Foster City, CA).

9.2.2 5-ethyl-5-(hydroxymethyl)-β,β-dimethyl-1,3-dioxane-2-ethanol diacrylate Synthesis

5-ethyl-5-(hydroxymethyl)-β,β-dimethyl-1,3-dioxane-2-ethanol diacrylate (EHD) was synthesized based on previous protocols described by Kaihara et al.[246] Potassium carbonate (18.9 g, 0.25 equiv) was added to isobutyraldehyde (50 ml, 1 equiv) and formaldehyde (37% aqueous solution, 40.8 ml, 1 equiv) and the solution was stirred at 0°C overnight. The product 3-hydroxy-2,2-dimethylpropinaldehyde (HDP) was extracted three times with chloroform and then washed with water and brine. The chloroform layers were combined and dried with sodium sulfate and the solvent was evaporated under reduced pressure to obtain solid HDP. HDP (32.9 g, 1 equiv) and trimethylolpropane (86.6 g, 2 equiv) were dissolved in 1 M hydrochloric acid (200 ml) and stirred for 2 hrs at 80°C. The solution was then neutralized with sodium hydroxide and the product 5-ethyl-5-(hydroxymethyl)-β,β-dimethyl-1,3-dioxane-2-ethanol (HEHD) was extracted three times with chloroform and washed with water and brine. The chloroform layers were combined and again dried with sodium sulfate and evaporated under reduced pressure to obtain solid HEHD. The HEHD was purified using an ethyl ether wash to remove undesired byproducts and was dried under reduced pressure. HEHD (31.3 g, 1 equiv) was dissolved in chloroform and trimethylamine (65.4 ml, 3 equiv) and hydroquinone (0.034 g, 0.002equiv) were added. Acryloyl chloride (38.1 ml, 3 equiv) was added dropwise as the reaction was stirred at 0°C for 2 hrs. The insoluble salts were removed through filtration and the product, 5-ethyl-5-(hydroxymethyl)-β,β-dimethyl-1,3-dioxane-2-ethanol diacrylate (EHD), was extracted three times with chloroform and washed with water and brine.

The chloroform layers were combined and dried with sodium sulfate and evaporated under reduced pressure. The EHD was further purified by silica gel column chromatography using a chloroform/ethanol (10:1, v/v) as the eluent. The fractions that contained EHD were determined by thin layer chromatography and NMR.

9.2.3 Hydrogel Formation

Porous EH-PEG constructs were crosslinked using ammonium persulfate and N,N,N',N'-tetramethylethylenediamine at 15 mM using a sodium chloride-leaching technique. A saturated salt solution was used as the water component of the gel to slow the sodium chloride crystals from dissolving into the gel solution. The constructs were prepared using EHD and PEGDA Mn~ 700 at 1:10 molar EHD to PEGDA with 30 wt% initial monomer components. Sieves were used to sort sodium chloride to specified sizes. Gels were cut to 8 mm diameter with a cork borer and sodium chloride was leached out over 2 days in water. Gels were sterilized in 70% ethanol, washed in PBS and presoaked in control media plus FBS before cell loading.

In order to demonstrate the method of macroporous fabrication, EH-PEG hydrogels were imaged using Field Emission Environmental Scanning Electron Microscope (FE-ESEM) (FE-ESEM; Quanta 200F, FEI). Dried gels were placed on individual FE-ESEM sample stubs which were pre-coated with carbon adhesive. The stubs were mounted on a sample holder and loaded into the FE-ESEM. Each sample was analyzed at 25kV acceleration voltage and 500x magnification.

9.2.4 Human Mesenchymal Stem Cell Culture

hMSCs were purchased from Lonza and cultured according the manufacturer's specifications and as described in the literature.[265] Prior to the study, the hMSCs were cultured in control media composed of high glucose DMEM with 4 mM L-Glutamine, 0.1 mM non-essential amino acids, 1% penicillin/streptomycin (v/v) and 10% MSC qualified FBS. During the study, the osteogenic groups were supplemented with 100 nM dexamethasone, 10 mM Na-β-glyerophosphate, and 0.2 mM ascorbic acid. hMSCs were added to sterile, presoaked hydrogels in a concentrated cell solution. The cells were allowed to attach for 4 hours before filling the well with media. The media was changed every two days throughout the study.

9.2.5 Fibronectin Loading

The hydrogels were loaded with fibronectin in a sterile environment before use. Specifically, surface liquid was removed from hydrogels, and allowed to dry in a sterile environment for 1 hour. Then a concentrated solution of fibronectin was added and allowed to absorb for approximately 1 hour for final concentrations of 0.5, 2.5, and 10 μg fibronectin/gel. Then the hMSCs were added as previously described.

9.2.6 Deoxyribonucleic Acid Quantification

Deoxyribonucleic acid (DNA) was isolated from all samples to normalize the ALP and ELISA assays described below. Specifically, DNA was isolated using the DNeasy Tissue kit following standard protocols into 400 μL of eluate. DNA was

then quantified using the Quant-iT PicoGreen Kit following standard protocols for a 200 μL sample volume. Samples were incubated at room temperature for 5 minutes and read using the M5 SpectraMax plate reader (Molecular Devices, Sunnyvale, CA) with excitation/emission of 480/520 nm. All samples were completed in triplicate (n = 3).

9.2.7 Alkaline Phosphatase Assay

Protein was extracted using the M-per Mammalian Protein Extraction Reagent following standard protocols. Briefly, 50 μL of M-per was added to each sample and shaken for 10 min. Cell debris was removed by centrifugation at 14,000g for 15 min and the supernatant was used for analysis. A p-nitrophenyl phosphate liquid substrate system (pNPP) was used to analyze intracellular alkaline phosphatase (ALP) concentrations from the extracted protein. Briefly, the extracted protein sample was suspended in PBS and added to 100 μL of pNPP and incubated at room temperature for 30 min. The reaction was stopped by adding 50 μL of 2M NaOH. The absorbance was read using a M5 SpectraMax plate reader at 405 nm and normalized by the PicoGreen assay. All samples were completed in triplicate (n = 3).

9.2.8 Bone Morphogenetic Protein-2 Study

Hydrogel constructs were created, loaded with cells, and cultured as described above. At each time point, the media was removed and centrifuged to remove particulates and then frozen until analysis. The BMP-2 levels were measured using a

quantikine ELISA kit according to the manufacturer's instructions and read using a M5 SpectraMax platereader. Data was normalized to the DNA quantities as determined by the PicoGreen assay. All samples were completed in triplicate (n = 3).

9.2.9 Viability

Gels were cultured and analyzed throughout the study using the LIVE/DEAD assay as described previously.[269] At each timepoint, the gels were soaked in PBS for 1.5 hrs to remove FBS from the gel which can interact with the Live/Dead reagents. The gels were incubated with the Live/Dead reagents (2.5 μm ethidium homodimer-1 and 2.5 μm calcein AM) at room temperature for 30 min. Micrographs were then taken using a fluorescent microscope equipped with a digital camera.

9.2.10 Gene Expression

RNA was isolated from cells in monolayer using the RNeasy Mini Plus Kit following standard protocols. The RNA was isolated from the hMSCs in EH-PEG hydrogels using trizol and purified using the RNeasy mini kit following standard protocols. The isolated total RNA was reverse transcribed using High Capacity cDNA Archive Kit. The expression of BMP-2, BMP-RIA, BMP-R2, and osteocalcin was then investigated by quantitative real time polymerase chain reaction (qrt-PCR) on an ABI Prism 7000 sequence detector (Applied Biosystems) with GAPDH as an endogenous control. TaqMan Gene Expression assays were used for all genes and the sequences are proprietary. All samples were completed in triplicate (n = 3).

9.2.11 Tri-Layer Formation

Tri-layer scaffolds were constructed from two layers of porous EH-PEG bound to a central layer of porous EH polymer using a sodium chloride leaching technique. The EH-PEG layers were crosslinked using ammonium persulfate and N,N,N',N'-tetramethylethylenediamine at 40 mM. The constructs were prepared using EHD and PEGDA Mn~ 700 at 1:10 molar EHD to PEGDA with 30 wt% initial monomer components in a 40% acetone solution. The EH layer was crosslinked using 7 wt% benzoyl peroxide and 8 μL of N,N-Dimethyl-p-toludine per gram of EHD in acetone. Sieves were used to sort sodium chloride to specified sizes. Tri-layers were created with varying porosity and pore size; for all conditions the EH-PEG layer was held constant at 75 wt% while the EH layer was varied. The experimental groups included 70%, 75%, and 80% porosity at 250μm and 65%, 70%, and 75% porosity for 100μm. The two control groups were constructed from three layers of porous EH-PEG at each of the two pore sizes, lacking the central EH layer. Molds were used to construct each scaffold with the dimensions of 47 x 10mm. The scaffolds were constructed layer-by-layer, with the EHD being initiated as soon as polymerization of the bottom EH-PEG layer took place. The EH layer was then monitored closely and upon polymerization the final EH-PEG layer could be added to the top. Previous testing confirmed that interaction between the layers is time dependent. Following polymerization, the scaffolds were soaked in acetone for 15 minutes. Sodium chloride was then leached out over 2 days in water.

9.2.12 Mechanical Testing

Each scaffold was tested for flexural properties using a three-point bend test based on ASTM D 7264 Standard Test Method for Flexural Properties of Polymer matrix Composite Materials. An INSTRON 5565 mechanical tester was employed and Bluehill software was used to record load data until breaking. The pre-load was set at 0.01N and the extension rate at the standard 1 mm/min. Samples were prepared at a thickness of 4 mm (1.333 mm per layer) and a support span-to-thickness ratio of 8 was used for testing. Flexural strength was calculated as $\sigma_{fs}=(3F_fL)/(2bd^2)$ where F_f is the load at fracture, L is the distance between support points, and b and d are the width and height of the specimen, respectively.[273]

9.2.13 Statistical Analysis

Data from all studies was analyzed using ANOVA single factor analysis and Tukey's multiple comparison test ($p \leq 0.05$). All results are reported as mean ± standard deviation. Please note that only pertinent statistical relationships are noted in the figures.

9.3 Results

Creating macroporous hydrogels through porogen leaching is not an established technique. Here we implemented the use of a saturated salt solution for the water component of the gel in order to maintain porogen integrity by slowing the process of salt dissolving into the water-based system. To demonstrate the success of

the technique we analyzed the EH-PEG hydrogels using FESEM and phase contrast microscopy as demonstrated in Figure 34.

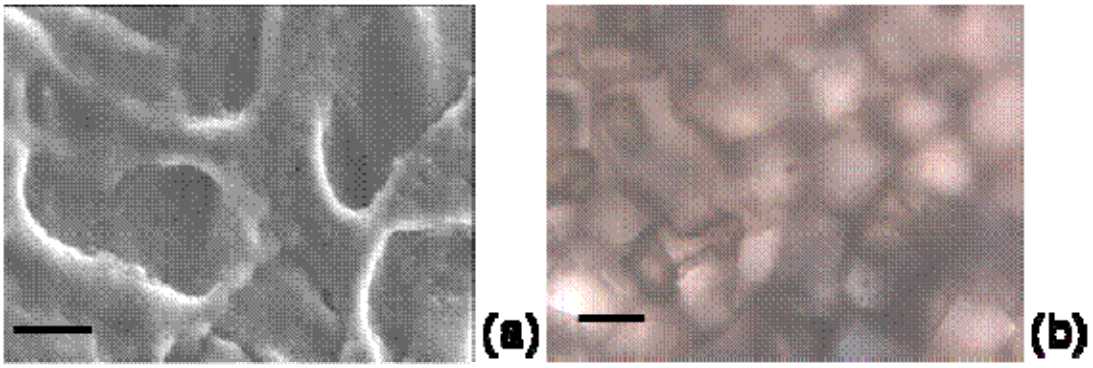

Figure 34: Micrographs of porous EH-PEG hydrogels with (a) FESEM and (b) phase contrast. Scale bar denotes 40 μm for FESEM and 200 μm for phase contrast.

We then investigated the effect of varying scaffold architecture. hMSCs were loaded into EH-PEG hydrogels with pore size/porosities of: 250 μm/75%, 250 μm/70%, 100 μm/70%, 100 μm/65%. The viability of hMSCs in EH-PEG hydrogels were analyzed throughout the study using the LIVE/DEAD assay, only images from the first and last timepoint are included for brevity (Figure 35). After one day of culture the cell populations appear viable in all groups independent of pore size and porosity. This was maintained throughout the study, and is represented by Figure 35 e-h at day 12 when the majority of the hMSCs appear viable in the EH-PEG hydrogels. It is important to note that during the study, while the hMSCs are viable in the EH-PEG hydrogels, they do not demonstrate a high degree of spreading common with hMSC culture.

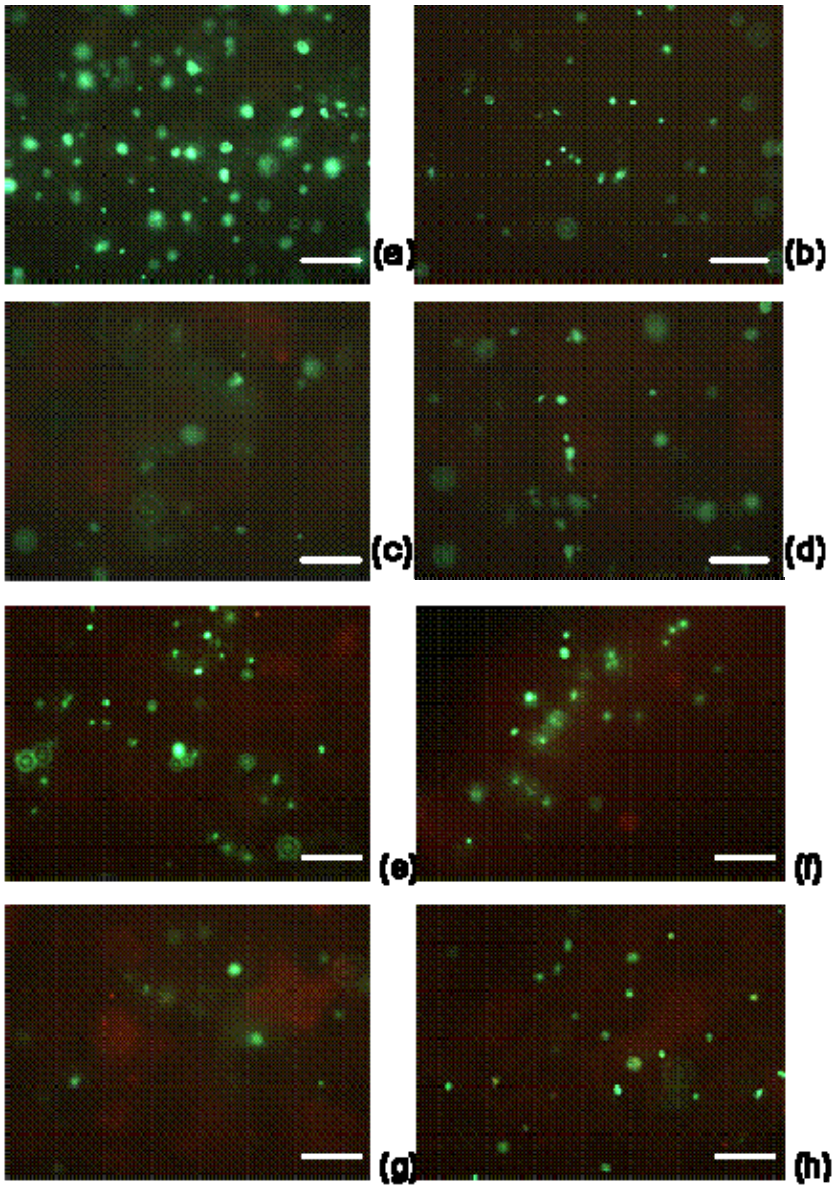

Figure 35: Viability of hMSCs in EH-PEG hydrogels. After one day of culture (a-d), and after twelve days of culture (e-h) the majority of the cell populations remain viable. (a, e) 100µm 65%, (b, f) 100µm 70%, (c, g) 250µm 70%, (d, h) 250µm 75%. Scale bar denotes 250µm.

Alkaline phosphatase levels were analyzed on days 1, 4, 8, and 12 days and normalized by DNA (Figure 36). The control groups were cultured in monolayer for all studies. The results indicate moderate changes from day 1 to day 4 for all groups. However, the hMSCs in the 100 µm EH-PEG hydrogels show significantly higher

expression than the controls at day 8 demonstrating a large increase from day 4. This represents a faster rate of expression when compared to the hMSCs in the 250 μm EH-PEG gels and the osteogenic control. From day 8 to day 12, the hMSCs in the 100 μm EH-PEG hydrogels decreased indicating the ALP expression had peaked for these groups, while the hMSCs in the 250 μm EH-PEG gels and the osteogenic control increased.

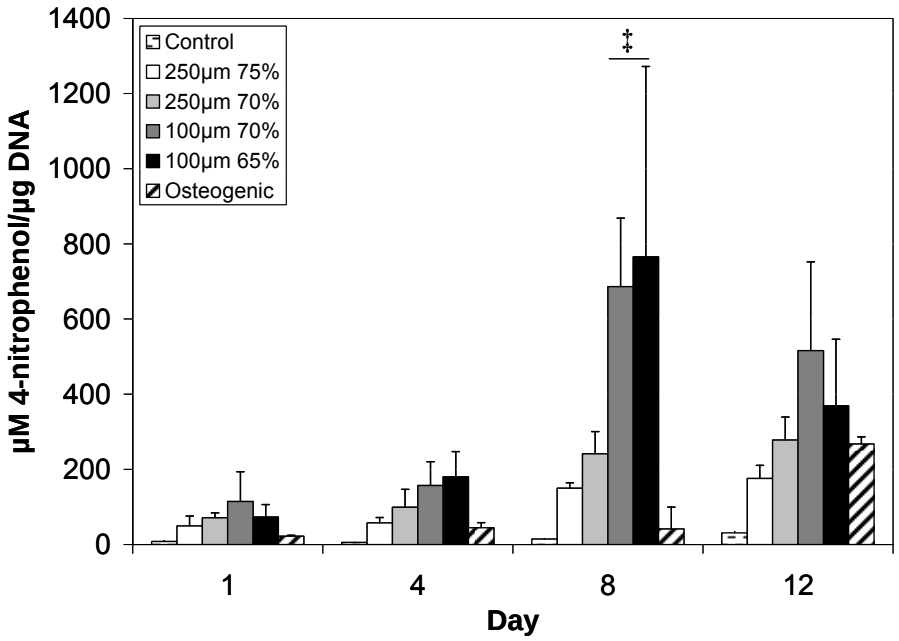

Figure 36: Alkaline phosphatase expression of cells after 1, 4, 8, and 12 d normalized by DNA. The results indicate moderate changes from day 1 to day 4 for all groups. The hMSCs in the 100μm EH-PEG gels showed a significant increase in expression from day 4 with a peak a day 8 demonstrating a faster rate of expression as compared to the osteogenic control. (‡) denotes statistical significance within that timepoint.

Bone morphogenetic protein-2 levels were measured by ELISA and normalized by DNA after 1, 4, 8, and 12 days (Figure 37). The results indicate similar levels for all groups at day one; however by day 4 the hMSCs in EH-PEG hydrogels show significantly higher levels as compared to the controls with no apparent trend to scaffold architecture. These elevated levels are increased at day 8

and maintained throughout the study, where at day 12 hMSCs within EH-PEG hydrogels show BMP-2 levels approximately 40-fold higher than that compared to hMSCs in monolayer controls.

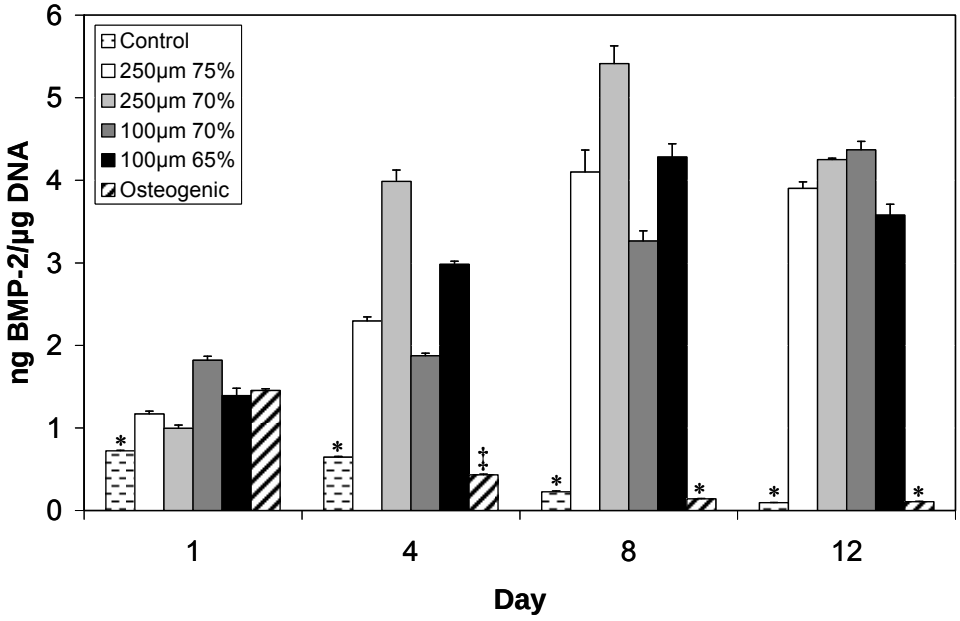

Figure 37: Bone morphogenetic protein-2 levels measured by ELISA and normalized by DNA after 1, 4, 8, and 12 days. The results indicate similar levels for all groups at day one; however by day 4 the hMSCs in EH-PEG hydrogels show significantly higher levels as compared to the controls. These elevated levels are maintained throughout the study. (‡, *) denote statistical significance within that timepoint.

hMSCs were cultured within EH-PEG hydrogels and analyzed on days 1, 4, 8, and 12 to investigate the effects of porosity and pore size on osteogenic signal expression. BMP-2 expression shows significantly elevated levels in all groups over the controls by day 1 and throughout the study independent of pore size or porosity (see Figure 38a.) Specifically, at day 12 hMSCs in the 250 µm EH-PEG gels had fold changes of 67 and 64 for 75 and 70%, respectively, and in the 100 µm EH-PEG gels a fold change of 26 and 90 for 70 and 65%, respectively over the monolayer control. Further analysis showed that this increase in BMP-2 expression correlated

with an increase in BMP receptor expression (Figures 38b, c) as demonstrated by significantly increased levels of BMP-RIA and BMP-R2. The increase in receptor expression was again independent of scaffold architecture; however the increase was not to the same magnitude as the BMP-2 increase as all groups demonstrated a fold change of approximately 2 at day 12. Osteocalcin expression was also analyzed; however only low levels were detected indicating the hMSCs were not expressing the late-stage differentiation marker.

(a)

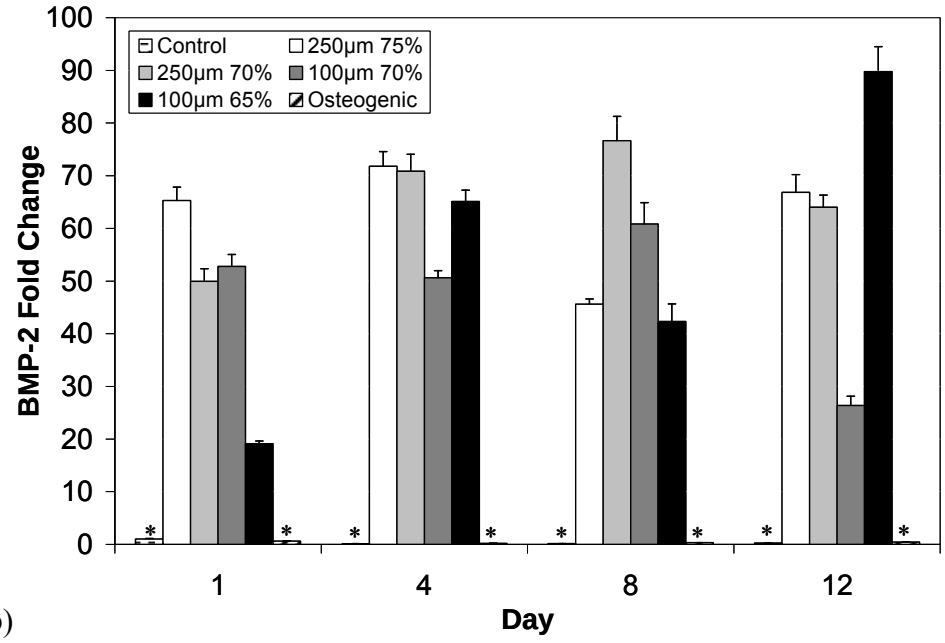

(b)

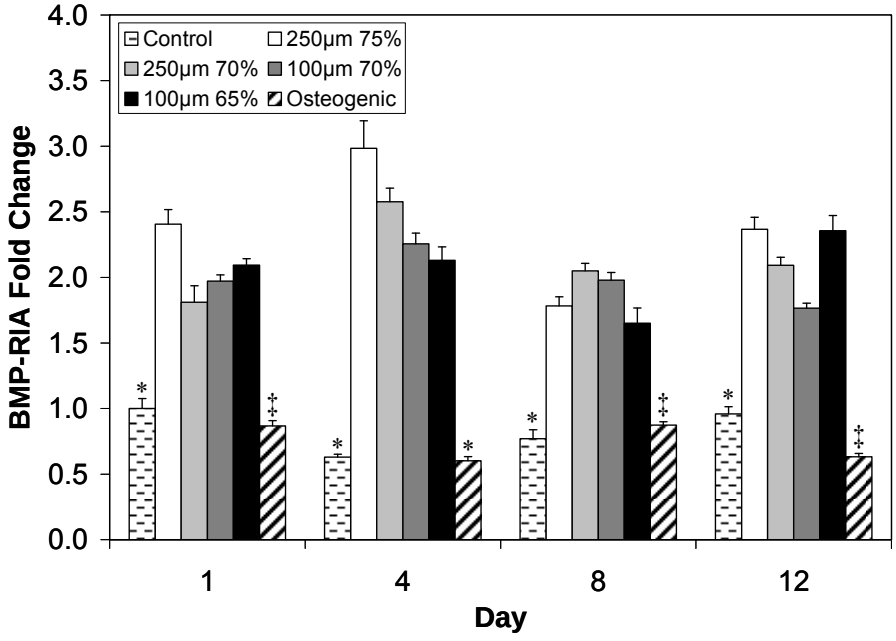

(c)

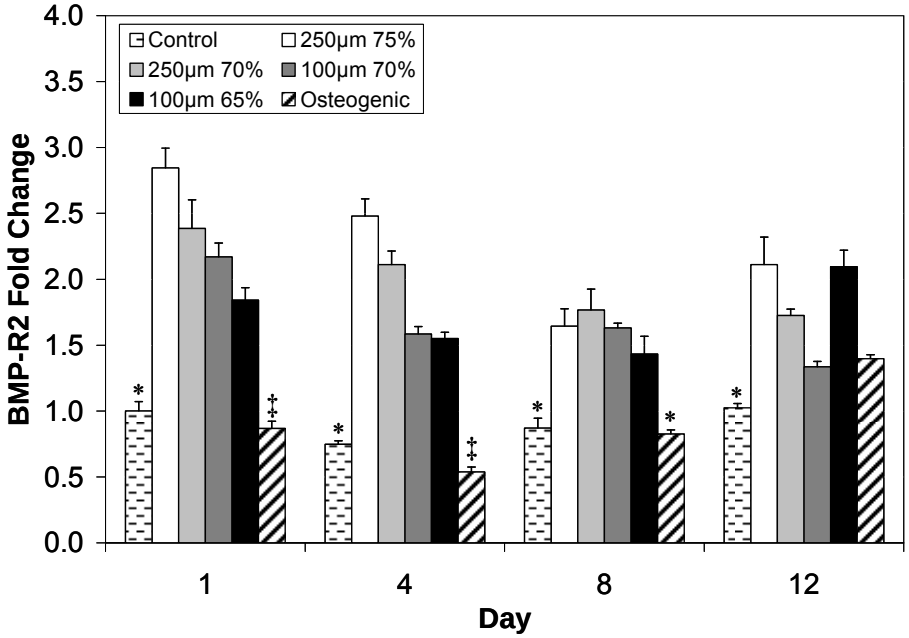

Figure 38: Quantitative RT-PCR analysis after 1, 4, 8, and 12 days for (a) bone morphogenetic protein-2, (b) bone morphogenetic protein- receptor type IA, and (c) bone morphogenetic protein- receptor type 2. BMP-2 expression shows significantly elevated levels over all controls throughout the study independent of pore size and porosity. The increase of BMP-2 correlated with a significant increase in receptor expression (b, c). The elevated levels of BMP receptor expression is maintained throughout the study and is independent of pore size and porosity. (‡, *) denote statistical significance within that timepoint.

From the previous studies we chose to move forward with the 100µm 65% EH-PEG hydrogels and added fibronectin at concentrations of 0.5, 2.5, and 10 µg/gel. The viability of EH-PEG hydrogels with increasing concentrations of fibronectin was assessed throughout the study using the LIVE/DEAD assay. For the duration of the investigation the majority of the hMSCs appeared viable as shown in Figure 39 where at days 4 and 8 the populations of hMSCs are fluorescing green. In addition, the hMSCs on EH-PEG hydrogels with higher concentrations of fibronectin demonstrated cell spreading.

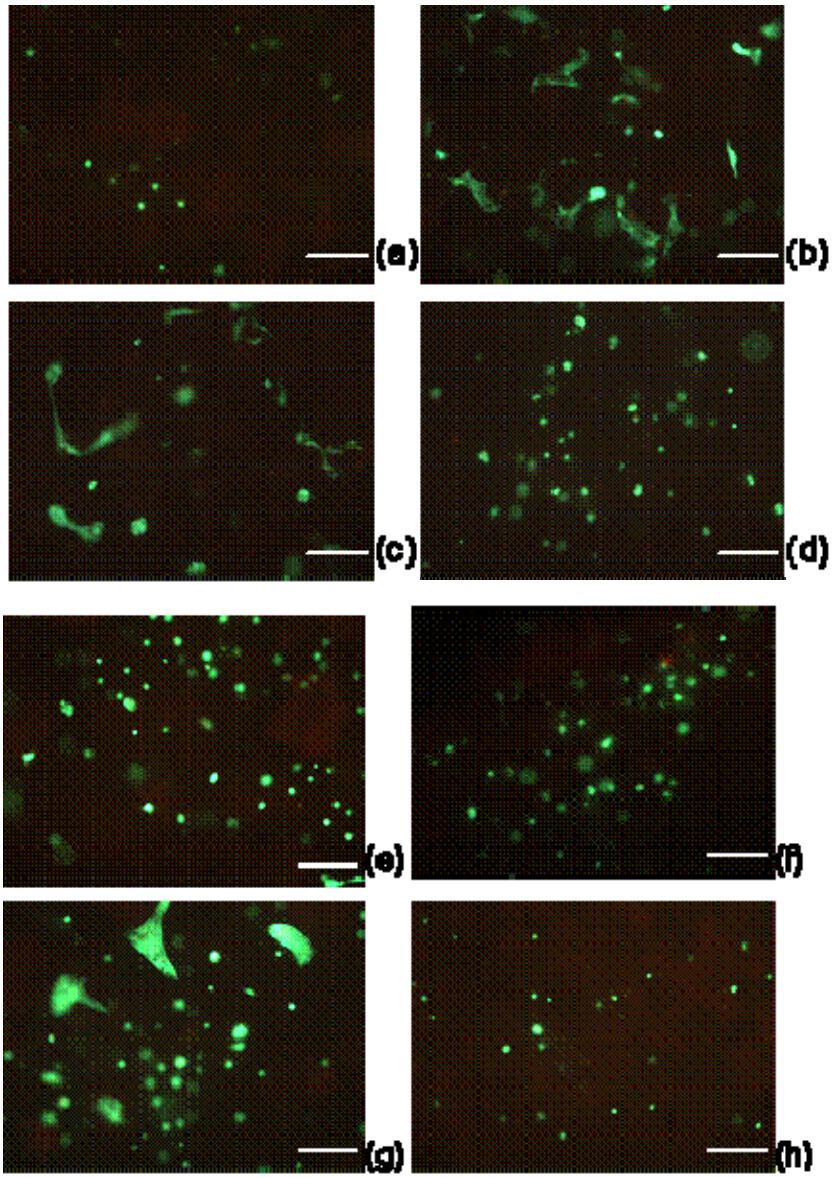

Figure 39: Viability of hMSCs in EH-PEG hydrogels with increasing concentrations of fibronectin. After four days of culture (a-d) and after eight days of culture (e-h) the majority of the cell populations were viable. Higher concentrations of fibronectin demonstrate cell spreading. (a, e) 0.5µg fib/gel, (b, f) 2.5µg fib/gel, (c, g) 10µg fib/gel, (d, h) osteogenic control. Scale bar denotes 250µm.

hMSCs were cultured on EH-PEG hydrogels and analyzed on days 1, 4, and 8 to investigate the effects of fibronectin concentration on osteogenic signal expression. BMP-2 expression shows significantly elevated levels in all groups over the controls throughout the study, with a slight increase from day 1 to day 4 (see Figure 40a.) In

addition, at day 4 and day 8, the hMSCs in EH-PEG gels with the highest concentrations of fibronectin demonstrated the highest expression of BMP-2. Specifically, at day 8, the hMSCs cultured in the 10µg fibronectin/gel EH-PEG gels showed a fold change of 60 over the control. Further analysis showed that the increase in BMP-2 expression correlated with an increase in BMP receptor expression (Figures 40b, c) as demonstrated by significantly increased levels of BMP-RIA and BMP-R2. For days 1 and 4 the increase in receptor levels is independent of fibronectin concentration. However, at day 8 the increase appears to be dependant on fibronectin concentration, where the higher concentrations demonstrate significantly higher receptor level expression for both BMP-RIA and BMP-R2 as compared to the other concentrations. As shown in the previous section, the increase in receptor expression was not to the same magnitude as the BMP-2 increase where the BMP-RIA increase was approximately two-fold and the BMP-R2 increase was approximately 1.5 fold at day 12.

(a)

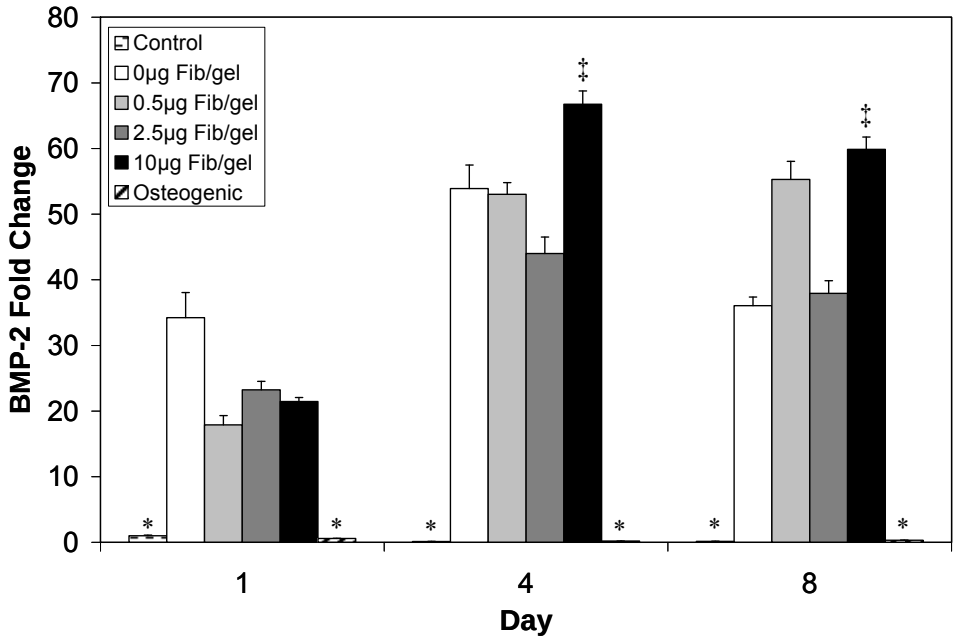

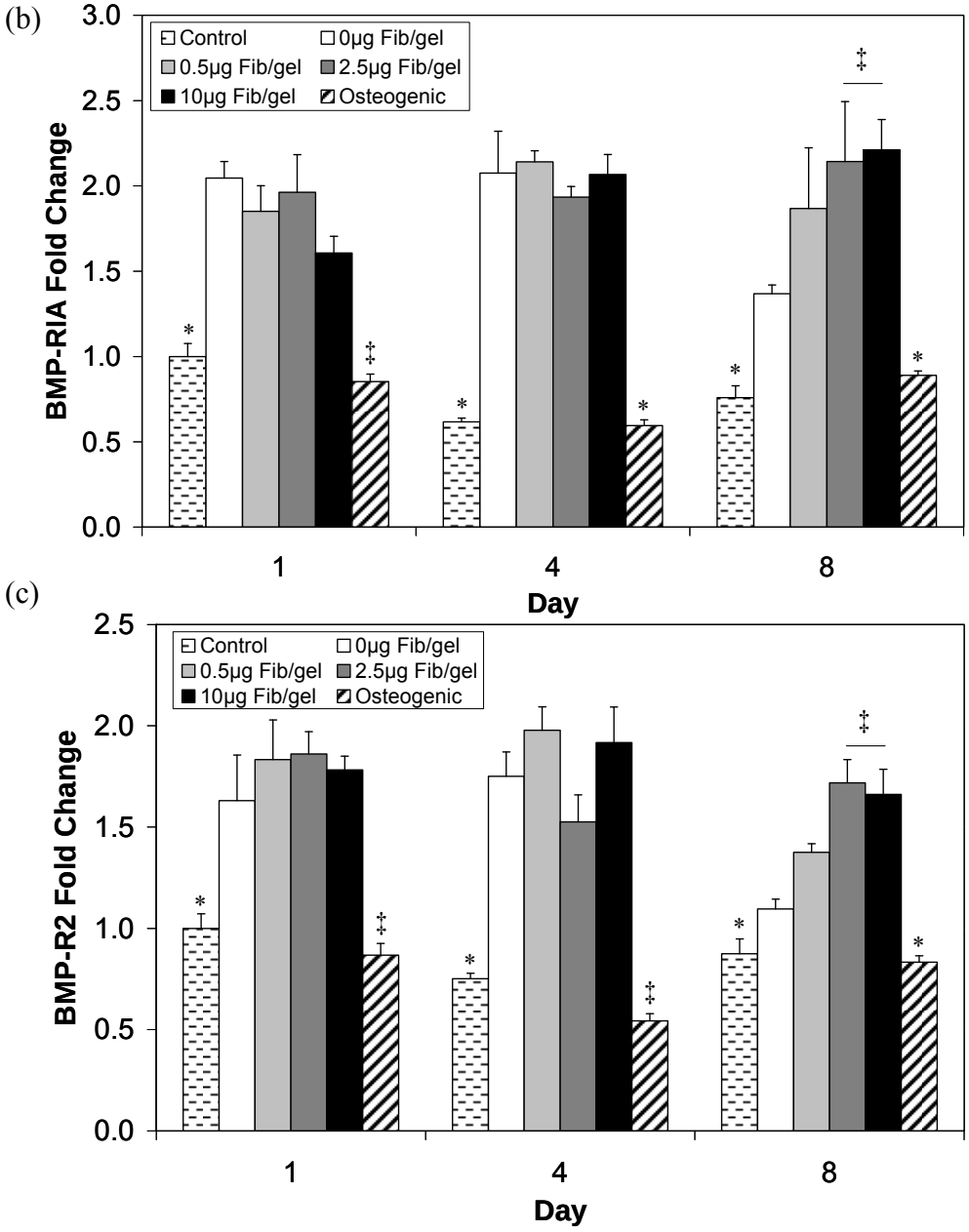

Figure 40: Quantitative RT-PCR analysis after 1, 4, and 8 days for (a) bone morphogenetic protein-2, (b) bone morphogenetic protein- receptor type 1A, and (c) bone morphogenetic protein- receptor type 2. BMP-2 expression shows significantly elevated levels over all controls throughout the study, with a slight increase from day 1 to day 4. The increase of BMP-2 correlated with a significant increase in receptor expression (b, c). The elevated levels of BMP receptor expression is maintained throughout the study and appears to have a slight dependence on fibronectin concentration, where the higher concentrations demonstrate higher receptor expression. (‡, *) denote statistical significance within that timepoint.

Tri-layer scaffolds were created with varying porosity and pore size to test for flexural properties using a three-point bending test (Figure 41). The results indicate that the scaffolds showed increasing strength with decreasing porosity when comparing scaffolds with the same pore size (Figure 42). The tri-layer scaffolds at 250 μm did show a slight increase in strength over the EH-PEG control. However, the tri-layer scaffolds at 100 μm showed significantly higher strength when compared to the control and to the 250 μm scaffolds.

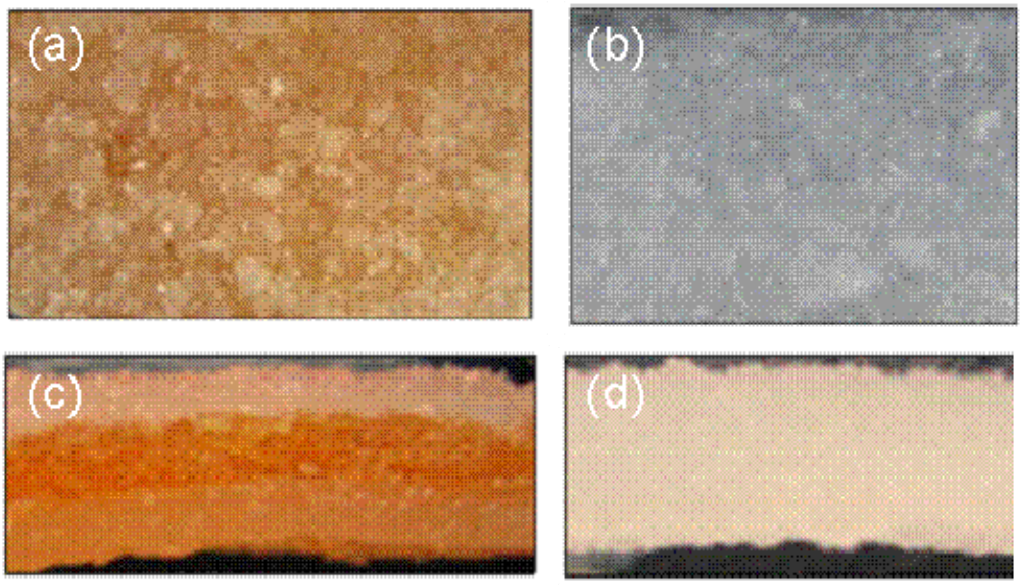

Figure 41: Scaffolds for mechanical testing. Tri-layer scaffolds (a, c) and control EH-PEG gels (b, d). Top view of the scaffold (a, b) and side view demonstrates layers (c, d).

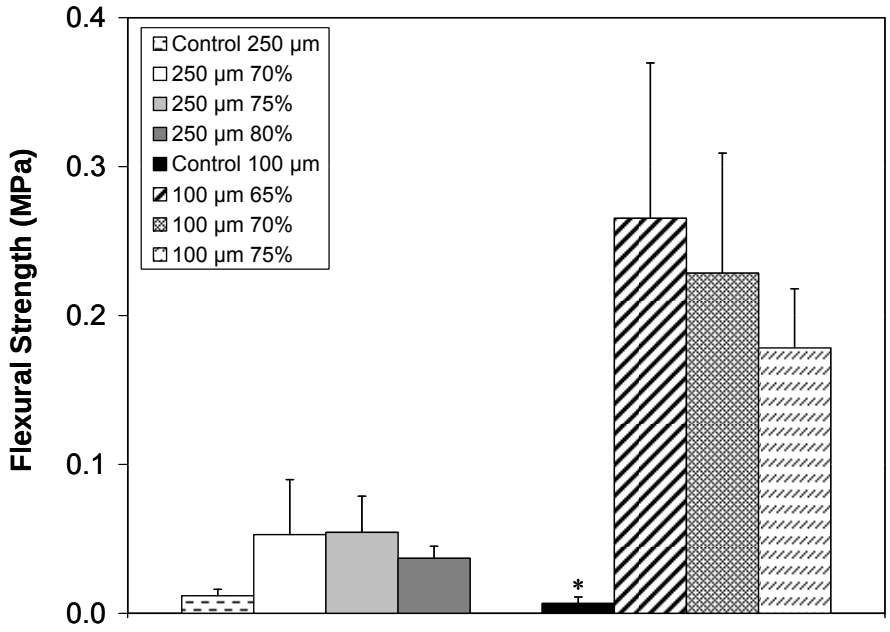

Figure 42: Tri-layer scaffolds with varying porosity and pore size were created and a three-point bend test was performed to analyze flexural strength. The results indicate increasing strength with decreasing porosity with the same pore size. The tri-layer scaffolds at 100 µm showed significantly higher strength when compared to the control and to the 250 µm scaffolds. (*) denotes statistical significance within that pore size.

9.4 Discussion

Scaffold architecture is important in determining the success of a tissue engineering construct. Specifically, the porosity of a scaffold is essential as it supports integration with the surrounding tissue. Furthermore, increased porosity allows for cellular infiltration and therefore increased cell density within the scaffold. This change in cell density will augment cell interaction and, as a result, cell signaling.

The objective of this work was to (1) investigate the effects of scaffold architecture, through varying porosity and pore size, in EH-PEG hydrogels on osteogenic signal expression. From this study we anticipated the results would

indicate an optimal architecture for the EH-PEG hydrogels to use in further investigations. Therefore, our next objective was to (2) examine the effect of cell adhesion through incorporation of fibronectin in EH-PEG hydrogels with an optimal architecture on osteogenic signal expression. Lastly, as varying architecture can alter the strength of the scaffold, we (3) investigated the strength of EH-PEG scaffolds with varying pore size and porosity.

First, we created macroporous EH-PEG hydrogels using porogen leaching, and demonstrated the success of the technique through FESEM and phase-contrast microscopy (Figure 34). To maintain porogen integrity, a saturated salt solution was used as the water component which slowed the dissolution of salt during crosslinking. As this technique is easily used, it should be considered when making macroporous hydrogels.

In order to evaluate the effect of varying architecture on osteogenic signal expression of hMSCs, cells were seeded on EH-PEG scaffolds with varying porosity and pore size and compared to cells cultured in monolayer. Viability was monitored throughout the study, and results demonstrated that the cell populations maintained viability throughout the study independent of architecture. When analyzing the morphology of the cells, the hMSCs do not appear as spread as in standard cultures, indicating a modification to the scaffold may be necessary.

Next, hMSCs within EH-PEG hydrogels were analyzed for alkaline phosphatase expression, an early osteogenic marker. The results demonstrate higher expression for the EH-PEG hydrogels when compared to the monolayer controls. In addition, further analysis demonstrates that the EH-PEG hydrogels with a pore size of

100 μm show higher expression at day 8 as compared to all other groups and also represent a faster rate of expression. This difference, dependent on scaffold architecture, could be due to a decrease in proliferation or cell aggregation caused by the smaller pores.

hMSCs were also loaded in EH-PEG hydrogels and analyzed for osteogenic signal expression as measured by BMP-2, BMP-RIA, and BMP-R2 expression levels. BMP-2 showed increased expression for all groups independent of pore size and porosity over the controls. Furthermore, this large increase in BMP-2 expression was associated with approximately a two-fold increase in receptor expression for all groups. This demonstrates that the increase in BMP-2 signal expression does not require an equal increase in receptor expression to aid in signal transduction. While it is clear that the EH-PEG hydrogels significantly enhance osteogenic signal expression of hMSCs, it does not appear to be dependent on scaffold architecture. Studies have demonstrated the ability of substrate stiffness to impact the differentiation of hMSCs.[274] Specifically, after several weeks in culture, cells commit to a lineage specified by matrix elasticity. While, this may have an effect on the hMSCs in our EH-PEG hydrogels, the osteogenic signal expression increased significantly by day one, so there may be other factors involved as well, such as proliferation rates and possible cell aggregation. Osteocalcin expression was also measured; however, only low levels were detected revealing that the late osteogenic marker is not being expressed. This indicates that over the length of this study, the EH-PEG scaffolds have been optimized for early osteogenic differentiation of hMSCs

as demonstrated by the early osteogenic marker alkaline phosphatase and the early signaling expression of BMP-2 and the related receptors.

Results from the previous studies indicate that the ideal EH-PEG architecture to use for hMSC culture was 100 μm/65% porosity. We then chose to add the extracellular matrix protein fibronectin to the EH-PEG hydrogels, as fibronectin is known to aid in hMSC attachment.[275,276] This environment is conducive to differentiation and therefore may enhance osteogenic cell signaling.

First, results indicate that the majority of the cells remained viable during the 8 days, independent of fibronectin concentration. Furthermore, the morphology of the cells was altered when compared to the previous studies. The hMSCs with higher concentrations of fibronectin demonstrated more cell spreading as compared EH-PEG hydrogels with no fibronectin, consistent with what is predicted from the literature.

Next, the effect of fibronectin addition to EH-PEG hydrogels on osteogenic signal expression was investigated. At day one there was a significant increase of BMP-2 expression over the controls with no dependence on fibronectin concentration. From day one to four the expression of BMP-2 increased and was maintained through day 8. At these last timepoints the highest level of BMP-2 expression correlated with the highest concentration of fibronectin concentration, however there does not appear to be a trend. This was also present in the receptor expression levels where at day one there was increased receptor expression independent of fibronectin concentration, but at the later timepoints, the highest expression appeared in the groups with the highest concentration. This suggests that

fibronectin may play a role in promoting the early osteogenic signaling which is involved in osteodifferentiation.

The importance of cell adhesion was investigated through the addition of fibronectin to the EH-PEG hydrogels. As demonstrated by the above results, when compared to monolayer controls, hMSCs cultured in EH-PEG hydrogels exhibit increased osteogenic signaling as shown by BMP-2 expression and BMP receptor expression. It is important to note that the increase in expression as a result in the change in architecture was similar to the increase shown by the hMSCs cultured on EH-PEG hydrogels with fibronectin. As these expression levels are both compared to hMSCs cultured in monolayer it can be determined that the increase in expression is predominately due to the change in architecture rather than as a result of an increase in cell adhesion from the incorporation of fibronectin in EH-PEG hydrogels.

As altering architecture can decrease the strength of the scaffold, it is important that the construct performs as required for the desired application. For orbital floor regeneration, the purpose of the orbital floor is to support the orbital contents. Therefore, one objective of this study was to modify the hydrogels by introducing a stiff, but still porous, central layer to improve support. The resulting tri-layer scaffolds were tested in a three-point bend test for flexural properties which simulate the physiological stresses *in situ* for orbital floors.

Tri-layer scaffolds were created with varying pore size and porosity. The results indicate increasing strength with decreasing porosity, as expected. Furthermore, the 250 μm tri-layer scaffolds did show some increase over the 250 μm EH-PEG control, however it was not significant. The 100 μm tri-layer scaffolds

showed significant improvement over the 100 μm EH-PEG hydrogel with the addition of the porous EH layer. In addition, the 100 μm scaffolds were significantly stronger than the 250 μm tri-layer scaffolds. It is possible that the scaffolds with the larger pore sizes and higher porosities may have improved interconnectivity which may cause decreased strength.

While it is interesting to see the difference in strength between the scaffolds with varying architecture, the most important question is whether the construct will support the orbital contents. It is difficult to perform mechanical studies on the human orbital floor as it is composed of portions of three bones, and the anatomy is difficult to simulate in animal models. However, the literature has reported that the combined weight of the human orbital contents is approximately 42.97 ± 4.05 g.[154] From this data, we can estimate the orbital contents would apply approximately 0.13 MPa which can be supported by our 100 μm scaffolds, but exceeds the strength of the 250 μm scaffolds. This analysis indicates that the 100 μm scaffolds are an appropriate construct for orbital floor repair, while the 250 μm scaffolds may need more adjustments before use.

9.5 Conclusions

The objectives of this work were to investigate the effects of varying pore size and porosity in EH-PEG hydrogels and incorporation of fibronectin on osteogenic signal expression, and investigate the strength of EH-PEG scaffolds with varying pore size and porosity. Alkaline phosphatase levels increased for hMSCs in EH-PEG gels with 100 μm pores. Furthermore, osteogenic signal expression analysis showed

elevated levels for all EH-PEG groups as demonstrated by BMP-2, BMP-RIA, and BMP-R2 expression levels. Further work demonstrated the inclusion of fibronectin in EH-PEG hydrogels shows increased hMSC attachment and spreading with increased fibronectin concentration. In addition, the increase in osteogenic signal expression in EH-PEG hydrogels with fibronectin is comparable to the increase seen when comparing expression levels of hMSCs in porous EH-PEG hydrogels to cells cultured in monolayer. This indicates the increase in expression may be due to the change in architecture rather than adhesion. Lastly, mechanical testing demonstrated the ability to increase the strength of EH-PEG hydrogels by creating a tri-layer scaffold with the central layer composed of a stiff, porous, EH sheet. This demonstrates that the EH-PEG hydrogels are a viable option for orbital floor repair.

Chapter 10: Summary

The goal of this project was to utilize tissue engineering strategies to regenerate orbital floor bone using a novel cyclic acetal scaffold with an osteoprogenitor cell population through enhanced osteogenic cell signaling. Construct design is an intricate process and must be tailored for different bone tissue engineering applications. Orbital bone engineering offers solutions to the current clinical techniques and can aid in regeneration of natural bone tissue that is similar in both form and function to the native orbital floor.

The first objective of our work was to harvest primary bone marrow stromal cells and induce differentiation through coculture with chondrocytes and the standard osteogenic media supplements dexamethasone and the Na-β–glycerolphosphate. We demonstrated that coculturing chondrocytes encapsulated in alginate hydrogels can effectively induce differentiation in a mechanism distinct from that of the media supplements dexamethasone and the Na-β–glycerolphosphate. Furthermore, we characterized this interaction as having separate temporal components, with brief exposure proving sufficient to induce early stages of differentiation, but extended exposure necessary for mature osteogenic development.

Next, we wanted to investigate whether EH-PEG hydrogels, and their fabrication components, permit bone marrow stromal cell viability, metabolic activity, and osteodifferentiation. The results demonstrated that the metabolic activity and viability of bone marrow stromal cells in monolayer are minimally affected by the APS-TEMED initiator system for extended time periods. In addition, it shows that on the time scale required for encapsulation, the initiator system does not significantly

affect expression of osteogenic markers, measured both at the mRNA and protein level. From these results, an optimal initiator concentration was chosen to crosslink EH-PEG hydrogels. Finally, encapsulated bone marrow stromal cells were shown to survive in EH-PEG hydrogels crosslinked using the optimal APS-TEMED concentration for 7 d. This work demonstrated that EH-PEG hydrogels are a viable platform for encapsulation and osteodifferentiation of bone marrow stromal cells.

Our next objective was to investigate the tissue response to EH-PEG hydrogels, characterize the release of BMP-2 from EH-PEG hydrogels, and analyze their ability to deliver BMP-2 *in vivo* and facilitate bone formation. The results indicate that the tissue surrounding the EH-PEG constructs showed a positive progression during the study, indicating that constructs were not eliciting a chronic response. In addition the release of BMP-2 from the construct was complete in 2-4 hours, and happened more quickly at the higher concentration. Lastly, the data shows the ability for EH-PEG gels to deliver BMP-2 as shown by the new bone growth in the area surrounding the constructs containing high concentrations of BMP-2 at 28 d. This demonstrates that EH-PEG constructs are a viable option for use *in vivo* and for delivery of BMP-2 *in vivo*.

The next objective of our work was to fabricate macroporous EH-PEG hydrogels and characterize the architecture using optical coherence tomography. In this work, macroporous EH-PEG hydrogels were produced using porogen-leaching demonstrating a simple technique for fabrication. OCT was used to quantify pore size and volume porosity. Reported pore sizes were within the expected range, as estimated from the starting materials, demonstrating the ability of OCT to quantify

pore size. In addition, OCT image analysis was able to be used to characterize volume porosity, a parameter not previously known. Further work combined OCT with confocal microscopy where viable cells were visualized within the scaffolds.

Last, we investigated the effects of varying pore size and porosity in EH-PEG hydrogels and incorporation of fibronectin on osteogenic signal expression, and investigate the strength of EH-PEG scaffolds with varying pore size and porosity. Alkaline phosphatase levels increased for hMSCs in EH-PEG gels with 100 μm pores. Furthermore, osteogenic signal expression analysis showed elevated levels for all EH-PEG groups as demonstrated by BMP-2, BMP-RIA, and BMP-R2 expression levels. Further work demonstrated the inclusion of fibronectin in EH-PEG hydrogels shows increased hMSC attachment and spreading with increased fibronectin concentration. In addition, the increase in osteogenic signal expression in EH-PEG hydrogels with fibronectin is comparable to the increase seen when comparing expression levels of hMSCs in porous EH-PEG hydrogels to cells cultured in monolayer. This indicates the increase in expression may be due to the change in architecture rather than adhesion. Lastly, mechanical testing demonstrated the ability to increase the strength of EH-PEG hydrogels by creating a tri-layer scaffold with the central layer composed of a stiff, porous, EH sheet. This demonstrates that the EH-PEG hydrogels are a viable option for orbital floor repair.

These studies have demonstrated the use of EH-PEG hydrogels as a tissue engineering construct with application for orbital floor repair. Specifically, through the demonstration of long term viability of encapsulated cells, growth factor delivery,

minimal tissue response *in vivo,* and enhanced osteogenic signaling of cell populations within the hydrogels.

Bibliography

1. Langer R, Vacanti JP. Tissue engineering. Science 1993;260(5110):920-6.
2. Angelova N, Hunkeler D. Rationalizing the design of polymeric biomaterials. Trends Biotechnol 1999;17(10):409-21.
3. Lee SH, Kim BS, Kim SH, Kang SW, Kim YH. Thermally produced biodegradable scaffolds for cartilage tissue engineering. Macromol Biosci 2004;4(8):802-10.
4. Gutowska A, Jeong B, Jasionowski M. Injectable gels for tissue engineering. Anat Rec 2001;263(4):342-9.
5. Yang S, Leong KF, Du Z, Chua CK. The design of scaffolds for use in tissue engineering. Part II. Rapid prototyping techniques. Tissue Eng 2002;8(1):1-11.
6. Yang S, Leong KF, Du Z, Chua CK. The design of scaffolds for use in tissue engineering. Part I. Traditional factors. Tissue Eng 2001;7(6):679-89.
7. Mikos AG, Bao Y, Cima LG, Ingber DE, Vacanti JP, Langer R. Preparation of poly(glycolic acid) bonded fiber structures for cell attachment and transplantation. J Biomed Mater Res 1993;27(2):183-9.
8. Lu L, Mikos AG. The importance of new processing techniques in tissue engineering. MRS Bull 1996;21(11):28-32.
9. Gomes ME, Sikavitsas VI, Behravesh E, Reis RL, Mikos AG. Effect of flow perfusion on the osteogenic differentiation of bone marrow stromal cells cultured on starch-based three-dimensional scaffolds. J Biomed Mater Res A 2003;67(1):87-95.
10. Mikos AG, Thorsen AJ, Czerwonka LA, Bao Y, Langer R, Winslow DN, Vacanti JP. Preparation and characterization of poly(L-lactic acid) foams. Polymer 1994;35(5):1068-77.
11. Taboas JM, Maddox RD, Krebsbach PH, Hollister SJ. Indirect solid free form fabrication of local and global porous, biomimetic and composite 3D polymer-ceramic scaffolds. Biomaterials 2003;24(1):181-94.
12. Oh SH, Kang SG, Kim ES, Cho SH, Lee JH. Fabrication and characterization of hydrophilic poly(lactic-co-glycolic acid)/poly(vinyl alcohol) blend cell scaffolds by melt-molding particulate-leaching method. Biomaterials 2003;24(22):4011-21.
13. Burdick JA, Frankel D, Dernell WS, Anseth KS. An initial investigation of photocurable three-dimensional lactic acid based scaffolds in a critical-sized cranial defect. Biomaterials 2003;24(9):1613-20.
14. Wolfe MS, Dean D, Chen JE, Fisher JP, Han S, Rimnac CM, Mikos AG. In vitro degradation and fracture toughness of multilayered porous poly(propylene fumarate)/beta-tricalcium phosphate scaffolds. J Biomed Mater Res 2002;61(1):159-64.
15. Hua FJ, Kim GE, Lee JD, Son YK, Lee DS. Macroporous poly(L-lactide) scaffold 1. Preparation of a macroporous scaffold by liquid--liquid phase

separation of a PLLA--dioxane--water system. J Biomed Mater Res 2002;63(2):161-7.
16. Nam YS, Park TG. Porous biodegradable polymeric scaffolds prepared by thermally induced phase separation. J Biomed Mater Res 1999;47(1):8-17.
17. Nam YS, Park TG. Biodegradable polymeric microcellular foams by modified thermally induced phase separation method. Biomaterials 1999;20(19):1783-90.
18. Zhang K, Wang Y, Hillmyer MA, Francis LF. Processing and properties of porous poly(L-lactide)/bioactive glass composites. Biomaterials 2004;25(13):2489-500.
19. Thomson RC, Yaszemski MJ, Powers JM, Mikos AG. Fabrication of biodegradable polymer scaffolds to engineer trabecular bone. J Biomater Sci Polym Ed 1995;7(1):23-38.
20. Hsu YY, Gresser JD, Trantolo DJ, Lyons CM, Gangadharam PR, Wise DL. Effect of polymer foam morphology and density on kinetics of in vitro controlled release of isoniazid from compressed foam matrices. J Biomed Mater Res 1997;35(1):107-16.
21. Sachlos E, Czernuszka JT. Making tissue engineering scaffolds work. Review: the application of solid freeform fabrication technology to the production of tissue engineering scaffolds. Eur Cell Mater 2003;5:29-39; discussion 39-40.
22. Whang K, Tsai DC, Nam EK, Aitken M, Sprague SM, Patel PK, Healy KE. Ectopic bone formation via rhBMP-2 delivery from porous bioabsorbable polymer scaffolds. J Biomed Mater Res 1998;42(4):491-9.
23. Mathieu LM, Mueller TL, Bourban PE, Pioletti DP, Muller R, Manson JA. Architecture and properties of anisotropic polymer composite scaffolds for bone tissue engineering. Biomaterials 2005.
24. Nam YS, Yoon JJ, Park TG. A novel fabrication method of macroporous biodegradable polymer scaffolds using gas foaming salt as a porogen additive. J Biomed Mater Res 2000;53(1):1-7.
25. Sheridan MH, Shea LD, Peters MC, Mooney DJ. Bioabsorbable polymer scaffolds for tissue engineering capable of sustained growth factor delivery. J Control Release 2000;64(1-3):91-102.
26. Giordano RA, Wu BM, Borland SW, Cima LG, Sachs EM, Cima MJ. Mechanical properties of dense polylactic acid structures fabricated by three dimensional printing. J Biomater Sci Polym Ed 1996;8(1):63-75.
27. Kim SS, Utsunomiya H, Koski JA, Wu BM, Cima MJ, Sohn J, Mukai K, Griffith LG, Vacanti JP. Survival and function of hepatocytes on a novel three-dimensional synthetic biodegradable polymer scaffold with an intrinsic network of channels. Ann Surg 1998;228(1):8-13.
28. Wu BM, Borland SW, Giordano RA, Cima LG, Sachs EM, Cima MJ. Solid free-form fabrication of drug delivery devices. Journal of Controlled Release 1996;40(1-2):77-87.
29. Mikos AG, Sarakinos G, Leite SM, Vacanti JP, Langer R. Laminated three-dimensional biodegradable foams for use in tissue engineering. Biomaterials 1993;14(5):323-30.

30. Cooke MN, Fisher JP, Dean D, Rimnac C, Mikos AG. Use of stereolithography to manufacture critical-sized 3D biodegradable scaffolds for bone ingrowth. Journal of Biomedical Materials Research Part B-Applied Biomaterials 2003;64B(2):65-69.
31. Mapili G, Lu Y, Chen S, Roy K. Laser-layered microfabrication of spatially patterned functionalized tissue-engineering scaffolds. J Biomed Mater Res B Appl Biomater 2005.
32. Cooke MN, Fisher JP, Dean D, Rimnac C, Mikos AG. Use of stereolithography to manufacture critical-sized 3D biodegradable scaffolds for bone ingrowth. J Biomed Mater Res 2003;64B(2):65-9.
33. Cao T, Ho KH, Teoh SH. Scaffold design and in vitro study of osteochondral coculture in a three-dimensional porous polycaprolactone scaffold fabricated by fused deposition modeling. Tissue Eng 2003;9 Suppl 1:S103-12.
34. Rohner D, Hutmacher DW, Cheng TK, Oberholzer M, Hammer B. In vivo efficacy of bone-marrow-coated polycaprolactone scaffolds for the reconstruction of orbital defects in the pig. J Biomed Mater Res B Appl Biomater 2003;66(2):574-80.
35. Zein I, Hutmacher DW, Tan KC, Teoh SH. Fused deposition modeling of novel scaffold architectures for tissue engineering applications. Biomaterials 2002;23(4):1169-85.
36. Hutmacher DW, Schantz T, Zein I, Ng KW, Teoh SH, Tan KC. Mechanical properties and cell cultural response of polycaprolactone scaffolds designed and fabricated via fused deposition modeling. J Biomed Mater Res 2001;55(2):203-16.
37. Ma PX, Zhang R. Synthetic nano-scale fibrous extracellular matrix. J Biomed Mater Res 1999;46(1):60-72.
38. Chen GP, Ushida T, Tateishi T. Development of biodegradable porous scaffolds for tissue engineering. Materials Science & Engineering C-Biomimetic and Supramolecular Systems 2001;17(1-2):63-69.
39. Lu Y, Chen SC. Micro and nano-fabrication of biodegradable polymers for drug delivery. Adv Drug Deliv Rev 2004;56(11):1621-1633.
40. Hutmacher DW. Scaffold design and fabrication technologies for engineering tissues--state of the art and future perspectives. J Biomater Sci Polym Ed 2001;12(1):107-24.
41. Middleton JC, Tipton AJ. Synthetic biodegradable polymers as orthopedic devices. Biomaterials 2000;21(23):2335-46.
42. Vehof JW, Fisher JP, Dean D, van der Waerden JP, Spauwen PH, Mikos AG, Jansen JA. Bone formation in transforming growth factor beta-1-coated porous poly(propylene fumarate) scaffolds. J Biomed Mater Res 2002;60(2):241-51.
43. Thomson RC, Wake MC, Yaszemski MJ, Mikos AG. Biodegradable polymer scaffolds to regenerate organs. Biopolymers Ii 1995;122:245-274.
44. Agrawal CM, Ray RB. Biodegradable polymeric scaffolds for musculoskeletal tissue engineering. J Biomed Mater Res 2001;55(2):141-50.

45. Ishaug-Riley SL, Okun LE, Prado G, Applegate MA, Ratcliffe A. Human articular chondrocyte adhesion and proliferation on synthetic biodegradable polymer films. Biomaterials 1999;20(23-24):2245-56.
46. El-Amin SF, Lu HH, Khan Y, Burems J, Mitchell J, Tuan RS, Laurencin CT. Extracellular matrix production by human osteoblasts cultured on biodegradable polymers applicable for tissue engineering. Biomaterials 2003;24(7):1213-21.
47. Hayashi T. Biodegradable Polymers for Biomedical Uses. Progress in Polymer Science 1994;19(4):663-702.
48. Dai NT, Williamson MR, Khammo N, Adams EF, Coombes AG. Composite cell support membranes based on collagen and polycaprolactone for tissue engineering of skin. Biomaterials 2004;25(18):4263-71.
49. Barralet JE, Wallace LL, Strain AJ. Tissue engineering of human biliary epithelial cells on polyglycolic acid/polycaprolactone scaffolds maintains long-term phenotypic stability. Tissue Eng 2003;9(5):1037-45.
50. Park YJ, Lee JY, Chang YS, Jeong JM, Chung JK, Lee MC, Park KB, Lee SJ. Radioisotope carrying polyethylene oxide-polycaprolactone copolymer micelles for targetable bone imaging. Biomaterials 2002;23(3):873-9.
51. Ciapetti G, Ambrosio L, Savarino L, Granchi D, Cenni E, Baldini N, Pagani S, Guizzardi S, Causa F, Giunti A. Osteoblast growth and function in porous poly epsilon -caprolactone matrices for bone repair: a preliminary study. Biomaterials 2003;24(21):3815-24.
52. Fisher JP, Vehof JWM, Dean D, van der Waerden JPCM, Holland TA, Mikos AG, Jansen JA. Soft and hard tissue response to photocrosslinked poly(propylene fumarate) scaffolds in a rabbit model. J Biomed Mater Res 2002;59(3):547-556.
53. Fisher JP, Timmer MD, Holland TA, Dean D, Engel PS, Mikos AG. Photoinitiated cross-linking of the biodegradable polyester poly(propylene fumarate). Part I. Determination of network structure. Biomacromolecules 2003;4(5):1327-34.
54. Fisher JP, Vehof JW, Dean D, van der Waerden JP, Holland TA, Mikos AG, Jansen JA. Soft and hard tissue response to photocrosslinked poly(propylene fumarate) scaffolds in a rabbit model. J Biomed Mater Res 2002;59(3):547-56.
55. Barr J, Woodburn KW, Ng SY, Shen HR, Heller J. Post surgical pain management with poly(ortho esters). Adv Drug Deliv Rev 2002;54(7):1041-8.
56. Davis KA, Anseth KS. Controlled release from crosslinked degradable networks. Crit Rev Ther Drug Carrier Syst 2002;19(4-5):385-423.
57. Heller J, Barr J, Ng SY, Abdellauoi KS, Gurny R. Poly(ortho esters): synthesis, characterization, properties and uses. Adv Drug Deliv Rev 2002;54(7):1015-39.
58. Andriano KP, Tabata Y, Ikada Y, Heller J. In vitro and in vivo comparison of bulk and surface hydrolysis in absorbable polymer scaffolds for tissue engineering. J Biomed Mater Res 1999;48(5):602-12.
59. Kumar N, Langer RS, Domb AJ. Polyanhydrides: an overview. Adv Drug Deliv Rev 2002;54(7):889-910.

60. Langer R. Biomaterials in drug delivery and tissue engineering: one laboratory's experience. Acc Chem Res 2000;33(2):94-101.
61. Burkoth AK, Anseth KS. A review of photocrosslinked polyanhydrides: in situ forming degradable networks. Biomaterials 2000;21(23):2395-404.
62. Burkoth AK, Burdick J, Anseth KS. Surface and bulk modifications to photocrosslinked polyanhydrides to control degradation behavior. J Biomed Mater Res 2000;51(3):352-9.
63. Gunatillake PA, Adhikari R. Biodegradable synthetic polymers for tissue engineering. Eur Cell Mater 2003;5:1-16; discussion 16.
64. Uhrich KE, Gupta A, Thomas TT, Laurencin CT, Langer R. Synthesis and Characterization of Degradable Poly(Anhydride-Co-Imides). Macromolecules 1995;28(7):2184-2193.
65. Muggli DS, Burkoth AK, Keyser SA, Lee HR, Anseth KS. Reaction behavior of biodegradable, photo-cross-linkable polyanhydrides. Macromolecules 1998;31(13):4120-4125.
66. Anseth KS, Svaldi DC, Laurencin CT, Langer R. Photopolymerization of novel degradable networks for orthopedic applications. Photopolymerization 1997;673:189-202.
67. Allcock HR, Cameron CG. Synthesis and Characterization of Photo-Cross-Linkable Small-Molecule and High-Polymeric Phosphazenes Bearing Cinnamate Groups. Macromolecules 1994;27(12):3125-3130.
68. Qiu LY, Zhu KJ. Novel biodegradable polyphosphazenes containing glycine ethyl ester and benzyl ester of amino acethydroxamic acid as cosubstituents: Syntheses, characterization, and degradation properties. Journal of Applied Polymer Science 2000;77(13):2987-2995.
69. Laurencin CT, Norman ME, Elgendy HM, el-Amin SF, Allcock HR, Pucher SR, Ambrosio AA. Use of polyphosphazenes for skeletal tissue regeneration. J Biomed Mater Res 1993;27(7):963-73.
70. Laurencin CT, El-Amin SF, Ibim SE, Willoughby DA, Attawia M, Allcock HR, Ambrosio AA. A highly porous 3-dimensional polyphosphazene polymer matrix for skeletal tissue regeneration. J Biomed Mater Res 1996;30(2):133-8.
71. Tangpasuthadol V, Pendharkar SM, Kohn J. Hydrolytic degradation of tyrosine-derived polycarbonates, a class of new biomaterials. Part I: Study of model compounds. Biomaterials 2000;21(23):2371-2378.
72. Ertel SI, Kohn J. Evaluation of a series of tyrosine-derived polycarbonates as degradable biomaterials. J Biomed Mater Res 1994;28(8):919-30.
73. Choueka J, Charvet JL, Koval KJ, Alexander H, James KS, Hooper KA, Kohn J. Canine bone response to tyrosine-derived polycarbonates and poly(L-lactic acid). J Biomed Mater Res 1996;31(1):35-41.
74. Lee SJ, Choi JS, Park KS, Khang G, Lee YM, Lee HB. Response of MG63 osteoblast-like cells onto polycarbonate membrane surfaces with different micropore sizes. Biomaterials 2004;25(19):4699-707.
75. Simon JL, Roy TD, Parsons JR, Rekow ED, Thompson VP, Kemnitzer J, Ricci JL. Engineered cellular response to scaffold architecture in a rabbit trephine defect. J Biomed Mater Res A 2003;66(2):275-82.

76. James K, Levene H, Parsons JR, Kohn J. Small changes in polymer chemistry have a large effect on the bone-implant interface: evaluation of a series of degradable tyrosine-derived polycarbonates in bone defects. Biomaterials 1999;20(23-24):2203-12.
77. Cai J, Bo S, Cheng R, Jiang L, Yang Y. Analysis of interfacial phenomena of aqueous solutions of polyethylene oxide and polyethylene glycol flowing in hydrophilic and hydrophobic capillary viscometers. J Colloid Interface Sci 2004;276(1):174-81.
78. Bourke SL, Kohn J. Polymers derived from the amino acid L-tyrosine: polycarbonates, polyarylates and copolymers with poly(ethylene glycol). Adv Drug Deliv Rev 2003;55(4):447-66.
79. Seal BL, Otero TC, Panitch A. Polymeric biomaterials for tissue and organ regeneration. Materials Science & Engineering R-Reports 2001;34(4-5):147-230.
80. Sims CD, Butler PE, Casanova R, Lee BT, Randolph MA, Lee WP, Vacanti CA, Yaremchuk MJ. Injectable cartilage using polyethylene oxide polymer substrates. Plast Reconstr Surg 1996;98(5):843-50.
81. Novikova LN, Novikov LN, Kellerth JO. Biopolymers and biodegradable smart implants for tissue regeneration after spinal cord injury. Curr Opin Neurol 2003;16(6):711-5.
82. Sawhney AS, Pathak CP, Hubbell JA. Bioerodible hydrogels based on photopolymerized poly(ethylene glycol)-co-poly(alpha-hydroxy acid) diacrylate macromers. Macromolecules 1993;26(4):581-587.
83. Kaito T, Myoui A, Takaoka K, Saito N, Nishikawa M, Tamai N, Ohgushi H, Yoshikawa H. Potentiation of the activity of bone morphogenetic protein-2 in bone regeneration by a PLA-PEG/hydroxyapatite composite. Biomaterials 2005;26(1):73-9.
84. Matsushita N, Terai H, Okada T, Nozaki K, Inoue H, Miyamoto S, Takaoka K. A new bone-inducing biodegradable porous beta-tricalcium phosphate. J Biomed Mater Res A 2004;70(3):450-8.
85. Lutolf MP, Weber FE, Schmoekel HG, Schense JC, Kohler T, Muller R, Hubbell JA. Repair of bone defects using synthetic mimetics of collagenous extracellular matrices. Nat Biotechnol 2003;21(5):513-8.
86. Schaefer D, Martin I, Shastri P, Padera RF, Langer R, Freed LE, Vunjak-Novakovic G. In vitro generation of osteochondral composites. Biomaterials 2000;21(24):2599-606.
87. Dar A, Shachar M, Leor J, Cohen S. Optimization of cardiac cell seeding and distribution in 3D porous alginate scaffolds. Biotechnol Bioeng 2002;80(3):305-12.
88. Cunliffe D, Pennadam S, Alexander C. Synthetic and biological polymers-merging the interface. European Polymer Journal 2004;40(1):5-25.
89. Shin H, Jo S, Mikos AG. Biomimetic materials for tissue engineering. Biomaterials 2003;24(24):4353-64.
90. Holy CE, Fialkov JA, Davies JE, Shoichet MS. Use of a biomimetic strategy to engineer bone. J Biomed Mater Res A 2003;65(4):447-53.

91. Hoffman AS. Hydrogels for biomedical applications. Adv Drug Deliv Rev 2002;54(1):3-12.
92. Drury JL, Mooney DJ. Hydrogels for tissue engineering: scaffold design variables and applications. Biomaterials 2003;24(24):4337-51.
93. Athanasiou KA, Zhu C, Lanctot DR, Agrawal CM, Wang X. Fundamentals of biomechanics in tissue engineering of bone. Tissue Eng 2000;6(4):361-81.
94. Yaszemski MJ, Payne RG, Hayes WC, Langer R, Mikos AG. Evolution of bone transplantation: molecular, cellular and tissue strategies to engineer human bone. Biomaterials 1996;17(2):175-85.
95. Rohl L, Larsen E, Linde F, Odgaard A, Jorgensen J. Tensile and compressive properties of cancellous bone. J Biomech 1991;24(12):1143-9.
96. Hollister SJ. Porous scaffold design for tissue engineering. Nat Mater 2005;4(7):518-24.
97. Hutmacher DW. Scaffolds in tissue engineering bone and cartilage. Biomaterials 2000;21(24):2529-43.
98. Lu JX, Flautre B, Anselme K, Hardouin P, Gallur A, Descamps M, Thierry B. Role of interconnections in porous bioceramics on bone recolonization in vitro and in vivo. J Mater Sci Mater Med 1999;10(2):111-20.
99. Shive MS, Anderson JM. Biodegradation and biocompatibility of PLA and PLGA microspheres. Adv Drug Deliv Rev 1997;28(1):5-24.
100. Anderson JM. Biological response to materials. Annual Review of Materials Research 2001;31(1):81-110.
101. Wake MC, Gerecht PD, Lu L, Mikos AG. Effects of biodegradable polymer particles on rat marrow-derived stromal osteoblasts in vitro. Biomaterials 1998;19(14):1255-68.
102. Mikos AG, McIntire LV, Anderson JM, Babensee JE. Host response to tissue engineered devices. Adv Drug Deliv Rev 1998;33(1-2):111-139.
103. Bergsma JE, de Bruijn WC, Rozema FR, Bos RR, Boering G. Late degradation tissue response to poly(L-lactide) bone plates and screws. Biomaterials 1995;16(1):25-31.
104. Yavuzer R, Tuncer S, Basterzi Y, Isik I, Sari A, Latifoglu O. Reconstruction of orbital floor fracture using solvent-preserved bone graft. Plast Reconstr Surg 2004;113(1):34-44.
105. Fonseca RJ, editor. Oral and Maxillofacial Surgery. Volume 3; 2000.
106. Waitzman AA, Posnick JC, Armstrong DC, Pron GE. Craniofacial skeletal measurements based on computed tomography: Part II. Normal values and growth trends. Cleft Palate Craniofac J 1992;29(2):118-28.
107. Chang EW, Manolidis S. Orbital floor fracture management. Facial Plast Surg 2005;21(3):207-13.
108. Metzger MC, Schon R, Tetzlaf R, Weyer N, Rafii A, Gellrich NC, Schmelzeisen R. Topographical CT-data analysis of the human orbital floor. Int J Oral Maxillofac Surg 2007;36(1):45-53.
109. Evans BT, Webb AA. Post-traumatic orbital reconstruction: anatomical landmarks and the concept of the deep orbit. Br J Oral Maxillofac Surg 2007;45(3):183-9.

110. Eski M, Sahin I, Deveci M, Turegun M, Isik S, Sengezer M. A retrospective analysis of 101 zygomatico-orbital fractures. J Craniofac Surg 2006;17(6):1059-64.
111. Rinna C, Ungari C, Saltarel A, Cassoni A, Reale G. Orbital floor restoration. J Craniofac Surg 2005;16(6):968-72.
112. Folkestad L, Aberg-Bengtsson L, Granstrom G. Recovery from orbital floor fractures: a prospective study of patients' and doctors' experiences. Int J Oral Maxillofac Surg 2006;35(6):499-505.
113. Manolidis S, Weeks BH, Kirby M, Scarlett M, Hollier L. Classification and surgical management of orbital fractures: experience with 111 orbital reconstructions. J Craniofac Surg 2002;13(6):726-37; discussion 738.
114. Ahmad F, Kirkpatrick NA, Lyne J, Urdang M, Waterhouse N. Buckling and hydraulic mechanisms in orbital blowout fractures: fact or fiction? J Craniofac Surg 2006;17(3):438-41.
115. Ahmad F, Kirkpatrick WN, Lyne J, Urdang M, Garey LJ, Waterhouse N. Strain gauge biomechanical evaluation of forces in orbital floor fractures. Br J Plast Surg 2003;56(1):3-9.
116. Jordan DR, St Onge P, Anderson RL, Patrinely JR, Nerad JA. Complications associated with alloplastic implants used in orbital fracture repair. Ophthalmology 1992;99(10):1600-8.
117. Donati L, Baruffaldi-Preis FW, Di Leo A, Donati V, Cavallini M, Marazzi M, Falcone L. Ten-year experience with craniofacial implants: clinical and experimental results. Int Surg 1997;82(4):325-31.
118. Guerra MF, Perez JS, Rodriguez-Campo FJ, Gias LN. Reconstruction of orbital fractures with dehydrated human dura mater. J Oral Maxillofac Surg 2000;58(12):1361-6; discussion 1366-7.
119. Kosaka M, Matsuzawa Y, Mori H, Matsunaga K, Kamiishi H. Orbital wall reconstruction with bone grafts from the outer cortex of the mandible. J Craniomaxillofac Surg 2004;32(6):374-80.
120. Lee HH, Alcaraz N, Reino A, Lawson W. Reconstruction of orbital floor fractures with maxillary bone. Arch Otolaryngol Head Neck Surg 1998;124(1):56-9.
121. Li KK. Repair of traumatic orbital wall defects with nasal septal cartilage: report of five cases. J Oral Maxillofac Surg 1997;55(10):1098-102.
122. Kontio RK, Laine P, Salo A, Paukku P, Lindqvist C, Suuronen R. Reconstruction of internal orbital wall fracture with iliac crest free bone graft: clinical, computed tomography, and magnetic resonance imaging follow-up study. Plast Reconstr Surg 2006;118(6):1365-74.
123. Tong L, Buchman SR. Facial bone grafts: Contemporary science and thought. J Craniomaxillofac Trauma 2000;6(1):31-41; discussion 42.
124. Ellis E, 3rd, Tan Y. Assessment of internal orbital reconstructions for pure blowout fractures: cranial bone grafts versus titanium mesh. J Oral Maxillofac Surg 2003;61(4):442-53.
125. Burnstine MA. Clinical recommendations for repair of isolated orbital floor fractures: an evidence-based analysis. Ophthalmology 2002;109(7):1207-10; discussion 1210-1; quiz 1212-3.

126. Orban JM, Marra KG, Hollinger JO. Composition options for tissue-engineered bone. Tissue Eng 2002;8(4):529-39.
127. Pittenger MF, Mackay AM, Beck SC, Jaiswal RK, Douglas R, Mosca JD, Moorman MA, Simonetti DW, Craig S, Marshak DR. Multilineage potential of adult human mesenchymal stem cells. Science 1999;284(5411):143-7.
128. Caplan AI. Mesenchymal stem cells. J Orthop Res 1991;9(5):641-50.
129. Leach JK, Mooney DJ. Bone engineering by controlled delivery of osteoinductive molecules and cells. Expert Opin Biol Ther 2004;4(7):1015-27.
130. Alhadlaq A, Mao JJ. Mesenchymal stem cells: isolation and therapeutics. Stem Cells Dev 2004;13(4):436-48.
131. Friedenstein AJ, Chailakhjan RK, Lalykina KS. The development of fibroblast colonies in monolayer cultures of guinea-pig bone marrow and spleen cells. Cell Tissue Kinet 1970;3(4):393-403.
132. Mao JJ, Giannobile WV, Helms JA, Hollister SJ, Krebsbach PH, Longaker MT, Shi S. Craniofacial tissue engineering by stem cells. J Dent Res 2006;85(11):966-79.
133. Wozney JM, Rosen V. Bone morphogenetic protein and bone morphogenetic protein gene family in bone formation and repair. Clin Orthop Relat Res 1998(346):26-37.
134. Hyun SJ, Han DK, Choi SH, Chai JK, Cho KS, Kim CK, Kim CS. Effect of recombinant human bone morphogenetic protein-2, -4, and -7 on bone formation in rat calvarial defects. J Periodontol 2005;76(10):1667-74.
135. Saito N, Murakami N, Takahashi J, Horiuchi H, Ota H, Kato H, Okada T, Nozaki K, Takaoka K. Synthetic biodegradable polymers as drug delivery systems for bone morphogenetic proteins. Adv Drug Deliv Rev 2005;57(7):1037-48.
136. Alden TD, Beres EJ, Laurent JS, Engh JA, Das S, London SD, Jane JA, Jr., Hudson SB, Helm GA. The use of bone morphogenetic protein gene therapy in craniofacial bone repair. J Craniofac Surg 2000;11(1):24-30.
137. Ramoshebi LN, Matsaba TN, Teare J, Renton L, Patton J, Ripamonti U. Tissue engineering: TGF-beta superfamily members and delivery systems in bone regeneration. Expert Rev Mol Med 2002;4(20):1-11.
138. Termaat MF, Den Boer FC, Bakker FC, Patka P, Haarman HJ. Bone morphogenetic proteins. Development and clinical efficacy in the treatment of fractures and bone defects. J Bone Joint Surg Am 2005;87(6):1367-78.
139. Wiesmann HP, Joos U, Meyer U. Biological and biophysical principles in extracorporal bone tissue engineering. Part II. Int J Oral Maxillofac Surg 2004;33(6):523-30.
140. Wozney JM, Seeherman HJ. Protein-based tissue engineering in bone and cartilage repair. Curr Opin Biotechnol 2004;15(5):392-8.
141. Yang XB, Green DW, Roach HI, Clarke NM, Anderson HC, Howdle SM, Shakesheff KM, Oreffo RO. Novel osteoinductive biomimetic scaffolds stimulate human osteoprogenitor activity--implications for skeletal repair. Connect Tissue Res 2003;44 Suppl 1:312-7.
142. Cheng H, Jiang W, Phillips FM, Haydon RC, Peng Y, Zhou L, Luu HH, An N, Breyer B, Vanichakarn P and others. Osteogenic activity of the fourteen

types of human bone morphogenetic proteins (BMPs). J Bone Joint Surg Am 2003;85-A(8):1544-52.
143. Lee DH, Park BJ, Lee MS, Lee JW, Kim JK, Yang HC, Park JC. Chemotactic migration of human mesenchymal stem cells and MC3T3-E1 osteoblast-like cells induced by COS-7 cell line expressing rhBMP-7. Tissue Eng 2006;12(6):1577-86.
144. Chu TM, Warden SJ, Turner CH, Stewart RL. Segmental bone regeneration using a load-bearing biodegradable carrier of bone morphogenetic protein-2. Biomaterials 2007;28(3):459-67.
145. Hidaka C, Cunningham ME, Rodeo SA, Maher SA, Zhu W. Modern biologics used in orthopaedic surgery. Curr Opin Rheumatol 2006;18(1):74-9.
146. Mistry AS, Mikos AG. Tissue engineering strategies for bone regeneration. Adv Biochem Eng Biotechnol 2005;94:1-22.
147. Jadlowiec JA, Celil AB, Hollinger JO. Bone tissue engineering: recent advances and promising therapeutic agents. Expert Opin Biol Ther 2003;3(3):409-23.
148. Schilephake H. Bone growth factors in maxillofacial skeletal reconstruction. Int J Oral Maxillofac Surg 2002;31(5):469-84.
149. Kong L, Ao Q, Wang A, Gong K, Wang X, Lu G, Gong Y, Zhao N, Zhang X. Preparation and Characterization of a Multilayer Biomimetic Scaffold for Bone Tissue Engineering. J Biomater Appl 2007.
150. Fiedler J, Etzel N, Brenner RE. To go or not to go: Migration of human mesenchymal progenitor cells stimulated by isoforms of PDGF. J Cell Biochem 2004;93(5):990-8.
151. White E, Shors EC. Biomaterial aspects of Interpore-200 porous hydroxyapatite. Dent Clin North Am 1986;30(1):49-67.
152. Gauthier O, Bouler JM, Aguado E, Pilet P, Daculsi G. Macroporous biphasic calcium phosphate ceramics: influence of macropore diameter and macroporosity percentage on bone ingrowth. Biomaterials 1998;19(1-3):133-9.
153. Hulbert SF, Morrison SJ, Klawitter JJ. Tissue reaction to three ceramics of porous and non-porous structures. J Biomed Mater Res 1972;6(5):347-74.
154. Haug RH, Nuveen E, Bredbenner T. An evaluation of the support provided by common internal orbital reconstruction materials. J Oral Maxillofac Surg 1999;57(5):564-70.
155. Betz MW, Caccamese JF, Coletti DP, Sauk JJ, Fisher JP. Tissue response and orbital floor regeneration using cyclic acetal hydrogels. J Biomed Mater Res A 2008.
156. Breitbart AS, Grande DA, Kessler R, Ryaby JT, Fitzsimmons RJ, Grant RT. Tissue engineered bone repair of calvarial defects using cultured periosteal cells. Plast Reconstr Surg 1998;101(3):567-74; discussion 575-6.
157. Schantz JT, Hutmacher DW, Lam CX, Brinkmann M, Wong KM, Lim TC, Chou N, Guldberg RE, Teoh SH. Repair of calvarial defects with customised tissue-engineered bone grafts II. Evaluation of cellular efficiency and efficacy in vivo. Tissue Eng 2003;9 Suppl 1:S127-39.

158. Dean D, Wolfe MS, Ahmad Y, Totonchi A, Chen JE, Fisher JP, Cooke MN, Rimnac CM, Lennon DP, Caplan AI and others. Effect of transforming growth factor beta 2 on marrow-infused foam poly(propylene fumarate) tissue-engineered constructs for the repair of critical-size cranial defects in rabbits. Tissue Eng 2005;11(5-6):923-39.
159. Kaihara S, Shuichi Matsumura, and John P. Fisher. Synthesis and Characterization of Cyclic Acetal Based Degradable Hydrogels. European Journal of Pharmaceutics and Biopharmaceutics 2007;Submitted.
160. Betz MW, Modi PC, Caccamese JF, Coletti DP, Sauk JJ, Fisher JP. Cyclic acetal hydrogel system for bone marrow stromal cell encapsulation and osteodifferentiation. J Biomed Mater Res A 2007.
161. Schantz JT, Teoh SH, Lim TC, Endres M, Lam CX, Hutmacher DW. Repair of calvarial defects with customized tissue-engineered bone grafts I. Evaluation of osteogenesis in a three-dimensional culture system. Tissue Eng 2003;9 Suppl 1:S113-26.
162. Heng BC, Cao T, Stanton LW, Robson P, Olsen B. Strategies for directing the differentiation of stem cells into the osteogenic lineage in vitro. J Bone Miner Res 2004;19(9):1379-94.
163. Mackenzie TC, Flake AW. Human mesenchymal stem cells persist, demonstrate site-specific multipotential differentiation, and are present in sites of wound healing and tissue regeneration after transplantation into fetal sheep. Blood Cells Mol Dis 2001;27(3):601-4.
164. Raisz LG, Pilbeam CC, Fall PM. Prostaglandins: mechanisms of action and regulation of production in bone. Osteoporos Int 1993;3 Suppl 1:136-40.
165. Weinreb M, Grosskopf A, Shir N. The anabolic effect of PGE2 in rat bone marrow cultures is mediated via the EP4 receptor subtype. Am J Physiol 1999;276(2 Pt 1):E376-83.
166. van Leeuwen JP, van Driel M, van den Bemd GJ, Pols HA. Vitamin D control of osteoblast function and bone extracellular matrix mineralization. Crit Rev Eukaryot Gene Expr 2001;11(1-3):199-226.
167. Peter SJ, Liang CR, Kim DJ, Widmer MS, Mikos AG. Osteoblastic phenotype of rat marrow stromal cells cultured in the presence of dexamethasone, beta-glycerolphosphate, and L-ascorbic acid. J Cell Biochem 1998;71(1):55-62.
168. Alvis M, Lalor P, Brown MK, Thorn MR, Block JE, Hornby S, Berg R, Reddi AH. Osteoinduction by a collagen mineral composite combined with isologous bone marrow in a subcutaneous rat model. Orthopedics 2003;26(1):77-80.
169. Niemeyer P, Krause U, Punzel M, Fellenberg J, Simank HG. [Mesenchymal stem cells for tissue engineering of bone: 3D-cultivation and osteogenic differentiation on mineralized collagen]. Z Orthop Ihre Grenzgeb 2003;141(6):712-7.
170. Rebaudi A, Silvestrini P, Trisi P. Use of a resorbable hydroxyapatite-collagen chondroitin sulfate material on immediate postextraction sites: a clinical and histologic study. Int J Periodontics Restorative Dent 2003;23(4):371-9.
171. Collin-Osdoby P, Nickols GA, Osdoby P. Bone cell function, regulation, and communication: a role for nitric oxide. J Cell Biochem 1995;57(3):399-408.

172. Evans DM, Ralston SH. Nitric oxide and bone. J Bone Miner Res 1996;11(3):300-5.
173. Wang FS, Wang CJ, Chen YJ, Chang PR, Huang YT, Sun YC, Huang HC, Yang YJ, Yang KD. Ras induction of superoxide activates ERK-dependent angiogenic transcription factor HIF-1alpha and VEGF-A expression in shock wave-stimulated osteoblasts. J Biol Chem 2004;279(11):10331-7.
174. Billotte WG, Hofmann MC. Establishment of a shear stress protocol to study the mechanosensitivity of human primary osteogenic cells in vitro. Biomed Sci Instrum 1999;35:327-32.
175. Yoshikawa T, Peel SA, Gladstone JR, Davies JE. Biochemical analysis of the response in rat bone marrow cell cultures to mechanical stimulation. Biomed Mater Eng 1997;7(6):369-77.
176. Gerstenfeld LC, Barnes GL, Shea CM, Einhorn TA. Osteogenic differentiation is selectively promoted by morphogenetic signals from chondrocytes and synergized by a nutrient rich growth environment. Connect Tissue Res 2003;44 Suppl 1:85-91.
177. Gerstenfeld LC, Cruceta J, Shea CM, Sampath K, Barnes GL, Einhorn TA. Chondrocytes provide morphogenic signals that selectively induce osteogenic differentiation of mesenchymal stem cells. J Bone Miner Res 2002;17(2):221-30.
178. Nurminskaya M, Magee C, Faverman L, Linsenmayer TF. Chondrocyte-derived transglutaminase promotes maturation of preosteoblasts in periosteal bone. Dev Biol 2003;263(1):139-52.
179. Kronenberg HM. Developmental regulation of the growth plate. Nature 2003;423(6937):332-6.
180. Provot S, Schipani E. Molecular mechanisms of endochondral bone development. Biochem Biophys Res Commun 2005;328(3):658-65.
181. Canalis E, Deregowski V, Pereira RC, Gazzerro E. Signals that determine the fate of osteoblastic cells. J Endocrinol Invest 2005;28(8 Suppl):3-7.
182. Sykaras N, Opperman LA. Bone morphogenetic proteins (BMPs): how do they function and what can they offer the clinician? J Oral Sci 2003;45(2):57-73.
183. Shimoyama A, Wada M, Ikeda F, Hata K, Matsubara T, Nifuji A, Noda M, Amano K, Yamaguchi A, Nishimura R and others. Ihh/Gli2 signaling promotes osteoblast differentiation by regulating Runx2 expression and function. Mol Biol Cell 2007;18(7):2411-8.
184. Ball SG, Shuttleworth AC, Kielty CM. Direct cell contact influences bone marrow mesenchymal stem cell fate. Int J Biochem Cell Biol 2004;36(4):714-27.
185. Moviglia GA, Varela G, Gaeta CA, Brizuela JA, Bastos F, Saslavsky J. Autoreactive T cells induce in vitro BM mesenchymal stem cell transdifferentiation to neural stem cells. Cytotherapy 2006;8(3):196-201.
186. Terada N, Hamazaki T, Oka M, Hoki M, Mastalerz DM, Nakano Y, Meyer EM, Morel L, Petersen BE, Scott EW. Bone marrow cells adopt the phenotype of other cells by spontaneous cell fusion. Nature 2002;416(6880):542-5.

187. Cancedda R, Mastrogiacomo M, Bianchi G, Derubeis A, Muraglia A, Quarto R. Bone marrow stromal cells and their use in regenerating bone. Novartis Found Symp 2003;249:133-43; discussion 143-7, 170-4, 239-41.
188. Glowacki J, Trepman E, Folkman J. Cell shape and phenotypic expression in chondrocytes. Proc Soc Exp Biol Med 1983;172(1):93-8.
189. Betz MW, Modi PC, Caccamese JF, Coletti DP, Sauk JJ, Fisher JP. Cyclic Acetal Hydrogel System for Bone Marrow Stromal Cell Encapsulation and Osteodifferentiation. Journal of Biomedical Materials Research Part A 2007;[accepted for publication].
190. Yoon DM, Fisher JP. Chondrocyte signaling and artificial matrices for articular cartilage engineering. Adv Exp Med Biol 2006;585:67-86.
191. Nakaoka R, Hsiong SX, Mooney DJ. Regulation of chondrocyte differentiation level via co-culture with osteoblasts. Tissue Eng 2006;12(9):2425-33.
192. Gregory CA GW, Peister A, Prockop DJ. An Alizarin red-based assay of mineralization by adherent cells in culture: comparison with cetylpyridinium chloride extraction. Analytical Biochemistry 2004;329(1):77-84.
193. Stanford CM, Jacobson PA, Eanes ED, Lembke LA, Midura RJ. Rapidly forming apatitic mineral in an osteoblastic cell line (UMR 106-01 BSP). J Biol Chem 1995;270(16):9420-8.
194. Puchtler H, Meloan SN, Terry MS. On the history and mechanism of alizarin and alizarin red S stains for calcium. J Histochem Cytochem 1969;17(2):110-24.
195. Hu Z, Peel SA, Ho SK, Sandor GK, Clokie CM. Role of bovine bone morphogenetic proteins in bone matrix protein and osteoblast-related gene expression during rat bone marrow stromal cell differentiation. J Craniofac Surg 2005;16(6):1006-14.
196. Jaiswal N, Haynesworth SE, Caplan AI, Bruder SP. Osteogenic differentiation of purified, culture-expanded human mesenchymal stem cells in vitro. J Cell Biochem 1997;64(2):295-312.
197. Harris SE, Bonewald LF, Harris MA, Sabatini M, Dallas S, Feng JQ, Ghosh-Choudhury N, Wozney J, Mundy GR. Effects of transforming growth factor beta on bone nodule formation and expression of bone morphogenetic protein 2, osteocalcin, osteopontin, alkaline phosphatase, and type I collagen mRNA in long-term cultures of fetal rat calvarial osteoblasts. J Bone Miner Res 1994;9(6):855-63.
198. Cowles EA, DeRome ME, Pastizzo G, Brailey LL, Gronowicz GA. Mineralization and the expression of matrix proteins during in vivo bone development. Calcif Tissue Int 1998;62(1):74-82.
199. Barnes GL, Kostenuik PJ, Gerstenfeld LC, Einhorn TA. Growth factor regulation of fracture repair. J Bone Miner Res 1999;14(11):1805-15.
200. Leeman MF, Curran S, Murray GI. The structure, regulation, and function of human matrix metalloproteinase-13. Crit Rev Biochem Mol Biol 2002;37(3):149-66.
201. Pelttari K, Steck E, Richter W. The use of mesenchymal stem cells for chondrogenesis. Injury 2008;39 Suppl 1:S58-65.

202. Behonick DJ, Xing Z, Lieu S, Buckley JM, Lotz JC, Marcucio RS, Werb Z, Miclau T, Colnot C. Role of matrix metalloproteinase 13 in both endochondral and intramembranous ossification during skeletal regeneration. PLoS ONE 2007;2(11):e1150.
203. Merz D, Liu R, Johnson K, Terkeltaub R. IL-8/CXCL8 and growth-related oncogene alpha/CXCL1 induce chondrocyte hypertrophic differentiation. J Immunol 2003;171(8):4406-15.
204. Dodla MC, Bellamkonda RV. Anisotropic scaffolds facilitate enhanced neurite extension in vitro. J Biomed Mater Res A 2006;78(2):213-21.
205. Yoshida M, Babensee JE. Differential effects of agarose and poly(lactic-co-glycolic acid) on dendritic cell maturation. J Biomed Mater Res A 2006;79(2):393-408.
206. Barralet JE, Wang L, Lawson M, Triffitt JT, Cooper PR, Shelton RM. Comparison of bone marrow cell growth on 2D and 3D alginate hydrogels. J Mater Sci Mater Med 2005;16(6):515-9.
207. Yoon DM, Hawkins EC, Francke-Carroll S, Fisher JP. Effect of construct properties on encapsulated chondrocyte expression of insulin-like growth factor-1. Biomaterials 2007;28(2):299-306.
208. Hong Y, Mao Z, Wang H, Gao C, Shen J. Covalently crosslinked chitosan hydrogel formed at neutral pH and body temperature. J Biomed Mater Res A 2006;79(4):913-22.
209. Kong L, Ao Q, Wang A, Gong K, Wang X, Lu G, Gong Y, Zhao N, Zhang X. Preparation and characterization of a multilayer biomimetic scaffold for bone tissue engineering. J Biomater Appl 2007;22(3):223-39.
210. VandeVord PJ, Matthew HW, DeSilva SP, Mayton L, Wu B, Wooley PH. Evaluation of the biocompatibility of a chitosan scaffold in mice. J Biomed Mater Res 2002;59(3):585-90.
211. Lee CH, Singla A, Lee Y. Biomedical applications of collagen. Int J Pharm 2001;221(1-2):1-22.
212. Ma L, Gao C, Mao Z, Zhou J, Shen J. Enhanced biological stability of collagen porous scaffolds by using amino acids as novel cross-linking bridges. Biomaterials 2004;25(15):2997-3004.
213. Baier Leach J, Bivens KA, Patrick CW, Jr., Schmidt CE. Photocrosslinked hyaluronic acid hydrogels: natural, biodegradable tissue engineering scaffolds. Biotechnol Bioeng 2003;82(5):578-89.
214. Cui FZ, Tian WM, Hou SP, Xu QY, Lee IS. Hyaluronic acid hydrogel immobilized with RGD peptides for brain tissue engineering. J Mater Sci Mater Med 2006;17(12):1393-401.
215. Altman GH, Diaz F, Jakuba C, Calabro T, Horan RL, Chen J, Lu H, Richmond J, Kaplan DL. Silk-based biomaterials. Biomaterials 2003;24(3):401-16.
216. Meinel L, Hofmann S, Betz O, Fajardo R, Merkle HP, Langer R, Evans CH, Vunjak-Novakovic G, Kaplan DL. Osteogenesis by human mesenchymal stem cells cultured on silk biomaterials: comparison of adenovirus mediated gene transfer and protein delivery of BMP-2. Biomaterials 2006;27(28):4993-5002.

217. Martens PJ, Bryant SJ, Anseth KS. Tailoring the degradation of hydrogels formed from multivinyl poly(ethylene glycol) and poly(vinyl alcohol) macromers for cartilage tissue engineering. Biomacromolecules 2003;4(2):283-92.
218. Moreau JL, Kesselman D, Fisher JP. Synthesis and properties of cyclic acetal biomaterials. J Biomed Mater Res A 2007;81(3):594-602.
219. Kaihara S, Matsumura S, Fisher JP. Synthesis and characterization of cyclic acetal based degradable hydrogels. Eur J Pharm Biopharm 2008;68(1):67-73.
220. Jabbari E. Release characteristics of a model plasmid DNA encapsulated in biodegradable poly(ethylene glycol fumarate)/acrylamide hydrogel microspheres. J Microencapsul 2004;21(5):525-38.
221. Baskaran S, Grande D, Sun XL, Yayon A, Chaikof EL. Glycosaminoglycan-mimetic biomaterials. 3. Glycopolymers prepared from alkene-derivatized mono- and disaccharide-based glycomonomers. Bioconjug Chem 2002;13(6):1309-13.
222. Vandijkwolthuis WNE, Franssen O, Talsma H, Vansteenbergen MJ, Vandenbosch JJK, Hennink WE. Synthesis, Characterization, and Polymerization of Glycidyl Methacrylate Derivatized Dextran. Macromolecules 1995;28(18):6317-6322.
223. Vervoort L, Vinckier I, Moldenaers P, Van den Mooter G, Augustijns P, Kinget R. Inulin hydrogels as carriers for colonic drug targeting. Rheological characterization of the hydrogel formation and the hydrogel network. Journal of Pharmaceutical Sciences 1999;88(2):209-214.
224. Temenoff JS, Park H, Jabbari E, Conway DE, Sheffield TL, Ambrose CG, Mikos AG. Thermally cross-linked oligo(poly(ethylene glycol) fumarate) hydrogels support osteogenic differentiation of encapsulated marrow stromal cells in vitro. Biomacromolecules 2004;5(1):5-10.
225. Temenoff JS, Park H, Jabbari E, Sheffield TL, LeBaron RG, Ambrose CG, Mikos AG. In vitro osteogenic differentiation of marrow stromal cells encapsulated in biodegradable hydrogels. J Biomed Mater Res A 2004;70(2):235-44.
226. Batorsky A, Liao J, Lund AW, Plopper GE, Stegemann JP. Encapsulation of adult human mesenchymal stem cells within collagen-agarose microenvironments. Biotechnol Bioeng 2005;92(4):492-500.
227. Nuttelman CR, Tripodi MC, Anseth KS. Synthetic hydrogel niches that promote hMSC viability. Matrix Biol 2005;24(3):208-18.
228. Sinikovic B, Kramer FJ, Swennen G, Lubbers HT, Dempf R. Reconstruction of orbital wall defects with calcium phosphate cement: clinical and histological findings in a sheep model. Int J Oral Maxillofac Surg 2007;36(1):54-61.
229. Burnstine MA. Clinical recommendations for repair of orbital facial fractures. Curr Opin Ophthalmol 2003;14(5):236-40.
230. Fonseca RJ, editor. Oral and Maxillofacial Surgery v.3 Trauma: W.B. Saunders Company; 2000. 205-243 p.

231. Polley JW, Ringler SL. The use of Teflon in orbital floor reconstruction following blunt facial trauma: a 20-year experience. Plast Reconstr Surg 1987;79(1):39-43.
232. Ng SG, Madill SA, Inkster CF, Maloof AJ, Leatherbarrow B. Medpor porous polyethylene implants in orbital blowout fracture repair. Eye 2001;15(Pt 5):578-82.
233. Villarreal PM, Monje F, Morillo AJ, Junquera LM, Gonzalez C, Barbon JJ. Porous polyethylene implants in orbital floor reconstruction. Plast Reconstr Surg 2002;109(3):877-85; discussion 886-7.
234. Ozturk S, Sengezer M, Isik S, Turegun M, Deveci M, Cil Y. Long-term outcomes of ultra-thin porous polyethylene implants used for reconstruction of orbital floor defects. J Craniofac Surg 2005;16(6):973-7.
235. Burm JS. Internal fixation in trapdoor-type orbital blowout fracture. Plast Reconstr Surg 2005;116(4):962-70.
236. Schon R, Metzger MC, Zizelmann C, Weyer N, Schmelzeisen R. Individually preformed titanium mesh implants for a true-to-original repair of orbital fractures. Int J Oral Maxillofac Surg 2006;35(11):990-5.
237. Rubin JP, Yaremchuk MJ. Complications and toxicities of implantable biomaterials used in facial reconstructive and aesthetic surgery: a comprehensive review of the literature. Plast Reconstr Surg 1997;100(5):1336-53.
238. Lee KY, Mooney DJ. Hydrogels for tissue engineering. Chem Rev 2001;101(7):1869-79.
239. Betz MW, PC Modi, JF Caccamese, DP Coletti, JJ Sauk, JP Fisher. Cyclic Acetal Hydrogel System for Bone Marrow Stromal Cell Encapsulation and Osteodifferentiation. J Biomed Mater Res A 2007;*Accepted*.
240. Woo BH, Fink BF, Page R, Schrier JA, Jo YW, Jiang G, DeLuca M, Vasconez HC, DeLuca PP. Enhancement of bone growth by sustained delivery of recombinant human bone morphogenetic protein-2 in a polymeric matrix. Pharm Res 2001;18(12):1747-53.
241. Inoda H, Yamamoto G, Hattori T. rh-BMP2-induced ectopic bone for grafting critical size defects: a preliminary histological evaluation in rat calvariae. Int J Oral Maxillofac Surg 2007;36(1):39-44.
242. Kofron MD, Laurencin CT. Bone tissue engineering by gene delivery. Adv Drug Deliv Rev 2006;58(4):555-76.
243. Degat MC, Dubreucq G, Meunier A, Dahri-Correia L, Sedel L, Petite H, Logeart-Avramoglou D. Enhancement of the biological activity of BMP-2 by synthetic dextran derivatives. J Biomed Mater Res A 2008.
244. Zhao B, Katagiri T, Toyoda H, Takada T, Yanai T, Fukuda T, Chung UI, Koike T, Takaoka K, Kamijo R. Heparin potentiates the in vivo ectopic bone formation induced by bone morphogenetic protein-2. J Biol Chem 2006;281(32):23246-53.
245. Jansen JA, Dhert WJ, van der Waerden JP, von Recum AF. Semi-quantitative and qualitative histologic analysis method for the evaluation of implant biocompatibility. J Invest Surg 1994;7(2):123-34.

246. Kaihara S, Matsumura S, Fisher JP. Synthesis and properties of poly[poly(ethylene glycol)-co-cyclic acetal] based hydrogels. Macromolecules 2007;40(21):7625-7632.
247. Mapili G, Lu Y, Chen S, Roy K. Laser-layered microfabrication of spatially patterned functionalized tissue-engineering scaffolds. J Biomed Mater Res B Appl Biomater 2005;75(2):414-24.
248. Mathieu A, Cournede PH, Barthelemy D, de Reffye P. Rhythms and alternating patterns in plants as emergent properties of a model of interaction between development and functioning. Ann Bot (Lond) 2008;101(8):1233-42.
249. Karageorgiou V, Kaplan D. Porosity of 3D biomaterial scaffolds and osteogenesis. Biomaterials 2005;26(27):5474-91.
250. Botchwey EA, Pollack SR, Levine EM, Laurencin CT. Bone tissue engineering in a rotating bioreactor using a microcarrier matrix system. J Biomed Mater Res 2001;55(2):242-53.
251. Dean D, Topham NS, Meneghetti SC, Wolfe MS, Jepsen K, He S, Chen JE, Fisher JP, Cooke M, Rimnac C and others. Poly(propylene fumarate) and poly(DL-lactic-co-glycolic acid) as scaffold materials for solid and foam-coated composite tissue-engineered constructs for cranial reconstruction. Tissue Eng 2003;9(3):495-504.
252. Maspero FA, Ruffieux K, Muller B, Wintermantel E. Resorbable defect analog PLGA scaffolds using CO2 as solvent: structural characterization. J Biomed Mater Res 2002;62(1):89-98.
253. Nazarov R, Jin HJ, Kaplan DL. Porous 3-D scaffolds from regenerated silk fibroin. Biomacromolecules 2004;5(3):718-26.
254. Zhang R, Ma PX. Poly(alpha-hydroxyl acids)/hydroxyapatite porous composites for bone-tissue engineering. I. Preparation and morphology. J Biomed Mater Res 1999;44(4):446-55.
255. Zhao F, Yin Y, Lu WW, Leong JC, Zhang W, Zhang J, Zhang M, Yao K. Preparation and histological evaluation of biomimetic three-dimensional hydroxyapatite/chitosan-gelatin network composite scaffolds. Biomaterials 2002;23(15):3227-34.
256. Kim HD, Valentini RF. Retention and activity of BMP-2 in hyaluronic acid-based scaffolds in vitro. J Biomed Mater Res 2002;59(3):573-84.
257. Park SN, Park JC, Kim HO, Song MJ, Suh H. Characterization of porous collagen/hyaluronic acid scaffold modified by 1-ethyl-3-(3-dimethylaminopropyl)carbodiimide cross-linking. Biomaterials 2002;23(4):1205-12.
258. Lin AS, Barrows TH, Cartmell SH, Guldberg RE. Microarchitectural and mechanical characterization of oriented porous polymer scaffolds. Biomaterials 2003;24(3):481-9.
259. Huang D, Swanson EA, Lin CP, Schuman JS, Stinson WG, Chang W, Hee MR, Flotte T, Gregory K, Puliafito CA and others. Optical coherence tomography. Science 1991;254(5035):1178-81.
260. Georgakoudi I, Rice WL, Hronik-Tupaj M, Kaplan DL. Optical spectroscopy and imaging for the noninvasive evaluation of engineered tissues. Tissue Eng Part B Rev 2008;14(4):321-40.

261. Tan W, Sendemir-Urkmez A, Fahrner LJ, Jamison R, Leckband D, Boppart SA. Structural and functional optical imaging of three-dimensional engineered tissue development. Tissue Eng 2004;10(11-12):1747-56.
262. Mason C, Markusen JF, Town MA, Dunnill P, Wang RK. The potential of optical coherence tomography in the engineering of living tissue. Phys Med Biol 2004;49(7):1097-115.
263. Tan W, Oldenburg AL, Norman JJ, Desai TA, Boppart SA. Optical coherence tomography of cell dynamics in three-dimensional tissue models. Optics Express 2006;14(16):7159-7171.
264. Andrews PM, Chen Y, Onozato ML, Huang SW, Adler DC, Huber RA, Jiang J, Barry SE, Cable AE, Fujimoto JG. High-resolution optical coherence tomography imaging of the living kidney. Lab Invest 2008;88(4):441-9.
265. Guo L, Kawazoe N, Hoshiba T, Tateishi T, Chen G, Zhang X. Osteogenic differentiation of human mesenchymal stem cells on chargeable polymer-modified surfaces. J Biomed Mater Res A 2008;87(4):903-12.
266. Lu Y, Chen SC. Micro and nano-fabrication of biodegradable polymers for drug delivery. Adv Drug Deliv Rev 2004;56(11):1621-33.
267. Fonseca R, editor. Oral and Maxillofacial Surgery v.3 Trauma: W. B. Saunders Company; 2000. 205-243 p.
268. Singhatanadgit W, Salih V, Olsen I. RNA interference of the BMPR-IB gene blocks BMP-2-induced osteogenic gene expression in human bone cells. Cell Biol Int 2008;32(11):1362-70.
269. Betz MW, Modi PC, Caccamese JF, Coletti DP, Sauk JJ, Fisher JP. Cyclic acetal hydrogel system for bone marrow stromal cell encapsulation and osteodifferentiation. J Biomed Mater Res A 2008;86(3):662-70.
270. Story BJ, Wagner WR, Gaisser DM, Cook SD, Rust-Dawicki AM. In vivo performance of a modified CSTi dental implant coating. Int J Oral Maxillofac Implants 1998;13(6):749-57.
271. Yuan H, Kurashina K, de Bruijn JD, Li Y, de Groot K, Zhang X. A preliminary study on osteoinduction of two kinds of calcium phosphate ceramics. Biomaterials 1999;20(19):1799-806.
272. Mathieu LM, Mueller TL, Bourban PE, Pioletti DP, Muller R, Manson JA. Architecture and properties of anisotropic polymer composite scaffolds for bone tissue engineering. Biomaterials 2006;27(6):905-16.
273. Callister WD. Fundamentals of materials science and engineering : an integrated approach. Hoboken, NJ: John Wiley & Sons; 2005. 1 v. (various pagings) p.
274. Engler AJ, Sen S, Sweeney HL, Discher DE. Matrix elasticity directs stem cell lineage specification. Cell 2006;126(4):677-89.
275. Ogura N, Kawada M, Chang WJ, Zhang Q, Lee SY, Kondoh T, Abiko Y. Differentiation of the human mesenchymal stem cells derived from bone marrow and enhancement of cell attachment by fibronectin. J Oral Sci 2004;46(4):207-13.
276. Salasznyk RM, Williams WA, Boskey A, Batorsky A, Plopper GE. Adhesion to Vitronectin and Collagen I Promotes Osteogenic Differentiation of Human Mesenchymal Stem Cells. J Biomed Biotechnol 2004;2004(1):24-34.